TESIS DOCTORAL

Multi-Aircraft Optimal 4D In-Flight Trajectory Planning Based On Embedded Optimal Control

Autor:

Dinesh Babu Seenivasan

Director:

Alberto Olivares González

Programa de Doctorado Interuniversitario en Multimedia y Comunicaciones

Escuela Internacional de Doctorado

2019

Abstract

The main goal of this dissertation is the in-flight 4D trajectory planning problem for multiple aircraft in converging and intersecting routes in the presence of multi-cell storms in development. The problem is solved using nonlinear model predictive control based on hybrid optimal control with logical constraints in disjunctive form which arise in modelling passage through waypoints, distance-based and time-based separation constraints, decision making processes, conflict resolution policies, no-fly zones, obstacles or storms avoidance.

Enforcing separation between aircraft, passage through waypoints, and obstacle or storm avoidance are especially demanding in terms of modelling efforts. Indeed, in general, the first one requires the introduction of auxiliary integer variables in the model, for the second one a multiphase optimal control approach is used, and for the last ones geometric approximations of the obstacles or storms are usually introduced. Multiple phases increase model complexity and the presence of integer variables in the model has the drawback of combinatorial complexity of the corresponding mixed-integer optimal control problem.

In this work, an embedding approach is employed to tackle the hybrid optimal control problems, that is, to transform logical constraints in disjunctive form into inequality and equality constraints which involve only continuous auxiliary variables. In this way, the hybrid optimal control problem is converted into a smooth optimal control problem which is solved using traditional techniques, thereby reducing the computational complexity of finding the solution. Moreover, the evolution of the storms is handled using the nonlinear model predictive control scheme, which iteratively re-plans the trajectories as a new estimation of the state of the storms is available. The presence of this feedback mechanism in this trajectory planning scheme makes it substantially different from open-loop trajectory planning methods. Since it is intended for trajectory planning with very short time horizon before the departure or during the flight, it has been herein called online trajectory planning.

The effectiveness of the approach is demonstrated through several realistic numerical experiments by computing the optimal trajectories of multiple aircraft in converging and intersecting arrival routes with time-based separation constraints, distance-based separation constraints, operational constraints, and storms avoidance constraints.

Resumen

La planificación óptima del vuelo de una única aeronave asociada a una carta de navegación implica la consideración de múltiples factores, los cuales pueden ser de naturaleza tanto continua como discreta. Entre dichos factores cabe destacar la dinámica no lineal de la aeronave, las condiciones de la atmósfera, el viento y las tormentas, la estructura del espacio aéreo, la cantidad de combustible en el despegue o las restricciones operacionales. Además, es habitual tener que modelar también procesos de toma de decisiones. La complejidad de este problema aumenta de forma significativa si, en lugar de una sola aeronave, se considera la presencia e interacción de múltiples aeronaves dentro de un entorno aeroportuario extendido (eTMA) donde, además de los factores mencionados anteriormente, se ha de tener en cuenta la modelización de la detección de conflictos y su resolución, tal y como ocurre, por ejemplo, al tratar de garantizar la separación y la secuenciación de las aeronaves cumpliendo los estándares de seguridad establecidos por las autoridades competentes. En este contexto, el objetivo principal de esta tesis doctoral es el desarrollo de técnicas de control óptimo para la planificación en vuelo de trayectorias 4D de múltiples aviones comerciales dentro del eTMA y en presencia de tormentas multicelulares en desarrollo.

Antecedentes

Bajo el paradigma tradicional de la planificación de vuelos de aeronaves comerciales, el método más utilizado fundamentalmente por las compañías aéreas ha sido la descomposición del problema en dos etapas: la optimización de la ruta en 2D y la optimización de los perfiles de altitud y velocidad sobre la ruta 2D previamente calculada. En la primera etapa, la optimización de las rutas 2D se calcula considerando la estructura del espacio aéreo, es decir, las zonas de exclusión aérea, las aerovías o los puntos de referencia, usando algoritmos de optimización de redes o métodos de programación lineal entera mixta. En la segunda etapa, los perfiles de altitud y la velocidad se calculan mediante técnicas heurísticas. La principal ventaja de estos métodos es la facilidad para incorporar restricciones que modelen procesos de toma de decisiones, obteniendo modelos bastante complejos que se pueden resolver en tiempos computacionales relativamente bajos.

Sin embargo, esta aproximación tradicional presenta serias deficiencias si se tiene en cuenta el nuevo paradigma de vuelo consistente en operaciones basadas en trayectorias

(TBO) establecido por programas de innovación en la gestión de tráfico aéreo (ATM) como SESAR en Europa, NextGen en Estados Unidos o CARATS en Japón. Todos ellos son paradigmas basados en la negociación de trayectorias por parte de los implicados. Bajo este nuevo marco TBO, una solución a un problema de planificación de trayectorias en el ámbito ATM pasa ineludiblemente por la optimización de las trayectorias en 4D (tres dimensiones espaciales más el tiempo). En este sentido, el problema de optimización de trayectorias puede ser estudiado como un problema de control óptimo en el que el objetivo es encontrar la trayectoria y los inputs de control que guían el estado de la aeronave (considerada como sistema dinámico) entre dos configuraciones, satisfaciendo un conjunto de restricciones sobre el estado y/o las variables de control, mientras se minimiza un cierto funcional objetivo.

A diferencia del tradicional método de descomposición, el uso de control óptimo permite considerar no linealidades en el sistema, dando como resultado una dinámica más exacta de la aeronave, de tal forma que la solución proporciona la trayectoria 4D completa junto con la velocidad, el consumo de combustible de la aeronave y los ángulos de actitud, todo ello en función del tiempo. Además, la solución también proporciona las leyes de control óptimo de tal manera que la aeronave pueda ser guiada de manera óptima por el piloto o el autopiloto. Dada la naturaleza del sistema dinámico de las aeronaves en las que aparecen diferentes configuraciones dinámicas dependiendo de la etapa de vuelo, la aproximación habitual en la literatura es la de plantear un problema de control óptimo multifase.

Si además de la dinámica continua de la aeronave se desea modelar otros aspectos de interés como el paso a través de puntos de ruta, restricciones de separación de seguridad basadas en la distancia o en el tiempo, procesos de toma de decisiones, políticas de resolución de conflictos, zonas de exclusión aérea, o evitar obstáculos o tormentas, han de tenerse en cuenta la aparición de variables discretas en el sistema. El problema, por tanto, se afronta como un problema de control óptimo híbrido debido a la presencia simultánea de variables continuas y discretas. En particular, forzar una separación de seguridad entre aeronaves, el paso a través de puntos de referencia y la evasión de obstáculos o tormentas son especialmente exigentes en términos de esfuerzos de modelado. De hecho, en general, las restricciones de separación requieren la introducción de variables enteras auxiliares en el modelo, para las restricciones de paso se utiliza un enfoque de control óptimo multifase entero mixto, y para las restricciones de evasión de obstáculos se introducen aproximaciones geométricas de los obstáculos. La introducción de múltiples fases aumenta la complejidad del modelo y la presencia de variables enteras en el modelo tiene el inconveniente de la complejidad combinatoria del problema de control óptimo entero mixto resultante.

Objetivos

Para la consecución del objetivo principal, es decir, el desarrollo de técnicas de control óptimo para la planificación en vuelo de trayectorias 4D de múltiples aviones comerciales dentro del eTMA y en presencia de tormentas multicelulares en desarrollo, se han alcanzado los siguientes objetivos intermedios:

- Revisión exhaustiva de la literatura sobre teoría de control óptimo híbrido y métodos numéricos para la resolución de problemas de control óptimo híbrido, tanto en lazo abierto como en lazo cerrado.
- Construcción de un modelo matemático adecuado para plantear el problema de planificación de vuelos de aeronaves comerciales que incluya la dinámica no lineal de la aeronave, el viento y las tormentas, las características de la atmósfera, la estructura del espacio aéreo, restricciones operacionales y procesos de toma de decisiones.
- Desarrollo de técnicas para la formulación y resolución numérica de problemas de control óptimo híbrido en lazo abierto que incluyan múltiples aeronaves, eventos discretos (en particular, condiciones lógicas) y procesos de toma de decisiones.
- Desarrollo de técnicas para la formulación y resolución numérica de problemas de control óptimo híbrido en lazo cerrado basadas en las técnicas en lazo abierto ya desarrolladas, y que incluyan múltiples aeronaves, eventos discretos (en particular, condiciones lógicas) y procesos de toma de decisiones.
- Aplicación práctica de las técnicas desarrolladas a la resolución de casos de estudio en entornos realistas que impliquen múltiples aeronaves en un entorno aeroportuario extendido siguiendo procedimientos operacionales descritos en cartas de navegación y en presencia de tormentas en desarrollo.

Metodología

Las características del problema descrito anteriormente conducen a la formulación de un problema de control óptimo híbrido que incluya la modelización de condiciones lógicas que permitan tener en cuenta no solo las condiciones operacionales sino también los procesos de toma de decisiones. En concreto, las restricciones para evitar tormentas se han obtenido aproximando cada celda de la tormenta como un elipsoide en movimiento y de tamaño cambiante. Además de las restricciones para evitar tormentas, también se han considerado las restricciones operativas, como aquellas que permiten seguir un procedimiento de llegada o salida, una separación de seguridad basada en el tiempo o el espacio entre aeronaves, o el paso por puntos de referencia.

El modelo resultante se ha resuelto utilizando un control predictivo del modelo no lineal (NMPC) basado en un control óptimo híbrido con restricciones lógicas en forma disyuntiva. Las restricciones lógicas en forma disyuntiva surgen al modelar las restricciones operativas y de evasión de tormentas, y también al modelar los procesos de toma de decisiones generales durante el vuelo, como el establecimiento de cuál de dos o más acciones se deben tomar para resolver una contingencia. La evolución de las tormentas se aborda utilizando el esquema NMPC, que re-planifica iterativamente las trayectorias a medida que está disponible una nueva estimación del estado de las tormentas. La presencia de este mecanismo de retroalimentación en el esquema de planificación de las trayectorias lo hace sustancialmente diferente de los métodos de planificación de trayectorias en lazo abierto. Por tanto, se trata de la planificación de trayectorias en vuelo, es decir, una planificación en lazo cerrado cuyo proceso recurrente

depende a su vez de la resolución de un problema de planificación en lazo abierto en cada iteración.

Para la integración eficiente de las condiciones lógicas dentro de cada problema de control óptimo en lazo abierto, el problema de control óptimo híbrido se ha abordado usando una aproximación de tipo control integrado para transformar las restricciones lógicas en forma disyuntiva en restricciones de desigualdad e igualdad que involucran solo variables auxiliares continuas. De esta manera, el problema de control óptimo con restricciones lógicas se convierte en un problema de control óptimo suave que se resuelve utilizando técnicas tradicionales, reduciendo así la complejidad computacional de encontrar la solución en comparación con el enfoque de control óptimo entero mixto usado en el estado del arte. En particular, el problema de control óptimo continuo resultante se ha resuelto usando un método numérico directo. Más específicamente, se ha empleado un método de colocación directa, conocido como método de Hermite-Simpson, para transcribir el problema de control óptimo de dimensión infinita en un problema de optimización de dimensión finita, que se ha resuelto numéricamente usando un solver de programación no lineal.

Resultados

La efectividad del enfoque se ha demostrado a través de varios experimentos numéricos que calculan las trayectorias óptimas de múltiples aeronaves con rutas intersecantes y convergentes, en presencia de tormentas, con restricciones de separación basadas en tiempo y en distancia, así como restricciones operativas. En todos los experimentos se han considerado aeronaves del tipo Airbus A-320 cuyos parámetros dinámicos han sido obtenidos de la base de datos BADA 3.14 de Eurocontrol y han sido simulados en el eTMA del aeropuerto Adolfo Suárez Madrid-Barajas.

Dichos experimentos se han realizado en dos fases. En una primera fase, se han considerado casos de estudio en lazo abierto sin tener en cuenta la presencia de viento ni tormentas, en los que se ha evaluado la eficiencia del uso del control integrado para el tratamiento de condiciones lógicas asociadas a restricciones operativas y de resolución de conflictos. Una vez completada la primera fase con éxito, se han considerado casos de estudio en lazo cerrado, basados en llamadas iterativas a modelos de lazo abierto, añadiendo la presencia de viento y tormentas, con el fin de simular la planificación de múltiples trayectorias en vuelo en un entorno más realista.

Los resultados computacionales de los experimentos llevados a cabo confirman la eficiencia de la metodología propuesta. Es decir, el tiempo de cálculo del paradigma de planificación de trayectoria propuesto es adecuado para la implementación en vuelo, ya que en dichos experimentos el tiempo de cálculo, basado en el esquema NMPC, es inferior al tiempo de vuelo. Es mas, el número de actualizaciones del NMPC es mucho mayor que el número de actualizaciones de la información meteorológica disponible en los productos meteorológicos actuales.

Conclusiones

En esta tesis doctoral, se ha estudiado el problema de la planificación en vuelo de trayectorias de múltiples aeronaves comerciales en el que se incluyen condiciones lógicas en forma disyuntiva en el modelo. Las condiciones lógicas en forma disyuntiva han permitido modelar la presencia de tormentas en desarrollo, la detección y resolución de conflictos entre las diferentes aeronaves y el cumplimiento de restricciones operacionales, así como procesos de toma de decisiones en general. Dichas condiciones lógicas se han transformado en restricciones de desigualdad e igualdad que implican solo variables auxiliares continuas mediante una técnica de control integrado. De esta manera, el problema de control óptimo con restricciones lógicas se ha convertido en un problema de control óptimo suave continuo que se ha resuelto utilizando técnicas estándar. Este enfoque en lazo abierto se ha incorporado dentro de un esquema de tipo control predictivo del modelo no lineal, en lazo cerrado, y se aplicado a la optimización del perfil de vuelo de múltiples aeronaves en rutas convergentes e intersectantes dentro del eTMA del aeropuerto Adolfo Suárez Madrid-Barajas. Los resultados de los experimentos numéricos muestran la eficiencia de la técnica propuesta y su compatibilidad con la planificación en vuelo.

Acknowledgments

To my parents, sister and my love to all my family, to those present your unconditional love and support to grow as a free man to achieve his dreams. My friends in Madrid and India, who helped and advised me in crucial situation, accommodated me as one of their family member, gave me beautiful and unforgettable memories from last six year of my stay in Madrid. Thank you for everyone!

I want to express my gratitude to my mentors Prof. Dr. Alberto Olivares and Prof. Dr. Ernesto Staffetti. Nothing done during these more than four years of conscientious work and dedication would have been possible without their constant supervision, their dedication and time, their comments and always seeking excellence, and, in short, without their guidance, sincere and committed. Thank you for the time invested in discussions, meetings, simulations, readings, proof readings, etc. that led to publishing a couple of nice papers, and also for sharing a lot of intercultural experiences. Thank you for your continuous support from beginning of this work. And thank you all colleagues and friends in Department of Signal Theory and Communications of the Rey Juan Carlos University.

I would also like to thank Prof. Dr. Moritz Diehl, who hosted me at the Systems Control and Optimization Laboratory, IMTEK, University of Freiburg, Germany, for his support and guidance during my stay for four months. Also, I would like to mention all those that I have had the pleasure to meet and work in Freiburg.

Finally, this work has been supported by the grants TRA2013-47619-C2-2-R and TRA2017-91203-EXP, and the predoctoral fellowship BES-2014-069586 of the Spanish Government.

Contents

Notation

Vectors are not explicitly denoted. Superindexes denote number of aircraft, whereas subindexes denote discretization samples. We provide a not exhaustive list of terms.

(x_w, y_w, z_w)	=	aircraft attached reference frame.
(x_e, y_e, z_e)	=	Earth reference frame.
a_l	=	maximum longitudinal acceleration for civil flights.
a_n	=	maximum normal acceleration for civil flights.
C_D	=	coefficient of drag.
C_{D_0}	=	coefficient of parabolic drag.
C_L	=	coefficient of lift.
$C_{L_{max}}$	=	maximum coefficient of lift.
C_V	=	minimum speed coefficient.
D	=	drag force $= 0.5\rho V^2 S C_D$.
d_t	=	safety time difference.
$d_{\lambda\theta}$	=	safety distance in the longitude and latitude.
d_h	=	safety distance in the altitude.
g	=	acceleration due to gravity.
h_e	=	altitude.
h_{M_0}	=	maximum reachable altitude.
h_{max}	=	maximum altitude at MTOW under ISA conditions.
h_u	=	maximum operative altitude at given mass of the aircraft.
L	=	lift force $= 0.5\rho V^2 S C_L$.
M	=	Mach number.
M_{M0}	=	maximum operating Mach number.
m	=	mass.
m_{max}	=	maximum mass.
m_{min}	=	minimum mass.
η	=	fuel efficiency coefficient.
$\hat{q}$	=	dynamic pressure, $\hat{q} = \frac{1}{2}\rho V^2$.
R	=	Earth radius.
S	=	reference wing surface area.
T	=	thrust.

T_{max}	=	maximum thrust.
T_{min}	=	minimum thrust.
V	=	true airspeed.
V_{CAS}	=	calibrated air speed.
V_{M_0}	=	maximum operating calibrated airspeed.
V_S	=	stall speed.
$V_{Wind\lambda_e}$	=	wind speed in the longitude.
$V_{Wind\theta_e}$	=	wind speed latitude.
α	=	angle of attack.
χ	=	heading angle.
γ	=	flight path angle.
γ_{min}	=	minimum flight path angle.
γ_{max}	=	maximum flight path angle.
λ_e	=	longitude.
μ	=	bank angle.
θ_e	=	latitude.
(λ_p, θ_p, h_p)	=	positions of aircraft p.
(λ_p, θ_q, h_q)	=	positions of aircraft q.
(λ_l, θ_l, h_l)	=	positions of lower corner of the cuboid.
(λ_u, θ_u, h_u)	=	positions of upper corner of the cuboid.
(λ_{min}, θ_{min}, h_{min})	=	minimum values of the state variables.
(λ_{max}, θ_{max}, h_{max})	=	maximum values of the state variables.
(λ_{W_l}, θ_{W_l}, h_{W_l})	=	positions of lower corner of the cuboid around a waypoint.
(λ_{W_u}, θ_{W_u}, h_{W_u})	=	positions of upper corner of the cuboid around a waypoint..

List of acronyms

AMANs	=	Arrival Managers.
APM	=	Aircraft Perfomance Model.
ATC	=	Air Traffic Control.
ATM	=	Air Traffic Management.
BADA	=	Base of Aircraft Data.
CAS	=	Calibrated AirSpeed.
CCO	=	Continuous Climb Operations.
CDA	=	Continuous Descent Approach.
COIN-OR	=	Computational Infrastructure for Operations Research
CNF	=	Conjunctive Normal Form
CPU	=	Central Processing Unit
CWAM	=	Convective Weather Avoidance Model
DOF	=	Degree Of Freedom.
DP	=	Dynamic Planner.
ETA	=	Estimated Time of Arrival.
FAA	=	Federal Aviation Administration.
FMS	=	Flight Management System.
HLGL	=	Hermite-Legendre-Gauss-Lobatto.
ICAO	=	International Civil Aviation Organization.
ISA	=	International Standard Atmosphere.
IPOPT	=	Interior Point OPTimizer.
NLP	=	Non-Linear Programming.
NLP BB	=	Non-Linear Programming based on Branch and Bound.
NM	=	Nautical Miles
NMPC	=	Nonlinear Model Predictive Control
NWCSAF	=	Nowcasting and Very Short-Range Forecasting.
MILP	=	Mixed-Integer Linear Programs.
MINLP	=	Mixed-Integer Non-Linear Programming.
OC	=	Operational Constraints.
OCP	=	Optimal Control Problem.
ODE	=	Ordinary Differential Equation.

OEW	=	Operating Empty Weight.
OLOCP	=	Open-loop Optimal Control Problem.
OPDs	=	Optimized Profile Descents
RAM	=	Random Access Memory
RDT	=	Rapidly Developing Thunderstorms.
RA	=	Route Analyzer
SESAR	=	Single European Sky ATM Research.
SID	=	Standard Instrumental Departure.
STA	=	Scheduled Times of Arrival.
STAR	=	Standard Terminal Arrival Route.
SWIM	=	System Wide Information Management.
TBO	=	Trajectory-Based Operations.
TMA	=	Terminal Maneuvering Areas.
e TMAs	=	Extended Terminal Maneuvering Areas.
TOP	=	Top-of-Descent.
TS	=	Traffic Synthesizer.
UAV	=	Unmanned Air Vehicle.
USA	=	United States of America.

List of Figures

List of Tables

1

Introduction

1.1 Motivation

In this dissertation, the in-flight trajectory planning problem is studied for multiple aircraft flying along converging routes in the presence of storms in development, which can be stated as follows: given the dynamic models of a set of aircraft, their initial and final states, a set of operational constraints, and a sequence of meteorological data about a multi-cell storm in development in the relevant airspace, find the optimal trajectories that steer the aircraft from the initial to the final states, avoiding the storm, fulfilling, if possible, all the operational constraints and optimizing an objective functional.

In Air Traffic Management (ATM), the flight of several aircraft can be modeled as a hybrid dynamical system, which can be regarded as a set of interacting continuous dynamical systems. A number of frameworks have been proposed to model hybrid dynamical systems, in which, in general, differential equations describe the dynamics of each system, whereas logical constrains describe the behavior of the systems during the interactions among them and the interaction with the environment in which they operate. In the ATM context, logical constraints describe, for instance, policies to apply in conflict detection and resolution and operational constraints to be fulfilled during flight. The main operational constraints to be fulfilled during flight are separation constraints, keep-out constraints to avoid no-fly zones and passage constraints through or by waypoints [1].

The problem studied in this dissertation can be classified into the category of Continuous Climb and Descent Operations (CCOs and CDOs). CCOs and CDOs are aircraft operating techniques enabled by airspace design, instrument procedure design and facilitated by Air Traffic Control (ATC). They allow aircraft to follow a flexible,

optimum flight path that delivers major environmental and economic benefits (reduced fuel burn, gaseous emissions, noise and fuel costs) without any adverse effect on safety [2].

Note that, although the numerical experiments considered in this dissertation are focused on CDOs, the methodology employed is presented as a general framework so that it could be straightfully applied to CCOs as well.

During a CDO, aircraft descend from the cruise altitude to the final approach fix at or near idle thrust without level segments at low altitude minimizing the need for high thrust levels to remain at a constant altitude and reducing the environmental impact. Actually, the term CDO makes reference to the different techniques to maximize operational efficiency and, at the same time, fulfilling local air space requirements and constraints. These operations are known as Continuous Descent Arrivals, Optimized Profile Descents (OPDs), Tailored Arrivals, 3D Path Arrival Management and Continuous Descent Approaches (CDAs). In particular, an OPD is a descent profile normally associated with a Standard Terminal Arrival Route (STAR) and designed to allow maximum use of a CDO. Planning CDOs is one of the functions of the so called Arrival Managers (AMANs) whose purpose is to ensure an optimal sequencing and spacing of arrival traffic [3].

Operations such us CDOs, OPDs and CDAs are part of a new ATM paradigm which has been developed in the last years and try to improve sustainability, efficiency and safety in civil aviation operations. Two of the main programmes devoted to devise an improved ATM system are the Next Generation of air transportation system (NextGen) [4] in the United States of America and the Single European Sky ATM Research (SESAR) Program [5] in Europe. This improved ATM system is intended to move from a clearance-based ATC paradigm to a Trajectory-Based Operations (TBO) paradigm [6] in which trajectories have become a key part and flight paths are negotiated. In this way, the business trajectory concept has been introduced to represent the trajectory that best meets the airlines business interests such us the minimization of the time for the flight, the consumption, the cost index, or the environmental impact. Although the airlines are considered to be the owners of the business trajectory, in-flight trajectory modifications usually carried out onboard Flight Management System (FMS) should be proposed by ATC and agreed with the airlines, since modifications in trajectories could result in changes in the cost effectiveness of the overall operation.

This TBO concept of operations based on the notion of business trajectory assumes that all necessary data regarding the trajectory is shared by all the stakeholders through a wide information management system, known as SWIM, in order to promote decision-making processes, and suppose aircraft to actually fly accurate 4D trajectories [7]. Since safety is always the main goal in civil aviation, under the TBO concept, airports, Terminal Manoeuvring Areas (TMAs) and extended TMAs (eTMAs) are still the congestion spots of the air navigation system so that the ATC intervention and the use of constraints are necessary as well. Thus, the TBO concept must also be designed under a constrained paradigm supervised by the ATC.

In particular, in this dissertation, the problem of optimal sequencing of arrival traffic has been studied taking into account multi-cell developing storms in the relevant airspace. Forecasting with precision the birth and evolution of convective weather phenomena at pre-tactical timescales (1-3 hours before departure) is not an easy task, which makes it hard for flight dispatchers to plan flights to avoid them. Although some meteorological conditions, which are required for storm formation, can be forecasted in advance, the specific location and timing of convective storms is difficult to determine. As a consequence, both thunderstorm forecasting and storm avoidance take place at short timescales, mainly at execution stage, that is, during flight.

Storm prediction is usually given in the form of deterministic nowcast such as the Rapidly Developing Thunderstorms (RDT) which is one of the meteorological products of the Satellite Application Facility on support to Nowcasting and Very Short-Range Forecasting (NWCSAF) consortium [1]. The RDT system characterizes thunderstorm activity providing images every 15 minutes with a horizontal resolution of 3 km. It identifies convective cells and describes them as polygons on a latitude-longitude map. It contains the identified convective storms, along with some of their features such as perimeter, direction of motion and speed and the cloud top pressure (the latter, needed to characterize the height of the storm). It also provides a description of the phase of the convective cell: triggering, triggering from split, growing, mature and decaying. These parameters are then employed to predict the evolution of the storm over a short time horizon and they are corrected as soon as a new observation becomes available.

Different approaches to the study of convective storms phenomena with data-driven methods oriented to aircraft routing problems have been presented in the literature. In [8], a characterization of the uncertainty in the thunderstorms movement detected by a radar-based system is conducted. In [9] the Convective Weather Avoidance Model (CWAM) has been introduced which is focused on analyzing and forecasting weather avoidance fields, that is, regions of space that pilots should avoid. The CWAM is performed by using statistical analysis to identify relationships between processed convection-related meteorological variables and weather-caused deviations of aircraft from the planned route, and has been extensively studied and employed in ATM research in the United States of America [10].

1.2 Goals

The main goal of this dissertation is to develop optimal control techniques for in-flight trajectory planning of multiple aircraft flying along converging and intersecting routes in the presence of storms in development.

To reach this main goal the following intermediate objectives has been achieved:

- Revision of the literature on optimal control theory and numerical methods for open-loop and closed-loop optimal control of nonlinear systems.

[1] http://www.nwcsaf.org/

- Revision of the literature on storms forecast and meteorological products availability.
- Modeling of the elements of the in-flight planning problem that include the aircraft performance model, the operational procedures, the multi-cell storm model, and decision-making processes.
- Definition of a framework to solve optimal control problems that include logical constraints arising from discrete events, such as operational constraints and decision-making processes.
- Validation of the approach by means of numerical experiments.

1.3 Methodology

The computation of the in-flight trajectory plan proposed in this dissertation is a complex task which involves the modelling of both continuous and discrete phenomena. On the one hand, the continuous models include aircraft performance, atmospheric conditions and meteorological conditions, such us the wind model. On the other hand, discrete models include operational constraints and procedures, and decision-making processes, such us choosing between flying through a waypoint or avoiding a storm. Therefore, the methodology proposed in this dissertation for the resolution of the in-flight trajectory planning problem looks for a trade-off between the computational complexity and solvability of the models, which must be accurate enough to represent reality in a reliable way and, at the same time, not too complex to be solvable with reasonable computational efforts.

Concerning to the dynamic model of the aircraft, in this dissertation a three-degrees-of-freedom dynamic model describing the point variable-mass motion of the aircraft has been assumed over a spherical, non rotating Earth model. The aircraft have been considered as conventional jet airplanes with fixed engines. The external actions acting on each aircraft have been decomposed into propulsive, aerodynamic, and gravitational. The aircraft has been supposed to have a plane of symmetry, and thus a symmetric flight has been considered.

Regarding the aircraft performance limitations model and parameters, they have been obtained from the Eurocontrol Base of Aircraft DAta (BADA), version 3.14 [11], which provides data for almost 300 types of aircraft, operations, and procedures. BADA is an Aircraft Performance Model (APM) developed and maintained by EUROCONTROL with the collaboration of aircraft manufacturers and airlines, which includes models for thrust, consumption, aerodynamics, and performance limitations, and is specifically designed for simulation and prediction of aircraft trajectories for research and operations in ATM. The BADA APM has two components: model specifications, which provide the theoretical models used to calculate aircraft performance parameters, and data sets, which give the aircraft-specific coefficients. BADA enables the standardization of aircraft models, the comparison of experimental results, and the automation of the flight plan

computation for different types of aircraft. There are two families of the BADA APM, based on the same modelling approach and with the same components: BADA Family 3 and BADA Family 4. The 3.14 release of BADA Family 3 has been used in this dissertation.

In relation to the atmospheric conditions, the standard model of atmosphere used in aviation and weather studies has been considered in this dissertation, that is, the density of air has been modelled as a function of the altitude given by the profiles established by the International Standard Atmosphere (ISA) in the different layers of the atmosphere.

As regards to the meteorological conditions, on one hand, a deterministic wind forecast model has been considered in which the wind in the vertical direction has been supposed to be zero. In particular, an stationary constant wind field has been assumed. On the other hand, a deterministic storm forecast model has been assumed. More specifically, multi-cell storms in development have been designed in which each cell has been modelled as a moving and size-changing ellipsoid in the 3D space.

Indeed, storms forecast, such us the RTD-based forecast introduced in Section 1.1, can be regarded as a moving horizon estimation, for which a well-suited scheme for in-flight trajectory planning is the Nonlinear Model Predictive Control (NMPC) scheme [12]. In the NMPC setting, the optimal trajectories for the aircraft can be calculated taking into account the prediction of the future dynamic behaviour of the storms over a certain time horizon, based on measurements obtained at a certain time instant.

Due to disturbances and modelling prediction errors, the behaviour of the storms will be different from the predicted behaviour and the trajectories of the aircraft will deviate from the planned trajectories. In order to incorporate some feedback mechanism to correct these mismatches, in the NMPC scheme the planned trajectories will be flown in open-loop until the next prediction of the storms becomes available. Then, the trajectory planning problem is solved again in a receding spatial and temporal horizon. For this reason, this control paradigm is also referred to as moving horizon control or receding horizon control. The presence of a feedback mechanism in this trajectory planning scheme, makes it substantially different from the open-loop trajectory planning methods. Since it is intended for in-flight trajectory planning, that is, with very short time horizon before the departure or during the flight, it has been herein called online trajectory planning.

Unlike offline approaches, online trajectory planning schemes are able to immediately respond to changes in the environment or perturbations on the aircraft during flight. In particular, in this dissertation, a NMPC scheme based on hybrid optimal control with logical constraints in disjunctive form has been employed in order to solve the problem. Logical constraints in disjunctive form arise in modelling of both storm avoidance and operational constraints but also in modelling general decision making processes during flight to establish which among two or more actions should be taken to solve a contingency, such us for instance when operational constraints cannot be fulfilled due to the presence of the storm. Finding the solution entails finding the

optimal trajectories of each aircraft, their optimal sequencing at merging waypoints, keeping safety separation, and taking the optimal decisions.

To solve hybrid optimal control problems with logical constraints in disjunctive form, the embedding technique presented in [13] and [14] has been used, which allows hybrid optimal control problems to be transformed into traditional smooth optimal control problems. This technique initially devised to tackle the discrete aspect of the system due to switches in the dynamic equations, was adapted in [15] to deal with the logical (discrete) components, which also might appear as constraints. In particular, the embedding technique proposed in [15] to model rectangular obstacle avoidance in the horizontal plane for Unmanned Aerial Vehicles (UAVs) path planning has been extended in this dissertation to model in the 3D space the following type of constraints in trajectory optimization for multiple aircraft:

- time-based separation constraints,
- distance-based separation constraints,
- passage through waypoints constraints, and
- storms avoidance constraints.

Given a set of aircraft, separation constraints between them can be expressed as follows: pairwise, they must keep a vertical distance greater than a minimum vertical safety distance or an horizontal distance greater than a minimum horizontal safety distance. The minimum horizontal separation distance can be fixed or variable. In the latter case, it can be established based on the turbulence generated by the preceding aircraft and the ability of the following aircraft to resist turbulence [16].

Regarding obstacles and no-fly zones, polyhedral regions of air space are in general considered. However, the corresponding keep-out constraints are usually introduced by bounding ellipsoids around obstacles. In some cases, this is a coarse approximation. Keep-out constraints from a polyhedral region of air space can be expressed as follows: each aircraft must stay outside one of the half-spaces defined by the planes that supports the faces of the polyhedron. This method for modelling keep-out constraints from obstacles can be extended to model passage constraints through windows or waypoints in the air space. In this manner, the multiphase modeling of the problem is avoided. This is an interesting possibility, since multiphase optimal control models imply the introduction of additional variables to the problem, such as the duration of the phases and additional constraints, such as the linkage constraints between them to enforce continuity of the state variables between contiguous phases [17].

In this dissertation, the modelling of passage constraints through waypoints has been done by defining vertical walls in the air space with a cuboidal window around the waypoint. In this way, introducing multiple phases in the model to enforce passage through waypoints is avoided. Moreover, the dimensions of the windows can be easily calibrated to induce a fly-by or a fly-through the waypoint.

Finally, the storm avoidance problem has been tackled like a moving obstacle avoidance problem in which, for each aircraft, a safety distance-based separation between the aircraft and the central point of the storm is guaranteed in the horizontal or vertical direction, and where each cell of the multi-cell storm has been represented by a moving and size-changing ellipsoid, as already mentioned above.

Therefore, following the proposed methodology, the in-flight trajectory planning problem studied in this dissertation has been solved using optimal control techniques. In particular, the multi-aircraft closed-loop optimal control problem has been transformed into a set of open-loop hybrid optimal control problems. Then, each of these open-loop hybrid optimal control problems has been converted into a smooth continuous optimal control problem through an embedding technique which has been transcribed into a NonLinear Programming (NLP) problem by means of a direct collocation technique. Finally, the resulting NLP problems have been solved using a NLP solver.

1.4 Previous Approaches

It is easy to see that all the constraints mentioned above in Section 1.3 can be expressed in disjunctive form. Standard modelling techniques are able to tackle constraints in disjunctive form using binary variables. The trajectory planning problem for multiple aircraft with logical constraints in disjunctive form can be solved as an Optimal Control Problem (OCP) for an hybrid dynamical system and a common approach for solving this class of problems is to formulate them as a mixed-integer programming problems. In [18], the optimal cooperative three-dimensional conflict resolution problem among multiple aircraft has been solved in which separation constraints among aircraft expressed in disjunctive form have been included in the model using continuous auxiliary variables. In [15], the optimal path planning problem for multiple UAVs in the horizontal plane with collision avoidance has been studied, in which constraints for collision avoidance with rectangular obstacles expressed in disjunctive form are included in the model using continuous auxiliary variables. In [19], the trajectory optimization problem for multiple aircraft landing on a single runway in the presence of constraints on the air space has been treated. The constraints considered are passage constraints through windows in the air space and optimal trajectories have been determined by solving a non-sequential constrained multiple-phase optimal control problem.

Most of the previous research on CDOs based on optimal control theory focused on the trajectory optimization of a single aircraft. In [20] a multi-phase optimal control method based on the pseudospectral technique has been employed to optimize vertical trajectories for individual aircraft in CDAs. Since the lateral path is assumed to be given by a STAR procedure, this work focused on optimizing vertical profile only using time and fuel consumption as performance indices. All the phases are formulated based on operational constraints and flap/gear schedules. The initial along track distance is free. Hence, it is possible to calculate both the optimal Top-of-Descent (TOD) and CDA trajectory. The optimal trajectories have been computed for two aircraft types:

a Boeing 737-500 and a Boeing 767-400. In [21], the vertical trajectory optimization for the en route descent phase of an aircraft has been studied in the presence of both along-track and cross winds, which are both modeled as functions of altitude. Flight idle thrust was assumed during the entire descent phase. The problem is formulated as an optimal control problem. The flight range was specified from a point during the latter stages of the cruise to the meter fix. CAS and Mach constraints, which are the state path constraints, are considered, along with flight path angle constraints, and a maximum descent rate limit, which is a mixed input and state path constraint. The descent trajectory is optimized with respect to two cost functionals: fuel and emissions. The effects of wind speed, windshear, and cross-wind on the optimal trajectory have been analyzed using the models of two types of aircraft, Boeing 737-500 and Boeing 767-400.

The interest in modelling the presence of storm within aircraft trajectories planning problems has increased mainly in the las years. In [22] the aircraft motion planning problem in converging flows of aircraft in the presence of convective storms in the en route airspace is solved using an algorithm based on NMPC. The optimal control sequence is computed over a fixed horizon using dynamic programming under aircraft separation constraints, bounds on aircraft turning rates and convective weather avoidance constraints.

In [23] a dynamic weather forecast product is used to formulate a receding horizon framework for planning trajectories for multiple aircraft that avoid hazardous weather regions in the en-route phase of the flight, in which the set to be avoided during the motion is assumed to be both time-varying and deterministic.

In [24] a dynamic programming based approach to a stochastic reach-avoid problem for a controlled discrete-time stochastic hybrid system is presented in which the set to be avoided during the motion is assumed to be both time-varying and probabilistic.

In [25] a path planning methodology is proposed to include several weather hazards but without taking into account the wind distribution, in which no trajectory optimization is carried out but weather avoidance is performed together with different criteria for the route decision making. Four options for weather hazard avoidance are defined, including moderate and severe convection, and three avoiding strategies are considered: hazard ignorance, avoiding from departing to arriving, and avoiding hazards as encountered within a 30-minute look-ahead time.

In [26] an approach to extract a probabilistic dynamic description of hazardous thunderstorm regions from nowcast data is presented. The stochastic thunderstorm model is integrated in a stochastic optimal trajectory planning tool based on the stochastic reach-avoid methodology presented in [24]. The resulting aircraft trajectories maximize the probability of reaching a specified goal set while avoiding multiple thunderstorm regions. However, the computational performance of this method is not compatible for online implementation due to the curse of dimensionality which appears as a consequence of the used of a planning algorithm based on dynamic programming in a 4D space.

In [27] a probabilistic weather map is constructed from ensemble forecasting with confidence bounds. A 3D receding horizon field D* search algorithm is used to find the optimal route. The probability of adverse weather in each grid cell of weather map, the probability of mission failure in each grid cell and along the entire route, and their associated confidence bounds is calculated to maximize the performance of an aerial vehicle and minimize the mission failure risk.

1.5 Contributions of the dissertation

In the previous approaches, presented in Section 1.4, less research efforts have been devoted to combined optimization of trajectories of multiple aircraft and sequencing for approaching a TMA in which all aircraft follow CDAs, whilst satisfying the operational requirements. Moreover, in most of these previous approaches to optimal trajectory planning under storm development a cell discretisation of the 3D or 4D space, in which the problem is represented, is performed. In these approaches, the model of the aircraft is oversimplified. Often, a kinematic model of a unicycle with upper bounds on the turning rate is used to represent aircraft. This implies that the actual performance of the aircraft involved is not taken into account. This fact does not guarantee the dynamic feasibility of the resulting trajectories. The problem is, in general, studied in the en-route phase of the flight of a single aircraft. The solution method is based on a discrete search which represents a further approximation of the problem, whose nature is indeed continuous. Furthermore, this search is computationally expensive and this makes the approach unsuitable for online applications.

All these facts have motivated this study so that, in the approach to optimal online trajectory planning for multiple aircraft in the presence of a multi-cell storm in development presented in this dissertation, all these drawbacks are overcome. In particular, the main contributions of this dissertation include:

- The optimization of trajectories of multiple aircraft have been combined and sequencing for approaching a TMA following CDAs procedures and, at the same time satisfying the operational requirements.
- Accurate models of the aircraft have been taken into account, which ensures dynamic feasibility of the trajectories.
- The problem is studied in the arrival phase of the flight of several aircraft along converging routes, in which modelling the scenario within an optimal control problem is much more complex than in other flight phases.
- All the logical constraints in disjunctive form are modelled using the embedding approach, which avoids integer or binary variables to be introduced in the model.
- The resulting problem is a smooth optimal control problem with continuous variables, which can be solved very efficiently within a NMPC scheme for online trajectory planning.

- Furthermore, as mentioned above, the methodology followed in this work is presented as a general framework so that it could be directly applied to CCOs as well.

1.6 Organization of the dissertation

This dissertation is structured as follows:

In Chapter 2, the general optimal control problem for multiple dynamical systems is stated and the closed-loop nonlinear model predictive control approach for its resolution, based on open-loop hybrid optimal control with logical constraints in disjunctive form, is explained.

In Chapter 3, the aircraft equations of motion and the flight envelope constraints are described, and the general approach to model logical constraints is presented, which is then particularized to model storm avoidance constraints and operational constraints.

In Chapter 4, the results of the application of the proposed method to solve several offline trajectory planning problems for multiple aircraft along converging and intersecting routes are reported and discussed.

In Chapter 5, the results of the application of the proposed method to solve several online trajectory planning problems for multiple aircraft along converging routes in the presence of a multi-cell storm in development are reported and discussed.

Finally, in Chapter 6, some conclusions and future lines of research are drawn.

2

Optimal Control

In this chapter, a theoretical background on NMPC-based closed-loop optimal control problems is presented. First, a general NMPC setting for discrete time systems is introduced. Then, the transformation of NMPC schemes for discrete time systems into NMPC settings for continuous time models, by means of sampled data systems, is described. Moreover, the basic NMPC algorithm is explained in detail together with its adaptation to the constrained NMPC case. The Open-loop Optimal Control Problem (OLOCP) for multiple dynamic systems which is solved in each iteration of the NMPC method is also stated in detailed, as well as its numerical resolution through the Hermite-Simpson direct collocation technique. Finally, the practical implementation of the NMPC closed-loop optimal control based on recursive iterations of OLOCPs is drawned.

2.1 Nonlinear Model Predictive Control

The multi-aircraft online trajectory problem considered in this dissertation has been tackled by means of a Model Predictive Control (MPC) approach, also known as Receding Horizon Control. The MPC technique, which is an optimization based method which provides feedback control of dynamic systems, will be described in this section following [12].

The MPC setting assumes a controlled process in the sense that, at each time instant, a control input, which steers the system to a subsequent state, can be selected. More specifically, given a reference trajectory, the goal of a tracking feedback control is to find the control input such that the state accurately follows it. Thus, the system will be steered to the reference trajectory when the current state is away from it or the system will be hold when the current state is close enough. In particular, if a constant reference trajectory is considered the tracking feedback control problem becomes a stabilization problem.

The basic idea behind MPC is both to predict and optimize the behavior of the system assuming that a model of the process is available which can be represented as

$$x^+ = \mathcal{F}(x, u), \tag{2.1}$$

where $\mathcal{F}$ is a known map usually called transition map, with $x \in \mathcal{X}$ and $u \in \mathcal{U}$ for some given state space $\mathcal{X}$ and set of controls $\mathcal{U}$, which provides the next state x^+ at the next time instant as a function of the current state x and a control value u. Then, an iterative procedure will provide a map $\mu_{\mathcal{L}} : \mathcal{X} \to \mathcal{U}$ for the computation of a control in the so called feedback form, that is, $u(\cdot) = \mu_{\mathcal{L}}(x(\cdot))$. In this way, the current state deviation from the reference trajectory is taken into account by this feedback control u.

2.1.1 Discrete Time Systems

In the original MPC method, control $u(n)$ and state measures $x(n)$ are considered at discrete time instants t_n for $n \in \mathbb{Z}^+$. Then, iterating (2.1), a prediction trajectory x_u can be built from the current state $x(n)$ and a given sequence of controls $u(0), u(1), \ldots, u(N-1)$ with horizon length $N \geq 2$, following

$$\begin{aligned} x_u(0) &= x(n), \\ x_u(k+1) &= \mathcal{F}\left(x_u(k), u(k)\right), \quad k = 0, 1, \ldots, N-1. \end{aligned}$$

This iterative procedure yields for each k a prediction $x_u(k)$ for the state $x(n+k)$, that is, a prediction for the value of the state at time instant t_{n+k}. Thus, a prediction of the behavior of the system through the control sequence $u(0), u(1), \ldots, u(N-1)$ is provided over the time interval $[t_n, t_{n+N}]$ at discrete time instants $t_n, t_{n+1}, \ldots, t_{n+N}$. The remaining question is how this control sequence is determined such that the reference trajectory, which will be denoted by x^*, is approximated as accurately as possible by the prediction x_u.

As pointed out above, model (2.1) generates predictions $x_u(k)$ which are needed in the optimization algorithm of the MPC scheme. Although this mathematical model do not provide exact predictions for the trajectories of real process, this idealized assumption is assumed in this dissertation so that for a given MPC feedback control law $\mu_{\mathcal{L}} : \mathcal{X} \to \mathcal{U}$ it is assumed that the resulting closed-loop system fulfils

$$x^+ = \mathcal{F}\left(x, \mu_{\mathcal{L}}(x)\right), \tag{2.2}$$

which is usually known as the nominal closed-loop system, and where $\mathcal{F}$ is the transition map in (2.1).

2.1.2 Sampled Data Systems

Many models of real life applications are given as continuous time models, usually in form of differential equations. This is the case of the kind of problems studied in this dissertation. To transform these models into the discrete time form (2.1), the notion of sampling is introduced. Suppose that the control system under study is given by an ordinary differential equation

$$\dot{x}(t) = f_C\left(x(t), v(t)\right), \tag{2.3}$$

where $x(t)$ denotes the unknown function $x : \mathbb{R} \to \mathbb{R}^{n_x}$, $v(t)$ the control function $v : \mathbb{R} \to \mathbb{R}^{n_u}$ and f_C is a vector field $f_C : \mathbb{R}^{n_x} \times \mathbb{R}^{n_u} \to \mathbb{R}^{n_x}$, and where $\dot{x}(t)$ denotes the derivative $\frac{dx}{dt}$ and $n_x, n_u \in \mathbb{N}$ are the dimensions of the state and the control vector, respectively. Note that, for the sake of clarity, symbol v has been introduced for the control function in order to remark the difference between the discrete time control $u(\cdot)$ in (2.1) and the continuous time control function $v(\cdot)$ in (2.3).

Under the assumption that the vector field f_C is continuous and Lipschitz in its first argument, Caratheodory's Theorem [28] guarantees that for each initial value $x_0 \in \mathbb{R}^{n_x}$, each initial time $t_0 \in \mathbb{R}$ and each locally Lebesgue integrable control function $v : \mathbb{R} \to \mathbb{R}^{n_u}$, equation (2.3) has a unique solution $x(t)$ with $x(t_0) = x_0$ defined for every time t contained in some open interval $I \subseteq \mathbb{R}$ with $t_0 \in I$. This solution can be denoted by $x^*(t, t_0, x_0, v)$ to account for all this information.

The notion behind the sampling approach is to define a discrete time system of the form (2.1) such that the trajectories of this discrete time system and the continuous time system concur at some predefined sampling times

$$t_0 < t_1 < t_2 < \ldots < t_N,$$

which split the time domain $[t_I, t_F]$ into N smaller subintervals $[t_n, t_{n+1}]$. Therefore, for appropriately chosen discrete time control $u(\cdot)$ and continuous time control function $v(\cdot)$, it holds

$$x^*(t, t_0, x_0, v) = x_u(n, x_0), \quad n = 0, 1, 2, \ldots, N.$$

In this way, the nominal closed-loop system (2.2) corresponds to the closed-loop sampled data system

$$x^+ = f_C(x(t), \mu_{\mathcal{L}}(x(t_n))(t - t_n)), \quad t \in [t_n, t_{n+1}), n = 0, 1, 2, \ldots, N-1,$$

with solution $x^*(t, t_0, x_0, \mu_{\mathcal{L}})$ at initial value $x_0 \in X$. Note that the term $(t - t_n)$ can be omitted in the case of constant control function $\mu_{\mathcal{L}}(x(t_n))$.

One of the main advantages of MPC is its capability to straightforwardly deal with nonlinear systems, being herein referred to as Nonlinear Model Predictive Control (NMPC). MPC can handle nonlinearities in an efficient way since they can directly be included in the right side of equation (2.3). MPC for linear systems became prominent in control engineering in the late 1970s [29], [30]. Not long after, many of the MPC techniques devised for linear systems [31], [32] showed to be useful for NMPC in the 1980s for both discrete time problems [33] and continuous time problems [34],[35].

The basic idea underlying the NMPC approach, which will be explained in more detail in the next section, is as follows: at each sampling instant n the predicted future behavior of the system over a finite time horizon $k = 0, 1, \ldots, N-1$ of length $N \geq 2$ is optimized and the first element of the resulting optimal control sequence is used as a feedback control value for the next sampling interval.

2.1.3 The Basic Nonlinear Model Predictive Control Algorithm

Following the ideas presented in the previous sections, a description of a standard unconstrained implementation of the NMPC algorithm is sketched below:

At each sampling time t_n, $n = 0, 1, 2 \ldots, N-1$,

(i) Measure the state $x(n) \in X$ of the system.

(ii) Set $x_0 = x(n)$ and solve the optimal control problem (OCP)

$$\min J_N(n, x_0, u(\cdot)) = \sum_{k=0}^{N-1} l(n + k, x_u(k, x_0), u(k)) \tag{2.4a}$$

$$\text{with respecto to } u(\cdot) \in \mathcal{U} \quad \text{and subject to} \tag{2.4b}$$

$$x_u(0, x_0) = x_0, \quad x_u(k+1, x_0) = f_C(x_u(k, x_0), u(k)) \tag{2.4c}$$

The obtained optimal control sequence is denoted by $u^*(\cdot) \in \mathcal{U}$.

(iii) Define the NMPC feedback value $\mu_{\mathcal{L}}^N(x(n)) = u^*(0) \in \mathcal{U}$ and use it in the next sampling time.

Note that in this sketch of the NMPC algorithm only the first element $u^*(0)$ of the corresponding minimizing control sequence is used in each step, so that the remaining terms $u^*(1), u^*(2), \ldots, u^*(N-1)$ are neglected. Since some numerical optimization algorithms for solving (2.4) usually work iteratively, these discarded terms can play an

important role in the implementation of the iterative procedure so that the minimizing sequence from a previous time step can be efficiently used to construct a good initial guess for the next time step. Note also that, if $l(\cdot)$ does not depend on n then algorithm, a particularized version of the algorithm (2.4) for the constant reference trajectory case is obtained.

2.1.4 The Constrained Nonlinear Model Predictive Control Algorithm

A key advantage of NMPC (and MPC in general) is its capability to straightforwardly take constraints into account. Constraints on both the control and the state can be considered introducing a nonempty state constraint set $\mathcal{X}_C \subset \mathcal{X}$ and, for each $x \in \mathcal{X}_C$, introducing a nonempty control constraint set $\mathcal{U}_C(x) \subset \mathcal{U}$, so that the trajectories must lie in $\mathcal{X}_C$ and the corresponding control values must lie in $\mathcal{U}_C(x)$. Note that $\mathcal{X}_C$ can be chosen independent of x.

NMPC can handle constraints in an efficient way since they can directly be included into the algorithm described in Section 2.1.3. Furthermore, a constrained version of algorithm (2.4) can be straightforward obtained replacing set $\mathcal{U}$ by a set $\mathcal{U}_C^N(x_0)$ in step (ii) of the the algorithm in order to formulate the corresponding optimization problem with state dependent control value set and constraints represented by $\mathcal{U}_C^N(x_0)$, that is, a sampled version of $\mathcal{U}_C(x)$. Note that for practical implementations of optimization algorithms for solving (2.4), constraints are not specified by means of sets $\mathcal{X}_C$ and $\mathcal{U}_C(x)$. In most approaches equality and inequality constraints in order to specify $\mathcal{X}_C$ and $\mathcal{U}_C(x)$ are considered. This is the case of this dissertation as explained in the next section.

2.2 Statement of the Open-Loop Optimal Control Problem

In the multi-aircraft online trajectory planning problem studied in this paper, the motion of each aircraft has been modeled with a set of differential-algebraic equations

$$\Sigma^p = \{f^p : \mathcal{X}^p \times \mathcal{U}^p \times \mathbb{R}^{n_s^p} \to \mathbb{R}^{n_x^p},\ g^p : \mathcal{X}^p \times \mathcal{U}^p \times \mathbb{R}^{n_s^p} \to \mathbb{R}^{n_z^p}\}$$

$p = 1, 2, \ldots, N_p$, where f^p describes the right-hand side of the differential equation

$$\dot{x}^p(t) = f^p(x^p(t), u^p(t), s^p)$$

and g^p describes the algebraic constraints

$$0 = g^p(x^p(t), u^p(t), s^p)$$

where $\mathcal{X}^p \subseteq \mathbb{R}^{n_x^p}$ and $\mathcal{U}^p \subseteq \mathbb{R}^{n_u^p}$ are the state and control sets, respectively, $x^p(t) \in \mathbb{R}^{n_x^p}$ is a n_x^p-dimensional state variable, $u^p(t) \in \mathbb{R}^{n_u^p}$ is a n_u^p-dimensional control input, and $s^p \in \mathbb{R}^{n_s^p}$ is a vector of parameters.

The OLOCP employed within the NMPC scheme is a multi-aircraft trajectory optimization problem which involves the optimization of a specified performance index

under operational and flight envelope constraints. It has been formulated as an optimal control problem of a set of dynamic systems, in which the goal is to find the control inputs and the corresponding trajectories that steer the state of the systems between two configurations, satisfying a set of constraints on the state and/or control variables while minimizing the objective functional.

Therefore, the OLOCP considered in this work can be stated as follows:

$$\begin{aligned}
&\min J(x(t), u(t), s, t) \\
&= \sum_{p=1}^{N_p} \Phi(t_F^p, x^p(t_F^p)) + \sum_{p=1}^{N_p} \int_{t_I^p}^{t_F^p} L^p(x^p(t), u^p(t), s^p, t)dt && \text{(2.5a)} \\
&\text{Subject to:} \\
&\dot{x}(t) = f(x(t), u(t), s, t) && \text{(2.5b)} \\
&0 = g(x(t), u(t), s, t) && \text{(2.5c)} \\
&\phi_l \leq \phi(x(t), u(t), s, t) \leq \phi_u && \text{(2.5d)} \\
&x(t_I) = x_I && \text{(2.5e)} \\
&\psi(x(t_F)) = 0 && \text{(2.5f)}
\end{aligned}$$

where

$$x = [x^1, x^2, \ldots, x^{N_p}]^T, u = [u^1, u^2, \ldots, u^{N_p}]^T, s = [s^1, s^2, \ldots, s^{N_p}]^T$$

and t_F^p denote de final time for aircraft $p = 1, 2, \ldots, N_p$. The objective functional

$$J : \mathbb{R}^{n_x} \times \mathbb{R}^{n_u} \times \mathbb{R}^{n_s} \times [t_I, t_F] \to \mathbb{R}$$

is given in Bolza form. It is expressed as a combination of a Mayer term

$$\sum_{p=1}^{N_p} \Phi(t_F^p, x^p(t_F^p))$$

and a Lagrange term

$$\sum_{p=1}^{N_p} \int_{t_I^p}^{t_F^p} L^p(x^p(t), u^p(t), s^p, t)dt$$

Functions

$$\Phi^p : [t_I^p, t_F^p] \times \mathbb{R}^{n_x^p} \to \mathbb{R} \quad \text{and} \quad L^p : \mathbb{R}^{n_x^p} \times \mathbb{R}^{n_u^p} \times \mathbb{R}^{n_z^p} \times [t_I^p, t_F^p] \to \mathbb{R}$$

are assumed to be twice differentiable. Function f is assumed to be piecewise Lipschitz continuous within the time interval $[t_I, t_F]$, and the derivative of the algebraic right-hand side function g with respect to z, that is,

$$\frac{\partial g}{\partial z} \in \mathbb{R}^{n_z \times n_z}$$

is assumed to be regular within the time interval $[t_I, t_F]$. Vector $x_I \in \mathbb{R}^{n_x}$ represents the initial conditions given at the initial time t_I and function

$$\psi : \mathbb{R}^{n_x} \to \mathbb{R}^{n_\psi}$$

provides the terminal conditions at the final time t_F, and it is assumed to be twice differentiable. The system must also satisfy algebraic path constraints within the time interval $[t_I, t_F]$ given by the vector function

$$\phi : \mathbb{R}^{n_x} \times \mathbb{R}^{n_u} \times \mathbb{R}^{n_s} \times [t_I, t_F] \to \mathbb{R}^{n_\phi}$$

with lower bound $\phi_l \in \mathbb{R}^{n_\phi}$ and upper bound $\phi_u \in \mathbb{R}^{n_\phi}$. Function ϕ is assumed to be twice differentiable.

In the objective functional (2.5a), the Lagrange term represents a running cost, whereas the Mayer terms represent a terminal cost. A usual Lagrange objective functional is to minimize the total amount of energy during the maneuver. A typical Mayer objective functional is to minimize the final time. Equations (2.5b) and (2.5c) represent the set of differential-algebraic equations that governs the motion of the dynamical systems. Equation (2.5d) models the performance limitations of the dynamical systems, typically expressed as upper and lower bounds on both states and control variables. Equations (2.5e) and (2.5f) denote the boundary (initial and final, respectively) conditions of the systems. Note that equations (2.5c) and (2.5d) also include logical constraints that model storm avoidance and operational constraints, as described in Sec. 3.2, which are of special interest for the problem studied in this paper.

Hence, the OLOCP 2.5 consists in finding an admissible control $u^*(t)$ such that the set of differential-algebraic subsystems follows an admissible trajectory $(x^*(t), u^*(t), s^*)$ between the initial and final state that minimizes the performance index $J(t, x(t), u(t), s, t)$. The final times, t_F^p, may be fixed or free.

2.3 Hermite-Simpson Direct Collocation Transcription of the Open-Loop Optimal Control Problem

A direct numerical method has been employed to transcribe the OLOCP into a Nonlinear Programming (NLP) problem. More specifically, a Hermite-Simpson direct collocation method [36] has been used. The Hermite-Simpson collocation method is a particular case of a family of direct transcription methods known as Hermite-Legendre-Gauss-Lobatto methods [37].

For the sake of simplicity, in this section a simplified unconstrained version of problem 2.5 has been considered, following [38]:

$$\min J(x(t), u(t), t) = \Phi(t_F, x(t_F)) + \int_{t_I}^{t_F} L(x(t), u(t))dt \tag{2.6a}$$

subject to:

$$\dot{x}(t) = f(x(t), u(t), t) \tag{2.6b}$$

$$x(t_I) = x_I \tag{2.6c}$$

$$x(t_F) = x_F \tag{2.6d}$$

where the initial conditions $x(t_I) = x_I$ are given at the fixed initial time t_I, and the final time t_F is also fixed. The symbols J, Φ, L, f, t, x, u have an analogous meaning to those of problem 2.5. The vector of parameters s has not been considered.

As shown in Figure 2.1, for the transcription of problem (2.6) the time domain $[t_I, t_F]$ has been split into N smaller subintervals

$$t_I = t_0 < t_1 < \ldots < t_{N-1} < t_N = t_F. \tag{2.7}$$

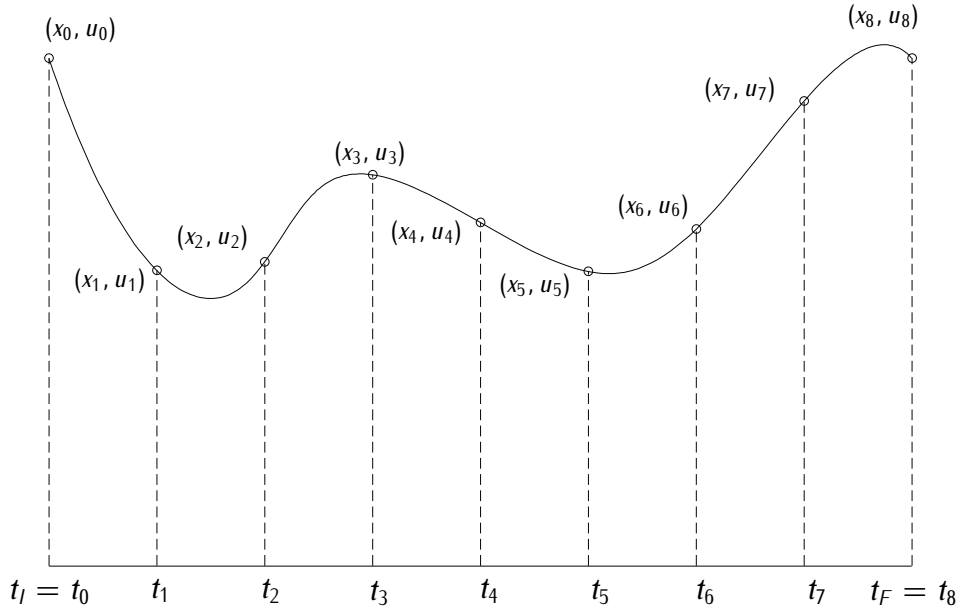

Figure 2.1: Time domain discretization with $N = 8$ subintervals.

In each time subinterval $[t_i, t_{i+1}]$, $x_i = x(t_i)$ and $u_i = u(t_i)$ are the values of the state and controls variables at the grid point t_i, respectively, and $h_i = \frac{t_F - t_I}{N}$ is the integration step size for step i, $i = 0, 1 \ldots, N-1$. Thus, the independent variables of the resulting NLP are

$$\{x_0, u_0, x_1, u_1, \ldots, x_N, u_N\},$$

together with other independent variables according to the integration rule and the control scheme employed. For instance, the values of both state and control at collocation points such as the center point of the subintervals $x_{i,C}$ and $u_{i,C}$ can be included.

Then, the ordinary differential equation (2.6b) is replaced by a finite number of equality constraints known as defect equations, that can be written in a general form as

$$c_i(x_i, x_{i+1}, u_i, u_{i+1}, x_{i,C}, u_{i,C}) = 0,\ i = 0, \ldots, N-1. \tag{2.8}$$

Each integration scheme leads to a different formulation of this set of transcribed constraints. In particular, the Hermite-Simpson method is based on the well-known Simpson's rule which can be used to numerically integrate a simplified form of differential equation (2.6b), that is, $\frac{dx}{dt} = f(t)$. The value of the integral of $f(t)$ over the subinterval $[t_i, t_{i+1}]$ using Simpson's rule is obtained by

$$\int_{t_i}^{t_{i+1}} f(t)dt \approx \frac{h_i}{6}[f(t_i) + 4f(t_{i,C}) + f(t_{i+1})], \tag{2.9}$$

with $h_i = (t_{i+1} - t_i)$, where the integrand is approximated using a quadratic polynomial which depends on the values of the integrand at the endpoints of the subinterval $[t_i, t_{i+1}]$ and at the midpoint $t_{i,C} = \frac{t_{i+1}+t_i}{2}$ of this subinterval. These points are known as collocation points.

Simpson's rule belong to the so called Gauss-Lobatto family of integration rules in which the degree of the integrated polynomial coincides with the number of discrete value of the integrand used to generate the interpolating polynomial. Thus, Simpson's rule is the third-degree Gauss-Lobatto integration rule.

2.3.1 Local and Global Truncation Errors

Usually, for the assessment of numerical integration methods, two kinds of truncation errors are considered which are known as local truncation error and global truncation error.

On the one hand, the local truncation represents the error in the approximate integration over a subinterval $[t_i, t_{i+1}]$ and it is a function of the subinterval length h_i to an integer power. This power should be as large as possible if a low local error is searched. Within the integration scheme a polynomial in time $p_m(t)$ of order m is constructed by choosing the coefficients associated with each term so that the resulting polynomial evaluates the integrand $f(t)$ at selected points in the subinterval $[t_i, t_{i+1}]$. Thus, the integration of $p_m(t)$ is an approximation of the integral of the function $f(t)$. Let the error in the integral of $p_m(t)$ over the subinterval $[t_i, t_{i+1}]$ be defined by

$$\varepsilon(f) = \int_{t_i}^{t_{i+1}} f(t)dt - \int_{t_i}^{t_{i+1}} p_m(t)dt.$$

Expression $\varepsilon(f)$ is called the local truncation error. In particular, the local truncation error for the Simpson's rule is proportional to h_i^5. This means that as h_i is reduced, the local truncation error of the Simpson's rule improves with a power of 5.

On the other hand, the global truncation error results from using a method to integrate a function over an interval that has been divided into a finite number of subintervals. Thus, the global truncation error results from the accumulation of local truncation errors. The order of accuracy of the approximation is that power of the step size h_i to which the truncation error is proportional. If the numerical method is employed only over one subinterval, the order of accuracy will be related to the local truncation error. Most commonly, as it is in our case, the numerical method will be employed over a finite number of subintervals, and thus the order of accuracy will be related to the global truncation error. Because the step size and the number of local truncation error values to be summed up are both proportional to the number of subintervals, the global truncation error is of order one less than the local truncation error. Therefore, the order of accuracy for the Simpson's rules is proportional to 4.

When analyzing the effectiveness of a numerical method to approximate a solution, the order of accuracy is one of the most important measures. The greater is the order of accuracy, the greater is the reduction in error if the step size is made smaller. Therefore, as the order of accuracy increases, a specified accuracy may be achieved with larger step sizes. However, in practice, it is necessary to seek an appropriate trade off between the number of subintervals for the discretization and the integration rule in order to achieve a determined accuracy while avoiding overfitting. The relatively high order of accuracy and the simplicity of the Simpson's rule makes it very efficient to be used in direct transcription methods for optimal control problems.

2.3.2 Collocation Points Determination

The collocation points used to formulate an integration rule must be chosen to increase the order of accuracy of the resulting integration rule to the highest order possible. In the case of the Gauss-Lobatto family integration rules the collocation points that maximize the power of h_i in the local truncation error are the roots of the corresponding Jacobi polynomials [39], which are the set of polynomials that are orthogonal on the interval $[-1, 1]$ with respect to the weight function $\mathcal{W} = (1-s)^{\alpha}(1+s)^{\beta}$. In particular, for the Gauss-Lobatto rules, $\alpha = \beta = 1$. Note that a subinterval with endpoints $[t_i, t_{i+1}]$ can be transformed to the interval $[-1, 1]$ using the relation $s = 2(t - t_i)/h_i - 1$. The interpolating polynomial can be calculated by interpolating $f(t)$ at the endpoints of the interval $[-1, 1]$ and at the zeros of the corresponding Jacobi polynomial.

In terms of this framework, Simpson's rule described in equation (2.9) is the third-degree Gauss-Lobatto integration rule and when it is applied to the differential equation $\frac{dx}{dt} = f(x)$, it is formulated considering a quadratic approximation of the integrand, and thus the state as a function of time $x(t)$ must be approximated by a cubic polynomial. Moreover, the polynomial used to interpolate $f(x)$ at the endpoints and center points of the subinterval is obtained as an integration of this cubic polynomial. In this

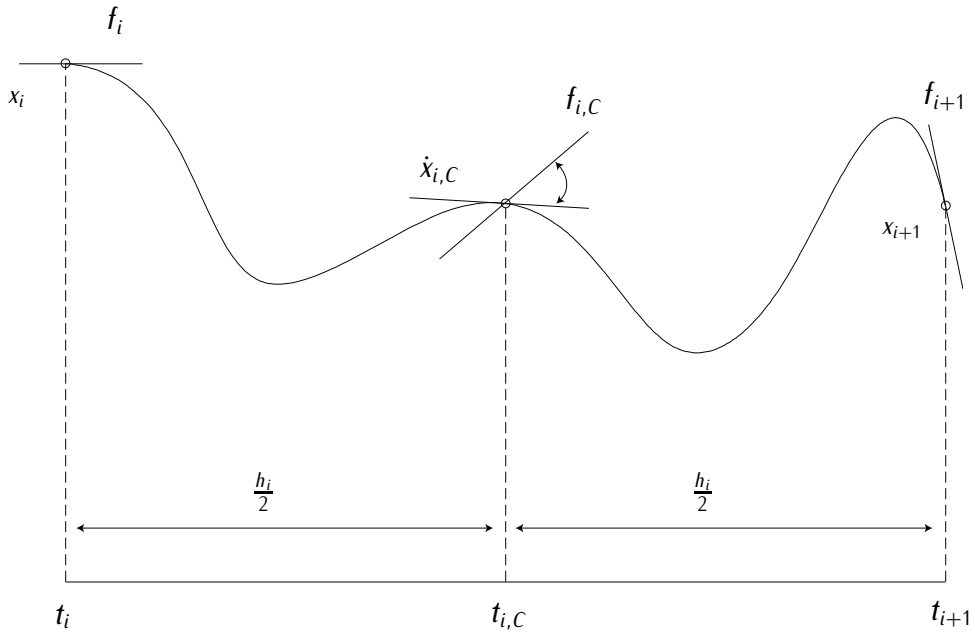

Figure 2.2: Hermite-Simson collocation scheme.

case, parameters representing the state at the endpoints x_i and x_{i+1} are used to formulate a constraint. Knowing the four peaces of information x_i, x_{i+1}, $f_i = f(x_i)$ and $f_{i+1} = f(x_{i+1})$, a Hermite-cubic polynomial representing the state $x(t)$ between the endpoint times t_i and t_{i+1} can be constructed such as both the values and first derivatives of the interpolant polynomial coincide with the values and first derivatives of function $f(x)$ at the extremes of the subinterval, as illustrated in Figure 2.2

Such polynomial is used to generate an internal collocation point $x_{i,C}$ per subinterval, whose numerical expression is

$$x_{i,C} = \frac{1}{2}(x_i + x_{i+1}) + \frac{h_i}{8}(f(x_i) - f(x_{i+1})), \tag{2.10}$$

where $x_{i,C}$ is a discrete approximation for $x(t)$ at $t_{i,C} = \frac{t_i + t_{i+1}}{2}$ and $i = 0, 1 \ldots, N-1$. The Simpson's system constraint is then formulated using $x_{i,C}$ to evaluate the system equation resulting in a discrete value at center point of the subinterval $f_{i,C} = f(x_{i,C})$. Then, by enforcing $f_{i,C}$ to be equal to the first time derivative of the Hermite-cubic interpolant polynomial at the center point of the subinterval, i.e., $\dot{x}_{i,C} = f_{i,C}$, one defect equation per subinterval is generated:

$$c_i(x_i, x_{i+1}) = x_i - x_{i+1} + \frac{h_i}{6}(f(x_i) + 4f(x_{i,C}) + f(x_{i+1})) = 0, \tag{2.11}$$

with $i = 0, 1 \ldots, N-1$. These constraints are known as Hermite-Simpson defect constraints [36].

For more details about the Hermite-Legendre-Gauss-Lobatto collocation schemes the reader is referred to [40, Chap. 4].

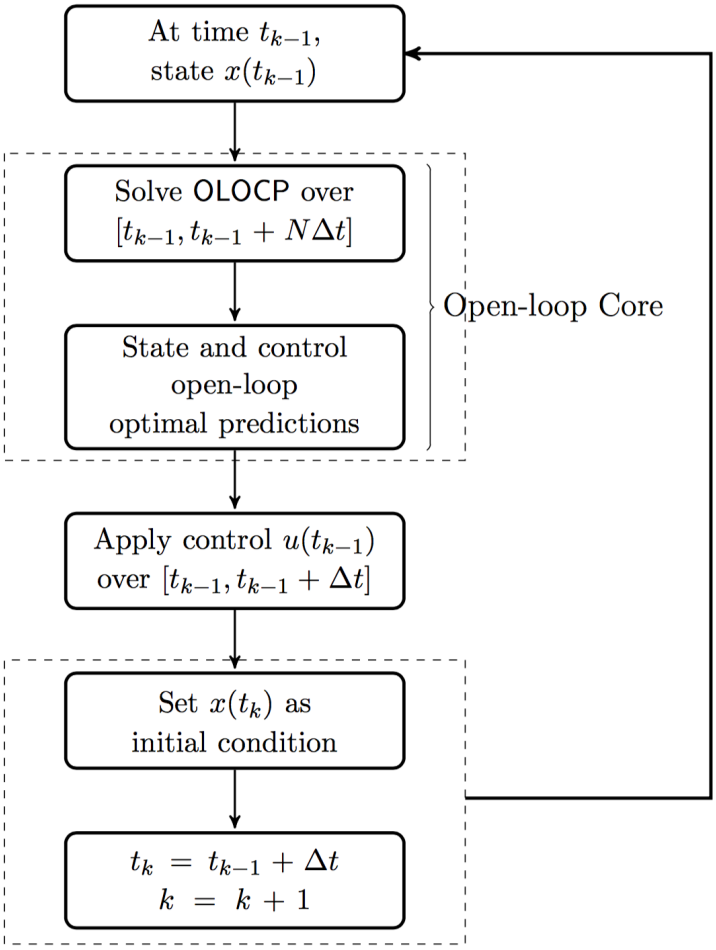

Figure 2.3: Flow diagram for the NMPC approach

2.4 Practical Implementation of the Closed-Loop Optimal Control

As pointed out in [41] the considered NMPC approach for the aircraft trajectories tracking can be viewed as an iterative decision-making process in which the decision made in each iteration is based on a suitable OLOCP Thus, the NMPC approach provides a kind of feedback control that accounts for the mismatch between actual states and previously assumed optimal states. As illustrated in Fig. 2.3, at each state and time instance, a OLOCP is solved, and the control is set to be equal to the first

term of the related optimal sequence of control actions.

Due to the time domain partition described in (2.7), the time interval $[t_I, t_F]$ is subdivided into N subintervals of equal length, Δt, whose endpoints are

$$\{t_0, t_1, \ldots, t_N\} \tag{2.12}$$

with $t_0 = t_I$ and $t_N = t_F$. In each subinterval $[t_i, t_{i+1}]$, $i = 0, \ldots, N-1$, the Hermite-Simpson numerical integration scheme is used. The set of constraints of the resulting NLP problem includes the Hermite-Simpson system constraints that correspond to the differential constraint (2.5b) and the discretized versions of the other constraints of the optimal control problem. They include the algebraic constraints (2.5c), the state and control envelope constraints (2.5d), and the boundary conditions (2.5e) and (2.5f). The unknowns of the NLP problem are the values of the state and the control variables at the endpoints of each subinterval $[t_i, t_{i+1}]$, $i = 0, \ldots, N-1$.

The practical implementation of the OLOCP described in Sec. 2.2 employed within a NMPC closed-loop scheme, whose practical implementation is sketched in Figure 2.3, can be summarized as follows:

(i) Consider the interval length Δt and the horizon length N, and set $k = 1$.

(ii) Solve the OLOCP 2.5 over the horizon $[t_{k-1}, t_{k-1} + N\Delta t]$ with initial state $x(t_{k-1})$ and obtain the control sequence $\{u(t_k), u(t_{k+1}), \ldots, u(t_{k+N})\}$.

(iii) Apply the control input $u(t_{k-1})$ for the time interval $[t_{k-1}, t_{k-1} + \Delta t]$ to the system in order to compute $x(t_k)$, and set $x(t_k)$ as the initial condition for the next iteration of the NMPC scheme.

(iv) Set $t_k = t_{k-1} + \Delta t$ and $k = k + 1$, and repeat steps (ii) and (iii) until the target is reached.

As a consequence, the closed-loop procedure $(i) - (iv)$ generates a sequence of NLP problems. To solve the resulting series of NLP problems, the open source IPOPT solver [42] has been employed. It implements an interior point line search filter method and it is able handle properly large-scale sparse nonconvex NLP problems, with a large number of equality and inequality constraints. Source and binary files are available at the Computational Infrastructure for Operations Research (COIN-OR) web site[1].

[1] https://www.coin-or.org/

3

Problem Modelling

In this chapter, the models used to solve the multi-aircraft trajectory planning problem proposed in this work are presented. Due to the intrinsic features of the problem, continuos phenomena, discrete phenomena, and decision-making processes have been considered. First, the continuos part of the model is described, that is, the aircraft equations of motion based on a three degrees of freedom model, together with the the aircraft performance limitations. Then, the general framework, based on embedded control techniques, devised to tackled the discrete aspects of the model by means of logical constraints in disjunctive form, has been set. Finally, the application of this technique to modelling time-based and distance-based separation constraints, obstacles or storms avoidance, passage through waypoints, and decision making processes, is explained in detail.

3.1 Aircraft Model Description

3.1.1 Equations of Motion

The aircraft dynamics has been represented using a common three-degree-of-freedom dynamic model, which describes the point variable-mass motion of the aircraft over a spherical Earth model. In particular, a symmetric flight has been considered. Thus, it has been assumed that there is no sideslip and all forces lie in the plane of symmetry of the aircraft. The following equations of motion of the aircraft has been considered:

$$\begin{aligned}
\dot{V}(t) &= \frac{T(t) - D(h_e(t), V(t), C_L(t)) - m(t) \cdot g \cdot \sin\gamma(t)}{m(t)}, \\
\dot{\chi}(t) &= \frac{L(h_e(t), V(t), C_L(t)) \cdot \sin\mu(t)}{m(t) \cdot V(t) \cdot \cos\gamma(t)}, \\
\dot{\gamma}(t) &= \frac{L(h_e(t), V(t), C_L(t)) \cdot \cos\mu(t) - m(t) \cdot g \cdot \cos\gamma(t)}{m(t) \cdot V(t)}, \\
\dot{\lambda_e}(t) &= \frac{V(t) \cdot \cos\gamma(t) \cdot \cos\chi(t) + V_{wind\lambda_e}}{R \cdot \cos\theta_e(t)}, \\
\dot{\theta_e}(t) &= \frac{V(t) \cdot \cos\gamma(t) \cdot \sin\chi(t) + V_{wind\theta_e}}{R}, \\
\dot{h_e}(t) &= V(t) \cdot \sin\gamma(t), \\
\dot{m}(t) &= -T(t) \cdot \eta(V(t)).
\end{aligned} \tag{3.1}$$

The three dynamic equations in (3.1) are expressed in an aircraft-attached reference frame (x_w, y_w, z_w) and the three kinematic equations are expressed in a ground based reference frame (x_e, y_e, z_e) as shown in Fig. 3.1.

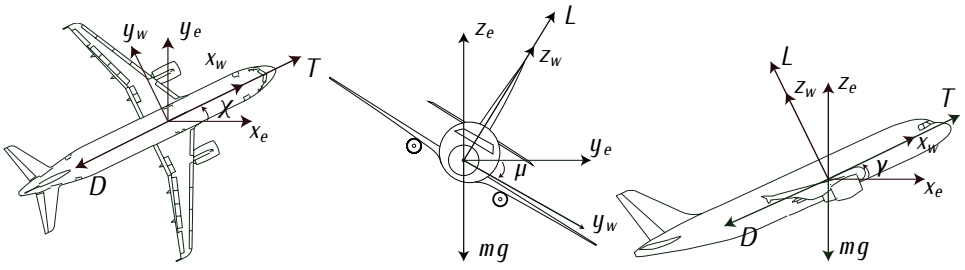

(a) Top view (b) Front view (c) Lateral view

Figure 3.1: Aircraft state and forces

The state variables of the system (3.1) are $V, \chi, \gamma, \lambda_e, \theta_e, h_e$ and m. Thus, $x(t) = (V(t), \chi(t), \gamma(t), \lambda_e(t), \theta_e(t), h_e(t), m(t))$. The state variables V, χ and γ are the true airspeed, the heading angle, and the flight path angle, respectively. The state

variables λ_e, θ_e and h_e are the 3D position, the longitude, the latitude and the altitude, respectively. The components of the aircraft position vector in two dimensions, (x_e, y_e), are approximated as $x_e = \lambda_e \cdot (R + h_e) \cdot \cos\theta_e$ and $y_e = \theta_e \cdot (R + h_e)$, respectively. Finally, the state variable m is the aircraft mass. The controls inputs of the system (3.1) are the bank angle μ, the engine thrust T, and the lift coefficient C_L. Thus, $u(t) = (T(t), \mu(t), C_L(t))$. The parameter R is the radius of the Earth, η is the speed-dependent fuel efficiency coefficient, and $V_{wind\lambda_e}$ and $V_{wind\theta_e}$ are the wind speed in the λ_e and θ_e components, respectively. Lift, $L = C_L S\hat{q}$, and drag, $D = C_D S\hat{q}$, are the components of the aerodynamic force. The parameter S is the reference wing surface area and $\hat{q} = \frac{1}{2}\rho V^2$ is the dynamic pressure. A parabolic drag polar $C_D = C_{D0} + KC_L^2$, and an International Standard Atmosphere (ISA) model are assumed. The lift coefficient C_L is a known function of the angle of attack α and the Mach number.

Note that differential equations (3.1) correspond to differential equation (2.5b) in the continuous OLOPC stated in Sec. 2.2.

3.1.2 Flight Envelope

The flight envelope constraints are derived from the geometry of the aircraft, the structural limitations, the engine power, and from the aerodynamic characteristics. The performance limitations model and the parameters have been obtained from the Base of Aircraft Data (BADA), version 3.14 [11]:

$$\begin{aligned} 0 \le h_e(t) \le \min[h_{M0}, h_u(t)], \quad & \gamma_{min} \le \gamma(t) \le \gamma_{max}, \\ M(t) \le M_{M0}, \quad & m_{min} \le m(t) \le m_{max}, \\ \dot{V}(t) \le \bar{a}_l, \quad & C_v V_s(t) \le V(t) \le V_{Mo}, \\ \dot{\gamma}(t)V(t) \le \bar{a}_n, \quad & 0.1 \le C_L(t) \le C_{L_{max}}, \\ \mu(t) \le \bar{\mu}, \quad & T_{min}(t) \le T(t) \le T_{max}(t). \end{aligned} \tag{3.2}$$

In (3.2), h_{M0} is the maximum reachable altitude and $h_u(t)$ is the maximum operative altitude at a given mass (it increases as fuel is burned). $M(t)$ is the Mach number and M_{M_0} is the maximum operating Mach number. C_v is the minimum speed coefficient, $V_s(t)$ is the stall speed, V_{M_0} is the maximum operating Calibrated Airspeed (CAS) and $\bar{a}_n$ and $\bar{a}_l$ are, respectively, the maximum normal and longitudinal accelerations for civilian aircraft. Finally, $T_{min}(t)$ and $T_{max}(t)$ correspond to the minimum and maximum available thrust, respectively, and $\bar{\mu}$ corresponds to the maximum bank angle due to structural limitations.

Note that inequality constraints (3.2) correspond to inequality (2.5d) of the continuous OLOPC stated in Sec. 2.2.

3.2 Logical Constraints Modelling

In this section, the method employed to model logical constraints in disjunctive form in the OLOCP without using binary variables will be described, in which the approach proposed in [15] has been followed. In this way a smooth formulation of the OLOCP is obtained and the inherent combinatorial complexity in solving a series of mixed integer NLP problems within a NMPC scheme is avoided. As said before, logical constraints in disjunctive form arise in modelling storm avoidance and operational constraints but also in modelling general decision making processes during flight.

It was shown in [43] that every Boolean expression can be transformed in Conjunctive Normal Form (CNF). Therefore, it has been assumed that any logical constraint considered in this paper can be written as a CNF expression

$$Q_1 \wedge Q_2 \wedge \ldots \wedge Q_n, \tag{3.3}$$

where

$$Q_i = P_i^1 \vee P_i^2 \vee \ldots \vee P_i^{m_i} \tag{3.4}$$

is in disjunctive form, in which only one of the propositions must be satisfied and the proposition P_i^j is either X_i^j or $\neg X_i^j$. The term X_i^j is a literal that can be either True or False and $\neg$ represents the negation or logical complement operator. The term X_i^j is used to represent statements such as "longitude $\lambda_e \leq 40$ deg". Therefore, P_i^j takes the form

$$P_i^j \equiv \{g_i^j(x(t)) \leq 0\}, \tag{3.5}$$

where $g_i^j : \mathbb{R}^{n_x} \to \mathbb{R}$ is assumed to be a $\mathcal{C}^1$ function. To include the logical constraint (3.3) into a smooth optimal control problem formulation, they must be converted into a set of equality or inequality constraints in which binary variables are not employed. Transcribing the conjunction in (3.3) is straightforward since it is equivalent to the following expression

$$\forall i \in \{1, 2, \ldots, n\} : \quad Q_i. \tag{3.6}$$

Thus, taking into account (3.4), the logical expression (3.3) can be represented as

$$\forall i \in \{1, 2, \ldots, n\} : \quad P_i^1 \vee P_i^2 \vee \ldots \vee P_i^{m_i}. \tag{3.7}$$

To describe these disjunctions in into a set of equality and inequality constraints, a continuos variable $\beta_i^j \in [0, 1]$ has been defined and related to each P_i^j in (3.5). Thus, (3.7) can be expressed as

$$\begin{aligned} \forall i \in \{1, 2, \ldots, n\} : \quad & \beta_i^j \cdot g_i^j(x(t)) \leq 0 \\ \text{and} \quad & 0 \leq \beta_i^j \leq 1 \\ \text{and} \quad & \sum_{j=1}^{m_i} \beta_i^j = 1. \end{aligned} \tag{3.8}$$

It is easy to see that if $\beta_i^j = 0$ in the first term in (3.8), then the constraint $g_i^j(x(t)) \leq 0$ is not fulfilled. On the other hand, if $0 < \beta_i^j \leq 1$ then $\beta_i^j \cdot g_i^j(x(t)) \leq 0$ is in fact $g_i^j(x(t)) \leq 0$, and thus constraint $g_i^j(x(t)) \leq 0$ is enforced. Finally, the last term in (3.8) guarantees that at least one of the propositions P_i^j holds.

Note that, as expected, equality and inequality constraints in (3.8) take the form of constraints (2.5c) and (2.5d) of the OLOPC stated in Sec. 2.2, respectively. In the following sections, the application of this technique to model logical constraints in disjunctive form relevant to the problem studied in this paper will be presented.

3.2.1 Time-Based Separation Between Aircraft

One of the problems of most interest in ATM is the conflict detection and resolution problem [44]. Two different instances of this problem will be presented in this section and in the next one. In this first instance, a collision avoidance problem among different aircraft along routes converging at the same waypoint has been considered, in which a safety time-based separation at the merging waypoint is guaranteed.

Let t_{p_F} and t_{q_F} be the unfixed arrival time at the merging waypoint of aircraft p and q, respectively, and let d_t be the safety time difference between these two consecutive aircraft. Taking into account the discretization (2.12), $t_{p_F} = t_{p_N}$ and $t_{q_F} = t_{q_N}$, and the multi-aircraft time-based separation constraints can be expressed as

$$\forall q > p: \qquad |t_{p_N} - t_{q_N}| \geq d_t, \tag{3.9}$$

where the condition $q > p$ prevents unnecessary duplication of constraints. Constraints (3.9) can be rewritten as

$$\begin{aligned} \forall q > p: \qquad & t_{p_N} - t_{q_N} \geq d_t \\ \text{or} \qquad & t_{q_N} - t_{p_N} \geq d_t. \end{aligned} \tag{3.10}$$

Following the technique described above to tackle constraints in disjunctive form, the new variables $\delta_{p_N,q_N}^1, \delta_{p_N,q_N}^2 \in [0,1]$ satisfying condition

$$\delta_{p_N,q_N}^1 + \delta_{p_N,q_N}^2 = 1,$$

must be defined. Eq. (3.10) can thus be transformed into

$$\begin{aligned} \forall q > p: \qquad & \delta_{p_N,q_N}^1 (t_{p_N} - t_{q_N} - d_t) \geq 0 \\ \text{and} \qquad & \delta_{p_N,q_N}^2 (t_{q_N} - t_{p_N} - d_t) \geq 0 \\ \text{and} \qquad & 0 \leq \delta_{p_N,q_N}^j \leq 1, j = 1,2 \\ \text{and} \qquad & \delta_{p_N,q_N}^1 + \delta_{p_N,q_N}^2 = 1. \end{aligned} \tag{3.11}$$

The last constraint in (3.11) ensures that at least one of the constraints in (3.10) is fulfilled, and therefore that the safety time-based separation between aircraft p and q is guaranteed.

3.2.2 Distance-Based Separation Between Aircraft

In this second instance, to model collision avoidance among different aircraft, at each endpoint of the subintervals of the discretization (2.12) and for every couple of aircraft, a safety distance-based separation is guaranteed in the horizontal or vertical directions, that is, $\lambda - \theta$ or h directions.

Let $(\lambda_{p_i}, \theta_{p_i}, h_{p_i})$ and $(\lambda_{q_i}, \theta_{q_i}, h_{q_i})$ be the positions of aircraft p and q at the endpoint t_i of the discretization, respectively. If the safety distance-based separation in the $\lambda - \theta$ and h directions are denoted by $d_{\lambda\theta}$ and d_h, respectively, then the distance-based separation constraints can be expressed as

$$\begin{aligned} \forall q > p, \forall i \in \{1, 2, \ldots, N\} : \quad & 2R \operatorname{atan2}\left(\sqrt{\zeta_i}, \sqrt{1-\zeta_i}\right) \geq d_{\lambda\theta} \\ \text{or} \quad & |h_{p_i} - h_{q_i}| \geq d_h \end{aligned} \tag{3.12}$$

where the haversine formula has been consider for the distance in the $\lambda - \theta$ direction with

$$\zeta_i = \sin^2\left(\frac{\theta_{q_i} - \theta_{p_i}}{2}\right) + \cos\theta_{p_i} \cos\theta_{q_i} \sin^2\left(\frac{\lambda_{q_i} - \lambda_{p_i}}{2}\right)$$

Condition $q > p$ again prevents unnecessary duplication of constraints and the set of constraints (3.12) can be rewritten as

$$\begin{aligned} \forall q > p, \forall i \in \{1, 2, \ldots, N\} : \quad & 2R \operatorname{atan2}\left(\sqrt{\zeta_i}, \sqrt{1-\zeta_i}\right) \geq d_{\lambda\theta} \\ \text{or} \quad & h_{p_i} - h_{q_i} \geq d_h \\ \text{or} \quad & h_{q_i} - h_{p_i} \geq d_h \end{aligned} \tag{3.13}$$

Again, following the technique described above, new variables $v^j_{p_i,q_i} \in [0,1]$ for $i = 1, 2, \ldots, N, j = 1, 2, 3$ satisfying condition

$$\sum_{j=1}^{3} v^j_{p_i,q_i} = 1,$$

are introduced, and Eq. (3.13) can be transformed into

$$\begin{aligned} \forall q > p, \forall i \in \{1, 2, \ldots, N\} : \quad & v^1_{p_i,q_i}\left(2R \operatorname{atan2}\left(\sqrt{\zeta_i}, \sqrt{1-\zeta_i}\right) - d_{\lambda\theta}\right) \geq 0 \\ \text{and} \quad & v^2_{p_i,q_i}(h_{p_i} - h_{q_i} - d_h) \geq 0 \\ \text{and} \quad & v^3_{p_i,q_i}(h_{q_i} - h_{p_i} - d_h) \geq 0 \\ \text{and} \quad & 0 \leq v^j_{p_i,q_i} \leq 1, j = 1, 2, 3 \\ \text{and} \quad & \sum_{j=1}^{3} v^j_{p_i,q_i} = 1 \end{aligned} \tag{3.14}$$

The last constraint in (3.14) ensures that at least one of the constraints in (3.13) is fulfilled, that is, aircraft p and q are guaranteed to be a safe distance apart. Moreover, since the approach employed to model logical constraint in disjunctive form is general, it allows any other distance-based separation model described in terms of Eq. (3.4) to be considered.

3.2.3 Obstacles Avoidance

In the third instance, an obstacle avoidance problem has been considered. Following [15], in which a set of stationary rectangular obstacles in a 2D environment were assumed, stationary obstacles in the three dimensional space have been enveloped by cuboids. This simple approach allows us to specify each cuboid by giving only the coordinates of two opposite corners as shown in Fig 3.4.

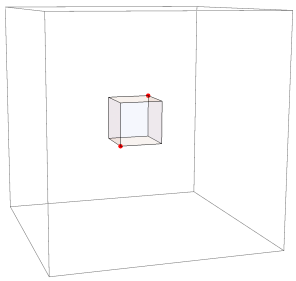

Figure 3.2: Two opposite corners of a cuboid in the 3D space.

Let $(\lambda_l, \theta_l, h_l)$ and $(\lambda_u, \theta_u, h_u)$ be the positions of opposite corners of the cuboid. Cuboid avoidance for a single aircraft involves that at every endpoint t_i of the subintervals of the discretization (2.12), the position of the aircraft $(\lambda_i, \theta_i, h_i)$ must remain outside it. In terms of logical constraints, this condition can be expressed as

$$\begin{aligned} \forall i \in \{1, 2, \ldots, N-1\}: \quad & \lambda_i - \lambda_l \leq 0 \\ \text{or} \quad & \lambda_u - \lambda_i \leq 0 \\ \text{or} \quad & \theta_i - \theta_l \leq 0 \\ \text{or} \quad & \theta_u - \theta_i \leq 0 \\ \text{or} \quad & h_i - h_l \leq 0 \\ \text{or} \quad & h_u - h_i \leq 0 \end{aligned} \tag{3.15}$$

Note that constraints (3.15) are not enforced at the initial and final points of the discretization, t_0 and t_N, since in practice both positions are fixed. Moreover, due to the nature of the collocation technique in Section 2.3, constraints are not enforced between the endpoints of the discretized differential system of equations. Therefore, small invasions into the cuboids might occur. A smaller discretization size implies a

larger intrusion, and viceversa. In practice, this drawback can be easily overcome by considering a sufficient safety margin in the modeling of the cuboids.

Following the same technique used in the previous sections, new variables $\xi_i^j \in [0,1]$ for $i = 1, 2, \ldots, N-1$, $j = 1, 2, \ldots, 6$ satisfying condition

$$\sum_{j=1}^{6} \xi_i^j = 1,$$

are introduced, and Eq. (3.15) can be transformed into

$$\begin{aligned} \forall i \in \{1, 2, \ldots, N-1\}: \quad & \xi_i^1(\lambda_i - \lambda_l) \leq 0 \\ \text{and} \quad & \xi_i^2(\lambda_u - \lambda_i) \leq 0 \\ \text{and} \quad & \xi_i^3(\theta_i - \theta_l) \leq 0 \\ \text{and} \quad & \xi_i^4(\theta_u - \theta_i) \leq 0 \\ \text{and} \quad & \xi_i^5(h_i - h_l) \leq 0 \\ \text{and} \quad & \xi_i^6(h_u - h_i) \leq 0 \\ \text{and} \quad & 0 \leq \xi_i^j \leq 1, j = 1, 2, \ldots, 6 \\ \text{and} \quad & \sum_{j=1}^{6} \xi_i^j = 1 \end{aligned} \tag{3.16}$$

Again, as mentioned above, the last constraint in (3.16) ensures that at least one of the constraints in (3.15) is fulfilled, which means that aircraft flies outside of the cuboid. Also note that this single-obstacle avoidance model for a single aircraft can be straightforwardly extended to multi-obstacle avoidance model for multiple aircraft. Moreover, as already pointed out in the previous section, since the approach employed to model logical constraint in disjunctive form is general, it allows any other obstacle model described in terms of Eq. (3.4) to be considered.

3.2.4 Storms Avoidance

As said before, each cell of the multi-cell storm has been represented by a moving and size-changing ellipsoid in the 3D space as shown in Fig. 3.3. This simple approach allows each cell of the storm to be specified by giving only the coordinates of one moving point in the 3D space. In this way, the storm avoidance problem is tackled like a moving obstacle avoidance problem in which, for each aircraft, a safety distance-based separation between the aircraft and the central point of the storm is guaranteed in the horizontal or vertical directions. Thus, the proposed approach to model storms avoidance consists of a mixture of the approaches presented in Sections 3.2.2 and 3.2.3.

Let $(\lambda_i, \theta_i, h_i)$ and $(\lambda_{C_i}, \theta_{C_i}, h_{C_i})$ be the positions of a single aircraft and the central point of a cell C of the storm at the endpoint t_i of the subintervals of the discretization (2.12) , respectively. Let the safety distance-based separation in the $\lambda - \theta$ and h

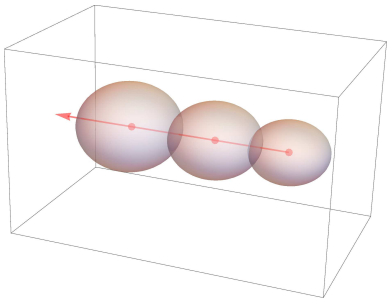

Figure 3.3: Moving and size-changing cell of a multi-cell storm representation in the 3D space.

directions at every endpoint t_i be denoted by $d_{\lambda\theta_i}$ and d_{h_i}, respectively. Note that changing the size of safety distances $d_{\lambda\theta_i}$ and d_{h_i} allows size-changing cells to be modelled. Then, the storm avoidance constraints can be expressed as the following moving obstacle avoidance constraints

$$\begin{aligned} \forall i \in \{1, 2, \ldots, N\}: \quad & 2R \operatorname{atan2}\left(\sqrt{\zeta_i}, \sqrt{1-\zeta_i}\right) \geq d_{\lambda\theta_i} \\ \text{or} \quad & |h_i - h_{C_i}| \geq d_{h_i}, \end{aligned} \tag{3.17}$$

where a haversine formula has been considered for the distance in the $\lambda - \theta$ direction with

$$\zeta_i = \sin^2\left(\frac{\theta_i - \theta_{C_i}}{2}\right) + \cos\theta_i \cos\theta_{C_i} \sin^2\left(\frac{\lambda_i - \lambda_{C_i}}{2}\right).$$

In practice, for safety reasons, the possibility of avoiding storms flying below them has not been considered in this work. Thus, the set of constraints (3.17) can be rewritten as

$$\begin{aligned} \forall i \in \{1, 2, \ldots, N\}: \quad & 2R \operatorname{atan2}\left(\sqrt{\zeta_i}, \sqrt{1-\zeta_i}\right) \geq d_{\lambda\theta_i} \\ \text{or} \quad & h_i - h_{C_i} \geq d_{h_i}. \end{aligned} \tag{3.18}$$

Again, following the technique described above, the new variables $\epsilon_i^j \in [0, 1]$, $i = 1, 2, \ldots, N, j = 1, 2$ satisfying condition

$$\sum_{j=1}^{2} \epsilon_i^j = 1,$$

are introduced, and Eq. (3.18) can be transformed into

$$\begin{aligned} & \forall i \in \{1, 2, \ldots, N\} : \\ & \epsilon_i^1 \left(2R \operatorname{atan2}\left(\sqrt{\zeta_i}, \sqrt{1-\zeta_i} \right) - d_{\lambda\theta_i} \right) \geq 0 \\ \text{and} \quad & \epsilon_i^2 (h_i - h_{C_i} - d_{h_i}) \geq 0 \\ \text{and} \quad & 0 \leq \epsilon_i^j \leq 1, j = 1, 2 \\ \text{and} \quad & \sum_{j=1}^{2} \epsilon_i^j = 1. \end{aligned} \tag{3.19}$$

The last constraint in (3.19) ensures that at least one of the constraints in (3.18) is fulfilled, that is, the aircraft and the cell are guaranteed to be a safe distance apart. Note that this single-cell storm avoidance model for a single aircraft can be straightforwardly extended to multi-cell storm avoidance model for multiple aircraft. Moreover, as already pointed out in the previous sections, since the approach employed to model logical constraint in disjunctive form is general, it allows any other storm avoidance model described in terms of Eq. (3.4) to be considered.

3.2.5 Waypoints

Finally, in this section, the model employed to enforce the passage constraint of an aircraft through a waypoint will be explained. The model has been based on the use of cuboids similar to those considered in Sec. 3.2.3. More specifically, a cuboid centered at each waypoint has been defined and passage constraints of an aircraft through a waypoint have been modelled as passage constraints through these cuboids. Thus, unlike the obstacle avoidance constraints, in this case the aircraft has been enforced to pass through the cuboid instead of avoiding it.

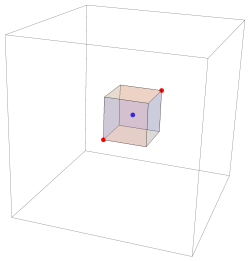

Figure 3.4: Two opposite corners of a cuboid centered at a waypoint in the 3D space.

Let $(\lambda_{W_l}, \theta_{W_l}, h_{W_l})$ and $(\lambda_{W_u}, \theta_{W_u}, h_{W_u})$ be the positions of the opposite corners of a cuboid surrounding a single waypoint as shown in Fig. 3.4. Flying by this waypoint, that is, passing through the corresponding cuboid, involves that at some endpoints t_i of the subintervals of the discretization (2.12), the position of the aircraft $(\lambda_i, \theta_i, h_i)$ must

remain inside it. In terms of logical constraints, this condition can be expressed as

$$\begin{aligned} \forall i \in \{1,2,\ldots,N-1\}: \quad & \lambda_{W_l} - \lambda_i \leq 0 \\ \text{and} \quad & \lambda_i - \lambda_{W_u} \leq 0 \\ \text{and} \quad & \theta_{W_l} - \theta_i \leq 0 \\ \text{and} \quad & \theta_i - \theta_{W_u} \leq 0 \\ \text{and} \quad & h_{W_l} - h_i \leq 0 \\ \text{and} \quad & h_i - h_{W_u} \leq 0. \end{aligned} \tag{3.20}$$

Note that, on one hand, constraints (3.20) are enforced at every endpoint of the discretization except for the initial and final points, t_0 and t_N, since there is no a priori knowledge about when the aircraft is going to fly by the waypoint. On the other hand, imposing these constraints makes sense only when the aircraft is close enough to the waypoint. To overcome this drawback, a second auxiliary cuboid is considered to model the free flight mode of the aircraft. Let $\lambda_{min}, \theta_{min}, h_{min}, \lambda_{max}, \theta_{max}$ and h_{max} be the minimum and maximum values of the state variables λ, θ and h, respectively. In terms of logical constraints, the free flight mode of the aircraft can be expressed as

$$\begin{aligned} \forall i \in \{1,2,\ldots,N-1\}: \quad & \lambda_{min} - \lambda_i \leq 0 \\ \text{and} \quad & \lambda_i - \lambda_{max} \leq 0 \\ \text{and} \quad & \theta_{min} - \theta_i \leq 0 \\ \text{and} \quad & \theta_i - \theta_{max} \leq 0 \\ \text{and} \quad & h_{min} - h_i \leq 0 \\ \text{and} \quad & h_i - h_{max} \leq 0. \end{aligned} \tag{3.21}$$

Then, the transcription into a logical disjunction, namely $\mathsf{WM} \vee \mathsf{FM}$, which allows the Waypoint Mode (WM) or the Freeflight Mode (FM), to be selected along the whole trajectory, can be expressed as

$$\begin{aligned} \forall i \in \{1,2,\ldots,N-1\}: \quad & \mathsf{WM}_i \\ \text{or} \quad & \mathsf{FM}_i, \end{aligned} \tag{3.22}$$

where WM_i and FM_i denote if at discretization time instant t_i the aircraft is in waypoint mode or in free flight mode, respectively.

Once again, following the technique described above, the new variables $\kappa_i^1, \kappa_i^2 \in [0,1]$ satisfying condition

$$\kappa_i^1 + \kappa_i^2 = 1, \quad \text{for all} \quad i = 1,2,\ldots,N-1,$$

are introduced, and Eq. (3.22) can be transformed into

$$
\begin{aligned}
\forall i \in \{1,2,\ldots,N-1\}: \quad & \kappa_i^1(\lambda_{W_l}-\lambda_i)\leq 0 \quad \text{and} \quad \kappa_i^2(\lambda_{min}-\lambda_i)\leq 0 \\
\text{and} \quad & \kappa_i^1(\lambda_i-\lambda_{W_u})\leq 0 \quad \text{and} \quad \kappa_i^2(\lambda_i-\lambda_{max})\leq 0 \\
\text{and} \quad & \kappa_i^1(\theta_{W_l}-\theta_i)\leq 0 \quad \text{and} \quad \kappa_i^2(\theta_{min}-\theta_i)\leq 0 \\
\text{and} \quad & \kappa_i^1(\theta_i-\theta_{W_u})\leq 0 \quad \text{and} \quad \kappa_i^2(\theta_i-\theta_{max})\leq 0 \\
\text{and} \quad & \kappa_i^1(h_{W_l}-h_i)\leq 0 \quad \text{and} \quad \kappa_i^2(h_{min}-h_i)\leq 0 \\
\text{and} \quad & \kappa_i^1(h_i-h_{W_u})\leq 0 \quad \text{and} \quad \kappa_i^2(h_i-h_{max})\leq 0 \\
\text{and} \quad & 0\leq \kappa_i^j\leq 1, j=1,2 \\
\text{and} \quad & \sum_{j=1}^{2}\kappa_i^j=1.
\end{aligned}
\tag{3.23}
$$

The last constraint in (3.23) ensures that at least one of the conditions in (3.22) is fulfilled, which means that at each discretization time instant t_i the aircraft flies in free flight mode or waypoint mode. Note that, depending on the performance index (2.5a) considered in the optimal control problem, two related undesired issues could potentially arise.

On one hand, the optimal solution could provide a trajectory in which the aircraft flies in free flight mode for each discretization time instant t_i. Therefore, in order to force the aircraft to actually fly by the waypoint, a penalty term must also be added to the numerical transcription of the performance index (2.5a). The use of this penalty term, which is set forth to encode the desired control objectives, implies that the numerical solution of the optimal control problem must combine the usual collocation technique described in Sec. 2.3 with a penalty function method. In particular, in this work, following [45], the continuation method has been implemented. In this specific case of waypoint modeling, the penalty term takes the form

$$
c_1\sum_{i=1}^{N-1}\kappa_i^1+c_2\sum_{i=1}^{N-1}\kappa_i^2, \tag{3.24}
$$

where c_1 and c_2 are suitable constants determined by the continuation method. In the context of a minimization of a performance index such as (2.5a), a value c_2 such that $c_2 \gg c_1 > 0$, large enough to penalize the free flight mode, guarantees that the aircraft actually flies by the waypoint.

On the other hand, the optimal solution could provide a trajectory in which the aircraft flies by the waypoint more than once. This situation can be easily avoided introducing the following constraint

$$
\sum_{i=1}^{N-1}\kappa_i^1\leq c_3,
$$

where $c_3 \in \{1,2,\ldots,N-1\}$ is a suitable constant. In the context of the problem considered in this work, to include the penalty term (3.24) in the objective functional, a small value of c_3 is enough to avoid this potential undesired issue.

Once again, note that this single-waypoint model for a single aircraft can be straightforwardly extended to a multi-waypoint model for multiple aircraft. Moreover, as already pointed out in the previous sections, since the approach employed to model logical constraint in disjunctive form is general, it allows any other waypoint model described in terms of Eq. (3.4) to be considered.

4

Multi-Aircraft Offline Trajectory Planning

In this chapter, to show the effectiveness of the multi-aircraft offline trajectory planning methodology described in Section 2.2 and Section 3.2, the following three numerical experiments have been carried out:

- Minimum-time continuous descent of three aircraft along routes converging at the same waypoint with time-based separation constraint among them.
- Minimum-time continuous descent of three aircraft along intersecting routes with distance-based separation constraint.
- Minimum-time STAR-based continuous descent of three aircraft along converging routes. The considered STAR procedure includes sequencing the aircraft at a merging point and passing through two other waypoints.

As already mentioned in the Introduction chapter, although these numerical experiments are focused on CDOs, the methodology employed could be straightfully applied to CCOs as well.

All of these numerical experiments involve Airbus A-320 BADA 3.14 aircraft models in which the performance index is the sum of the duration of the flights of the three aircraft. Constraints derived from current flight regulation have been introduced, namely, time-base separation and distance-based separation operational constraints have been imposed. In particular, a minimum horizontal distance separation between aircraft of 5000 m and vertical separation between aircraft of 1000 m have been considered whereas the considered minimum time separation between aircraft has been 200 s. This specific

values have been chosen taken as a reference the aviation regulation [46] in which, in general, aircraft have to be separated by at least 3 NM or 3 min in the TMA.

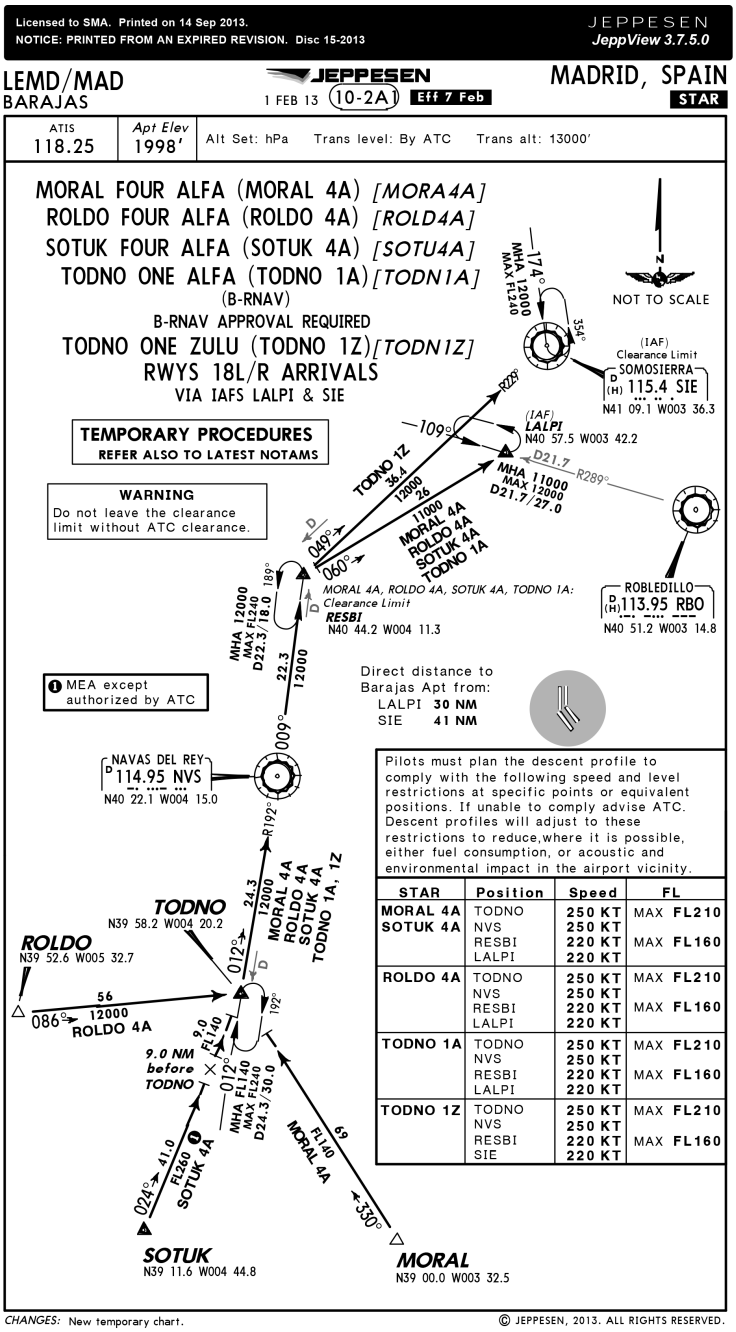

Figure 4.1: Chart of the Adolfo Suárez Madrid-Barajas (LEMD/MAD) STAR 10-2A1. Source: Jeppesen, A Boeing Company. Not for operational use.

4.1 Experiment 1. Minimum-time continuous descent along converging routes

In this experiment, CDA under vectoring has been considered, that is, the lateral path followed by the aircraft has been assumed to be specified through instructions provided by the ATC. In particular, the boundary conditions of the state variables have been selected from the chart of the Adolfo Suárez Madrid-Barajas (LEMD/MAD) TMA shown in Figure 4.1. This specific chart has been intentionally selected due to the high likelihood of potential conflicts that might arise among the involved aircraft. The initial position of Aircraft 1, Aircraft 2, and Aircraft 3 have been supposed to be coincident with the ROLDO, SOTUK, and MORAL waypoints, respectively. Their common final position has been assumed to be the LALPI waypoint. The three aircraft have been supposed to go directly from their initial positions to the final waypoint, that is, no constraints on the lateral path have been considered.

4.1.1 Case study A. Without time-based separation constraints

In a first instance, the problem has been formulated as an offline trajectory planning problem as described in Section 2.2 and it has been solved following Section 2.3. Neither time-based nor distance-based separation constraints have been included in the model. The initial mass of the three aircraft has been assumed equal to the maximum landing weight of the aircraft. The specific boundary conditions of the state variables are given in Table 4.1.

Table 4.1: Boundary conditions for Experiment 1 and Experiment 3

Symbol	Unit	Aircraft 1	Aircraft 2	Aircraft 3
h_I	m	7400	7000	7200
h_F	m	3350	3350	3350
θ_I	deg	39.526	39.116	39.000
θ_F	deg	40.575	40.575	40.575
λ_I	deg	-5.327	-4.448	-3.325
λ_F	deg	-3.422	-3.422	-3.422
V_I	m/s	130	130	130
V_F	m/s	110	110	110
μ_I	deg	0	0	0
γ_I	deg	0	0	0
χ_I	deg	356	294	240
m_I	kg	65000	65000	65000

In Figure 4.2 the 3D view of the paths obtained in the solution are represented, and in Figure 4.3 and Figure 4.4 the horizontal and vertical profiles, respectively, are shown for the three aircraft. The final mass for the three aircraft are depicted in Figure 4.5.

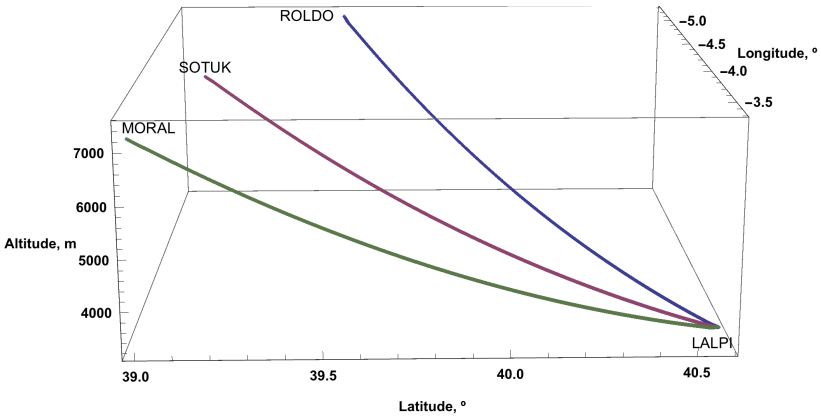

Figure 4.2: Experiment 1. Case study A. 3D view of the paths without time-based separation constraints.

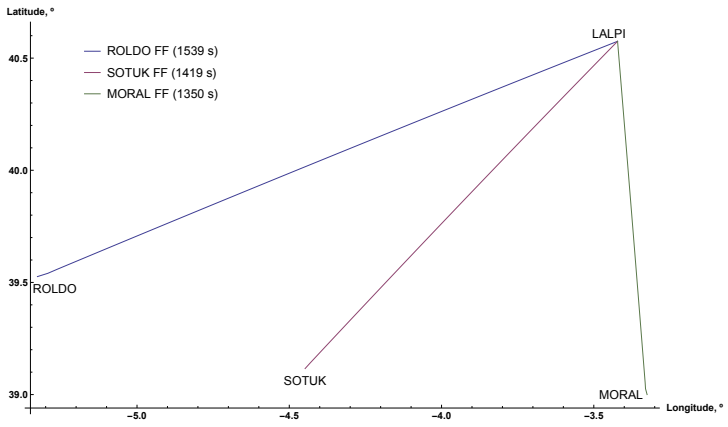

Figure 4.3: Experiment 1. Case study A. Horizontal profiles without time-based separation constraints.

The final time is 1539 s, 1419 s and 1350 s for Aircraft 1, Aircraft 2 and Aircraft 3, respectively, corresponding to 22-25 min of flight. The difference between the final time of Aircraft 2 and 3 is 69 s, between Aircraft 1 and 2 is 120 s, and between Aircraft 1 and 3 is 189 s. As expected, these differences in time among the three aircraft at `LALPI` waypoint are below the required time separation of 200 s established above. Note that, as mentioned before, the chart in Figure 4.1 has been intentionally selected

due to the high likelihood of potential conflicts that might arise among the involved aircraft. Therefore, a new experiment has been conducted in order to fix the conflict observed in Case study A.

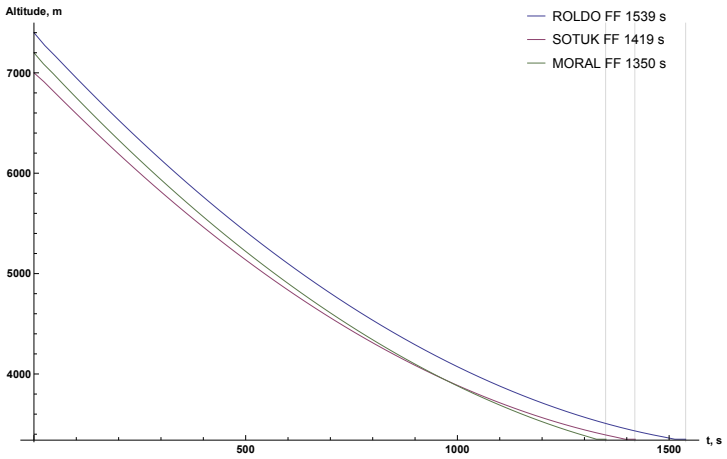

Figure 4.4: Experiment 1. Case study A. Vertical profiles without time-based separation constraints.

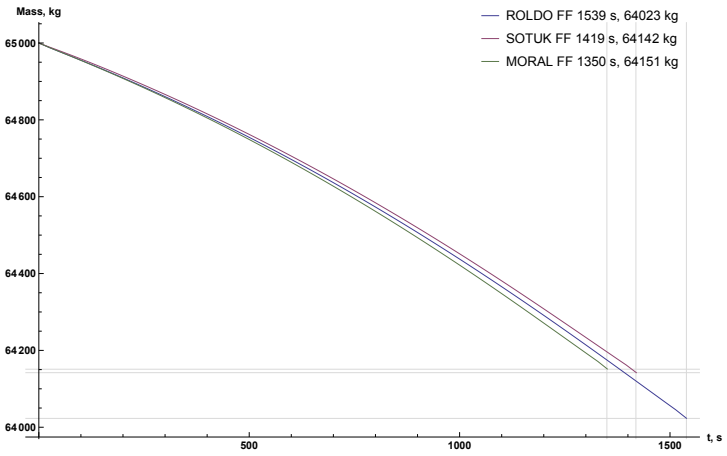

Figure 4.5: Experiment 1. Case study A. Mass consumption without time-based separation constraints.

4.1.2 Case study B. With time-based separation constraints

As mentioned above, a second experiment has been conducted which, besides the formulation used to model Case study A, includes time-based separation logical

constraint of at least 200 s between aircraft at the LALPI waypoint as described in Section 3.2.1.

In Figure 4.6 the 3D view of the paths obtained in the solution are represented, and in Figure 4.7 and Figure 4.8 the horizontal and vertical profiles, respectively, are shown for the three aircraft. The final mass for the three aircraft are depicted in Figure 4.9.

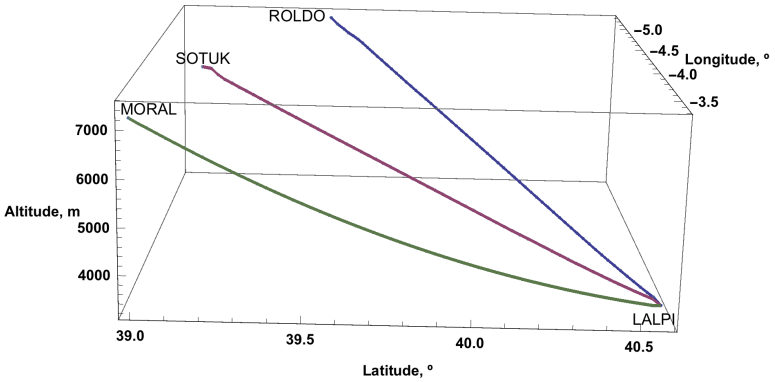

Figure 4.6: Experiment 1. Case study B. 3D view of the paths with time-based separation constraints.

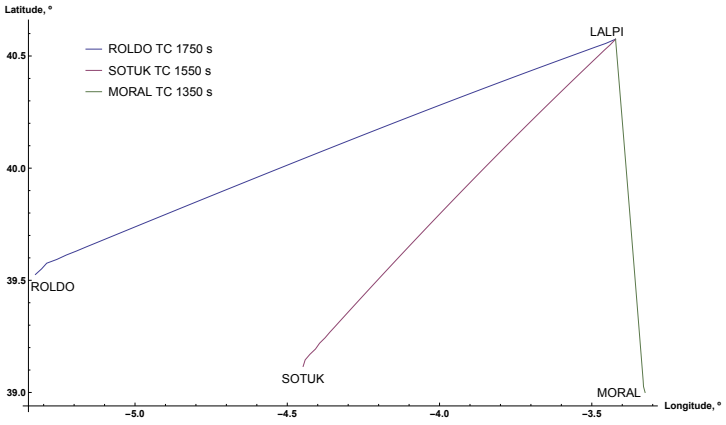

Figure 4.7: Experiment 1. Case study B. Horizontal profiles with time-based separation constraints.

Now, the final time is 1750 s, 1550 s and 1350 s for Aircraft 1, Aircraft 2 and Aircraft 3, respectively, corresponding to 22-29 min of flight. The difference between the final time of aircraft is 200 s in all cases. Thus, these differences in time among the three aircraft at LALPI waypoint fulfil the required time separation established above.

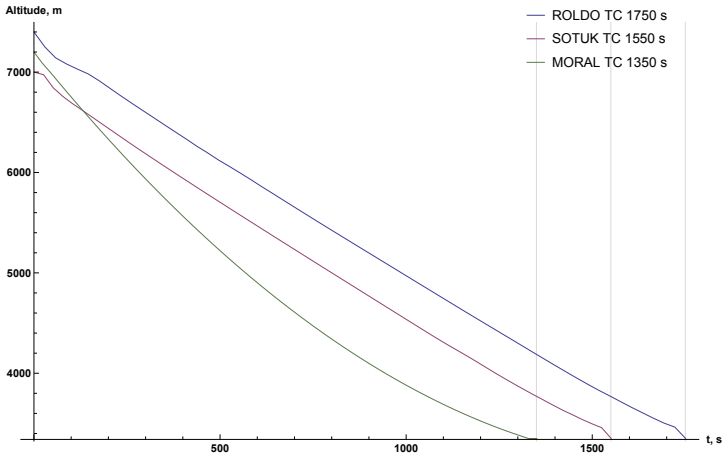

Figure 4.8: Experiment 1. Case study B. Vertical profiles with time-based separation constraints.

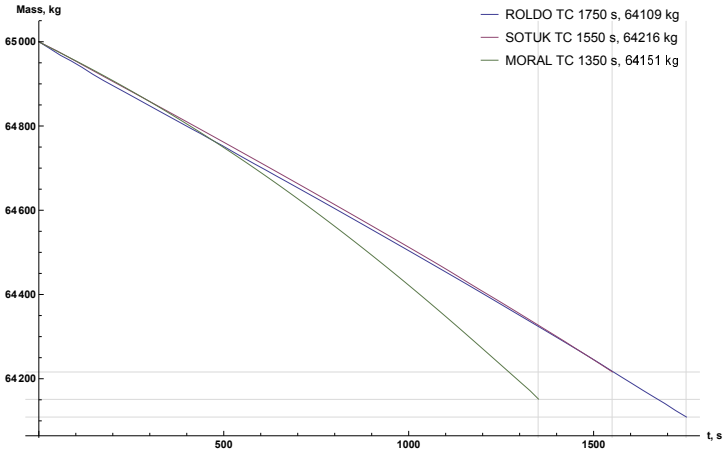

Figure 4.9: Experiment 1. Case study B. Mass consumption with time-based separation constraints.

4.1.3 Comparison and discussion on the results

In Figure 4.10 the 3D view of the paths obtained in the solution without time-based separation constraints are represented in thin lines whereas the 3D view of the paths obtained in the solution with time-based separation constraints are represented in thick lines. In Figure 4.11 and Figure 4.12 the horizontal and vertical profiles without time-based separation constraints are represented in solid lines whereas the horizontal and vertical profiles with time-based separation constraints are represented in dashed lines.

Note that whereas in Case Study A the three aircraft perform the minimum-time

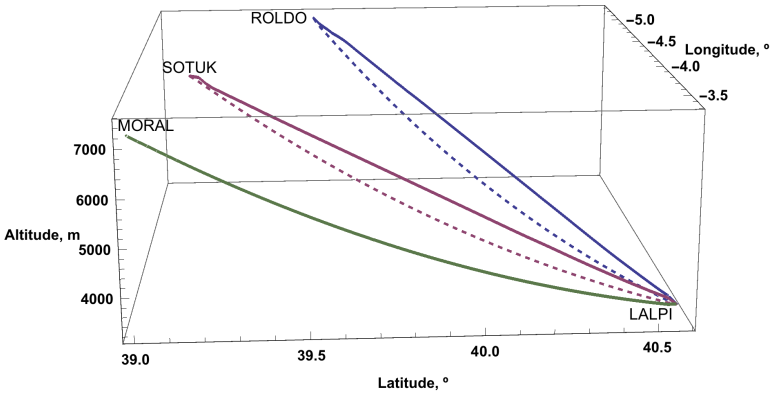

Figure 4.10: Experiment 1. Comparison. 3D view of the paths with (thick lines) and without (thin lines) time-based separation constraints.

Table 4.2: Results of Experiment 1

	# Aircraft	Final Time, s	Final mass, kg
Without time constraint	1	1539	64023
	2	1419	64142
	3	1350	64151
With time constraint	1	1750	64109
	2	1550	64216
	3	1350	64151

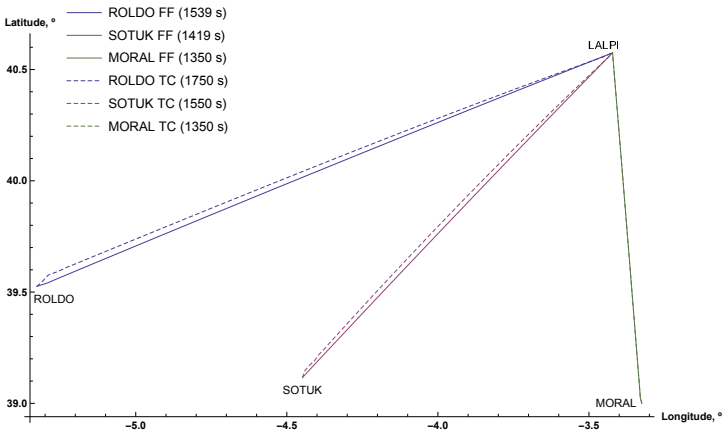

Figure 4.11: Experiment 1. Comparison. Horizontal profiles with (TC, dashed lines) and without (FF, solid lines) time-based separation constraints.

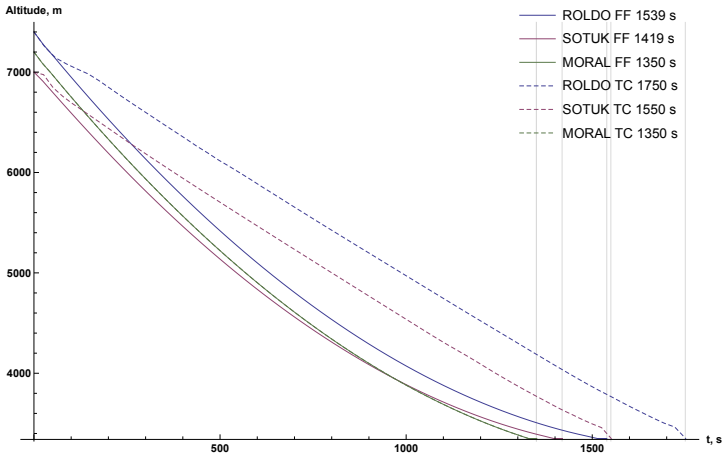

Figure 4.12: Experiment 1. Comparison. Vertical profiles with (TC, dashed lines) and without (FF, solid lines) time-based separation constraints.

descent path by means of a CDA procedure at almost idle thrust, in Case Study B, the vertical profiles of Aircraft 1 and Aircraft 2 changed significantly while there are slight changes in the horizontal profiles. Vertical and horizontal profiles of Aircraft 3 remain unchanged. These differences are obviously due to the inclusion of the time-based separation constraints which substantially modifies the control variables profiles of Aircraft 1 and Aircraft 2.

The final mass and time given by the solution with and without time-based separation constraints are reported for each aircraft in Table 4.2. The mass consumption is represented in Figure 4.13, in which the solution without time-based separation constraints is represented in solid lines whereas the solution with time-based separation constraints is represented in dashed lines. It can be seen that introducing time separation constraints increases the mass consumption of Aircraft 1 and Aircraft 2 in more than 70 kg, whereas that of Aircraft 3 remains unchanged.

Finally, note that, since the objective functional to be minimized is the sum of the duration of the flights, time-based separation constraints are saturated and aircraft in Case Study B maintain mutually the minimum required time-based separation of 200 s.

4.2 Experiment 2. Minimum-time continuous descent along intersecting routes

This experiment has been designed to test the effectiveness of the logical constraint formalism described in Section 3.2.2, where three aircraft start at and have to reach three different positions flying along intersecting routes in which a mid air conflict arises, in the sense that the experiment is intentionally designed in such a way that they reach

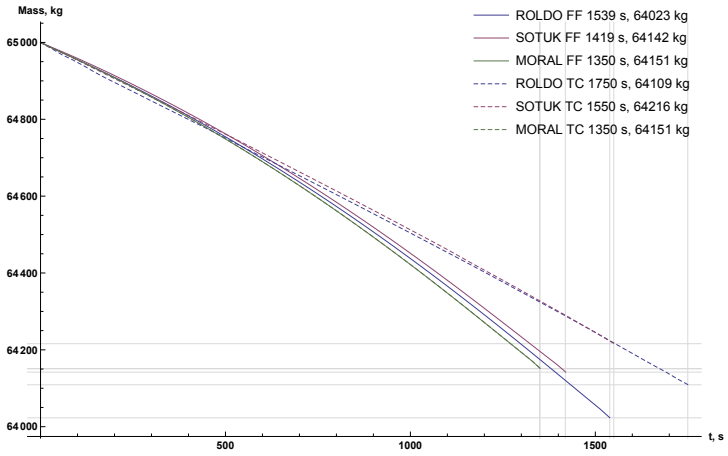

Figure 4.13: Experiment 1. Comparison. Mass consumption with (TC, dashed lines) and without (FF, solid lines) time-based separation constraints.

almost the same point at the same time.

4.2.1 Case study A. Without distance-based separation constraints

As in Section 4.1, in a first instance, the problem has been formulated as an offline trajectory planning problem as described in Section 2.2 and it has been solved following Section 2.3, and neither time-based nor distance-based separation constraints have been included in the model. Again, the initial mass of the three aircraft has been assumed equal to the maximum landing weight of the aircraft. The specific boundary conditions of the state variables are given in Table 4.3 and the information about the conflict is reported in Table 4.4.

Table 4.3: Boundary conditions for Experiment 2

Symbol	Unit	Aircraft 1	Aircraft 2	Aircraft 3
h_I	m	7400	7400	7400
h_F	m	3350	3350	3350
θ_I	deg	39.000	39.000	38.701
θ_F	deg	40.575	40.575	40.848
λ_I	deg	-5.327	-3.325	-4.320
λ_F	deg	-3.430	-5.215	-4.320
V_I	m/s	130	130	130
V_F	m/s	110	110	110
μ_I	deg	0	0	0
γ_I	deg	0	0	0
χ_I	deg	356	294	294
m_I	kg	65000	65000	65000

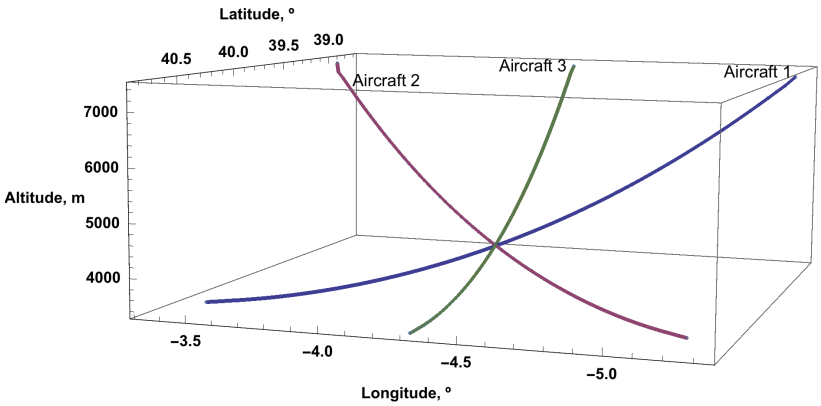

Figure 4.14: Experiment 2. Case study A. 3D view of the paths without distance-based separation constraints.

Table 4.4: Positions of aircraft at merging point (at time 980 s) without distance constraint for Experiment 2

Symbol	Unit	Aircraft 1	Aircraft 2	Aircraft 3
h_I	m	4176	4170	4194
θ_I	deg	39.8414	39.8449	39.8458
λ_I	deg	-4.3243	-4.3165	-4.3184

In Figure 4.14 the 3D view of the paths obtained in the solution are represented, and in Figure 4.15 and Figure 4.16 the horizontal and vertical profiles, respectively,

are shown for the three aircraft. The final mass for the three aircraft are depicted in Figure 4.17. Note that, as expected, the three aircraft perform similar profiles so that a mid air conflict arises at 980 s, and the final time of all of them is 1838 s. Therefore, a new experiment has been conducted in order to fix this conflict observed in Case study A.

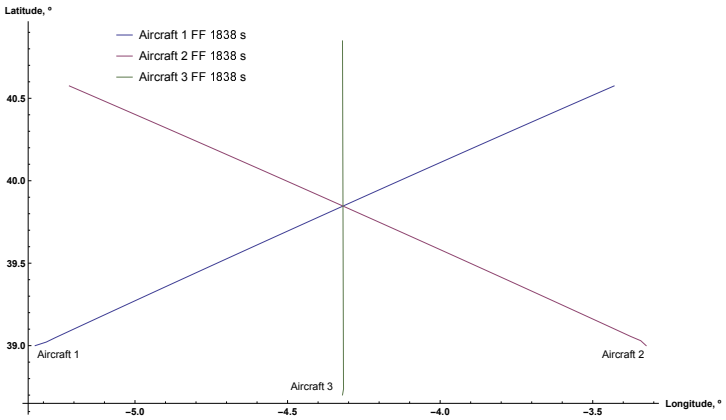

Figure 4.15: Experiment 2. Case study A. Horizontal profiles without distance-based separation constraints.

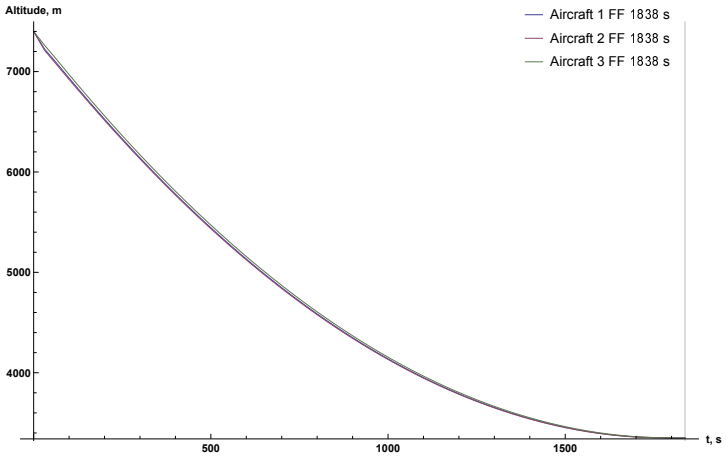

Figure 4.16: Experiment 2. Case study A. Vertical profiles without distance-based separation constraints.

4.2.2 Case study B. With distance-based separation constraints

To avoid the mid air conflict, a second experiment has been conducted which, besides the formulation used to model Case study A, includes distance-based separation logical

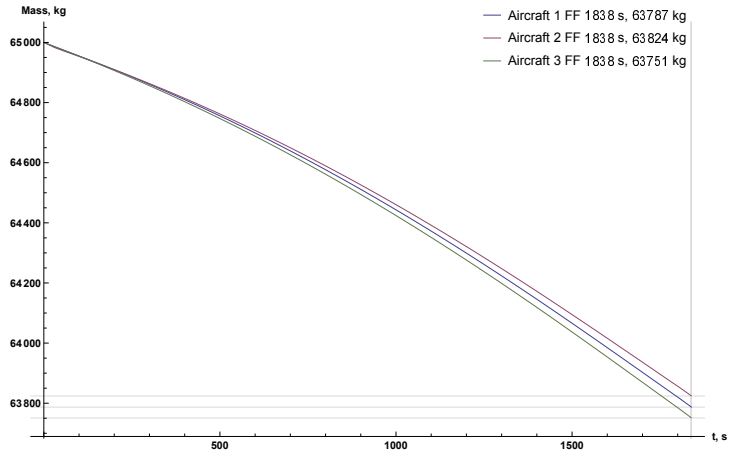

Figure 4.17: Experiment 2. Case study A. Mass consumption without distance-based separation constraints.

constraint between aircraft of at least 5000 m (2.7 NM) in the horizontal profile and at least 5000 m (2.7 NM) in the vertical profile as described in Section 3.2.2.

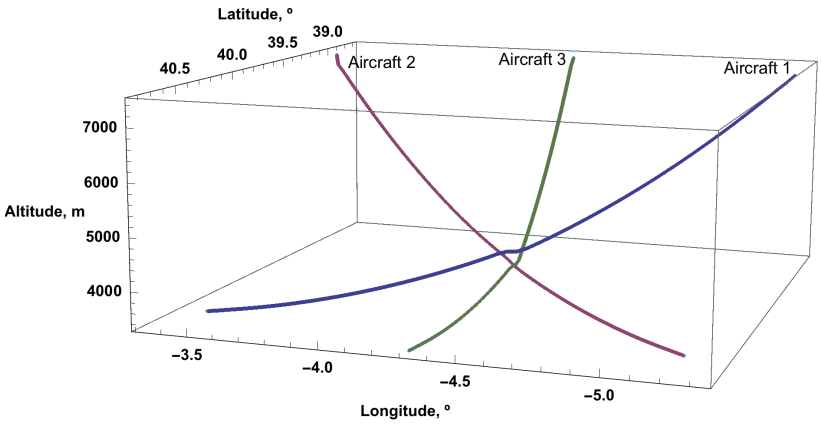

Figure 4.18: Experiment 2. Case study B. 3D view of the paths with distance-based separation constraints.

In Figure 4.18 the 3D view of the paths obtained in the solution are represented and in Figure 4.19 and Figure 4.20 the horizontal and vertical profiles, respectively, are shown for the three aircraft. The distances in the horizontal profile among aircraft along the trajectory are shown in Figure 4.21. The final mass for the three aircraft are depicted in Figure 4.22.

Unlike Case Study A, now it can be seen from Figure 4.19 and Figure 4.21 that the conflict is avoided by activating the logical constraints associated to the horizontal

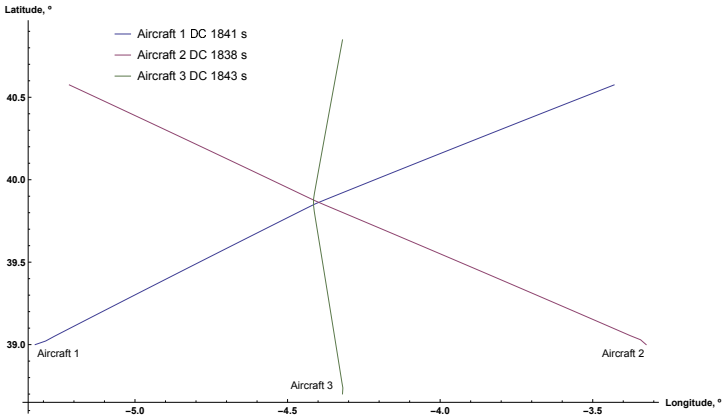

Figure 4.19: Experiment 2. Case study B. Horizontal profiles with distance-based separation constraints.

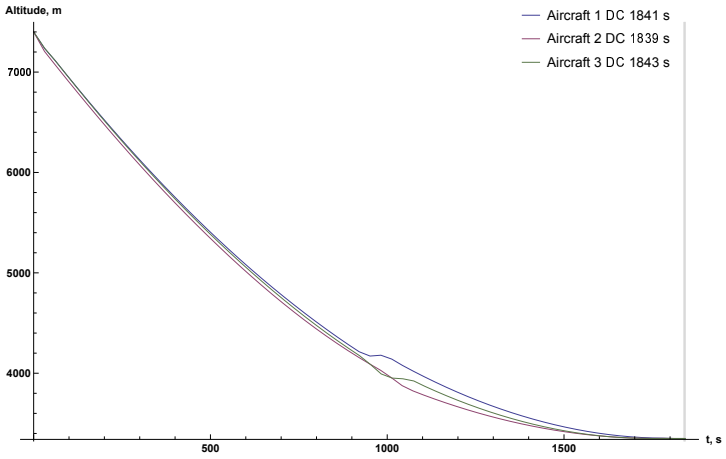

Figure 4.20: Experiment 2. Case study B. Vertical profiles with distance-based separation constraints.

profile. In particular, from Figure 4.21, it can be observed that the logical distance constraint between Aircraft 1 and Aircraft 2 is active in the interval $[982, 1012]$ s, between Aircraft 2 and Aircraft 3 is active in the interval $[1011, 1042]$ s, and between Aircraft 1 and Aircraft 3 is active in the interval $[952, 983]$ s. Although there is a change in the vertical profile of Aircraft 1 and Aircraft 3, this is not due to the inclusion of the logical distance-based constraint associated to the vertical profile since it is not activated at any time instant. The final time of Aircraft 1, Aircraft 2, and Aircraft 3 are similar, being 1841 s, 1838 s, and 1843 s, respectively.

Finally, it can be observed that now the mass consumption of Aircraft 1 and Aircraft 3 are similar whereas the mass consumption of Aircraft 2 is 128 kg higher.

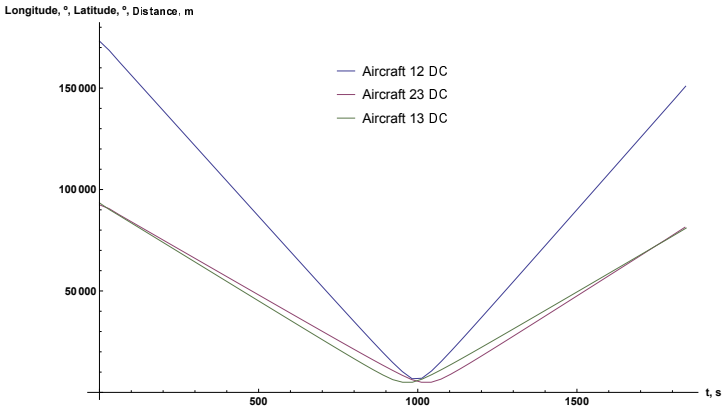

Figure 4.21: Experiment 2. Distance among aircraft with distance-based separation constraints (DC).

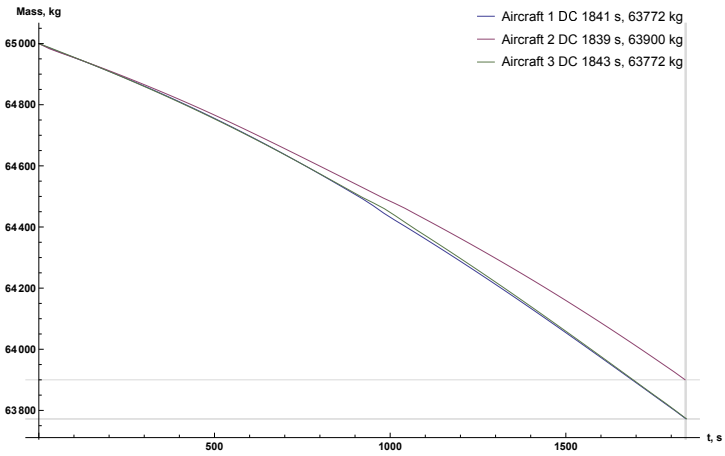

Figure 4.22: Experiment 2. Case study B. Mass consumption with distance-based separation constraints.

4.2.3 Comparison and discussion on the results

In Figure 4.23 the 3D view of the paths obtained in the solution without distance-based separation constraints are represented in thin lines whereas the 3D view of the paths obtained in the solution with distance-based separation constraints are represented in thick lines. In Figure 4.24 and Figure 4.25 the horizontal and vertical profiles without time-based separation constraints are represented in solid lines whereas the horizontal and vertical profiles with time-based separation constraints are represented in dashed lines. The final mass and time given by the solution with and without distance-based separation constraints are reported for each aircraft in Table 4.5.

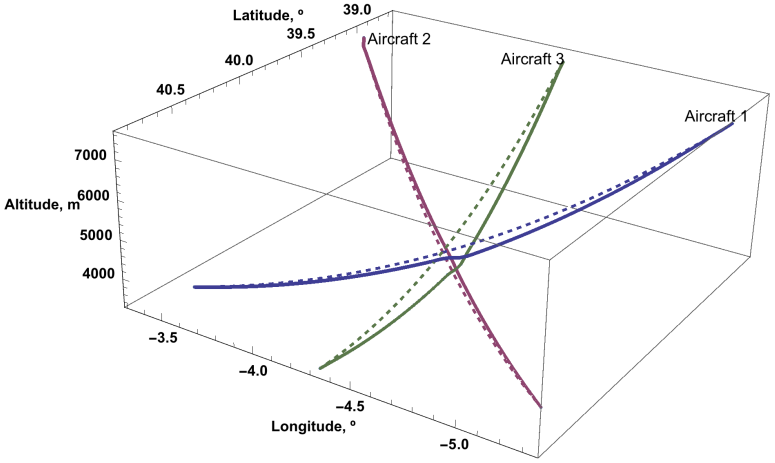

Figure 4.23: Experiment 2. Comparison. 3D view of the paths with (thick lines) and without (thin lines) distance-based separation constraints.

Table 4.5: Results of Experiment 2

	# Aircraft	Final Time, s	Final mass, kg
Without distance constraint	1	1838	63787
	2	1838	63824
	3	1838	63751
With distance constraint	1	1841	63772
	2	1839	63900
	3	1843	63772

Note that whereas in Case Study A the three aircraft perform the minimum-time descent path by means of a CDA procedure at almost idle thrust, in Case Study B the horizontal profiles of the three aircraft changed significantly, mainly during the time interval [952, 1042] s, while there are slight changes in the vertical profiles This differences are obviously due to the inclusion of the distance-based separation constraints which substantially modifies the control variables profiles of the three aircraft mainly during the mentioned time interval [952, 1042] s.

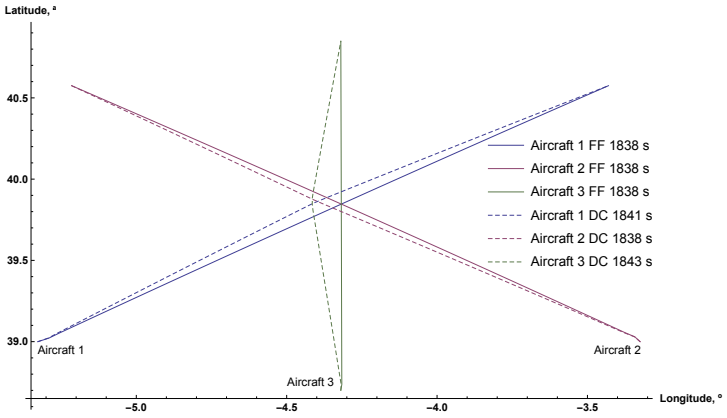

Figure 4.24: Experiment 2. Comparison. Horizontal profiles with (DC, dashed lines) and without (FF, solid lines) distance-based separation constraints.

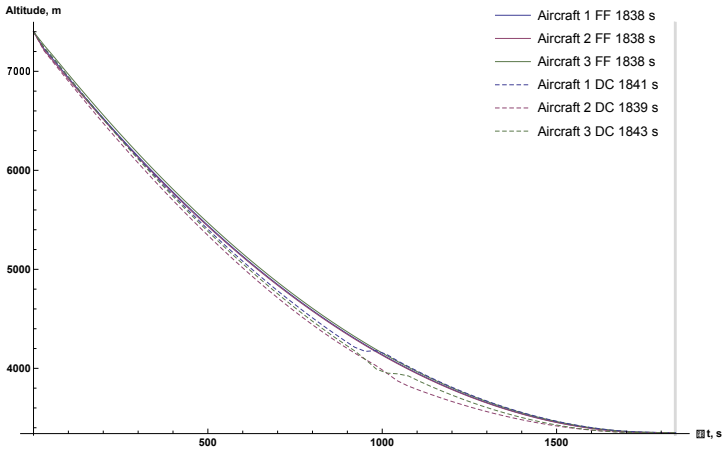

Figure 4.25: Experiment 2. Comparison. Vertical profiles with (DC, dashed lines) and without (FF, solid lines) distance-based separation constraints.

The mass consumption is depicted in Figure 4.26, in which the solution without distance-based separation constraints is represented in solid lines whereas the solution with distance-based separation constraints is represented in dashed lines. It can be seen that introducing distance separation constraints does not significantly change the mass consumption of Aircraft 1 and Aircraft 3, whereas the mass consumption of Aircraft 3 is 76 kg higher for Case Study B. Also, the final time of the three aircraft are very similar.

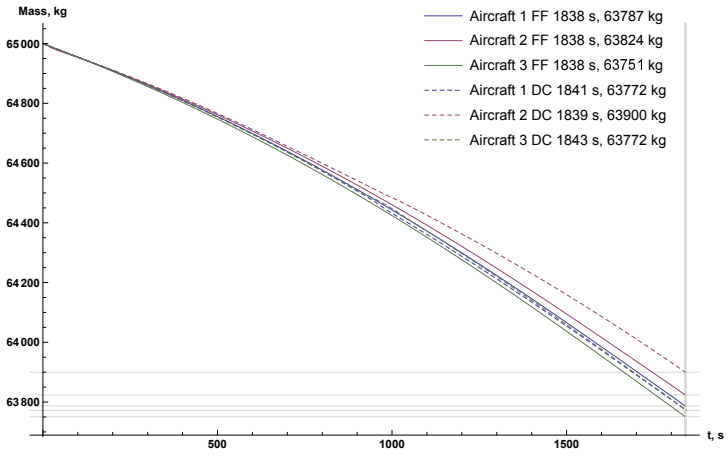

Figure 4.26: Experiment 2. Comparison. Mass consumption with (DC, dashed lines) and without (FF, solid lines) distance-based separation constraints.

4.3 Experiment 3. Minimum-time STAR-based continuous descent along converging routes

In this experiment, a STAR-based CDA has been considered, that is, the lateral path followed by the aircraft has been assumed to be specified in a navigation chart. In particular, as in Experiment 1, the boundary conditions of the state variables have been selected from the chart of the Adolfo Suárez Madrid-Barajas (LEMD/MAD) TMA shown in Figure 4.1. Again, the initial position of Aircraft 1, Aircraft 2, and Aircraft 3 are supposed to be coincident with the ROLDO, SOTUK, and MORAL waypoints, respectively. Aircraft are constrained to pass through TODNO and RESBI waypoints and their common final position is assumed to be the LALPI waypoint. For the setting of the cuboids centered at the given waypoints the modeling defined in (3.20) has been considered. In particular, the cuboid centered at TODNO waypoint has been defined by the two corners (39.560°,-4.24°, 5400 m) and (39.640°,-4.160°, 6000 m) whereas the cuboid centered at RESBI waypoint has been defined by the two corners (40.400°,-4.150°, 4200 m) and (40.480°,-4.070°, 4800 m).

As in the previous experiments, the initial mass of the three aircraft has been assumed equal to the maximum landing weight of the aircraft. The specific boundary conditions of the state variables are the same as in Experiment 1 and are given in Table 4.6.

Table 4.6: Boundary conditions for Experiment 1 and Experiment 3

Symbol	Unit	Aircraft 1	Aircraft 2	Aircraft 3
h_I	m	7400	7000	7200
h_F	m	3350	3350	3350
θ_I	deg	39.526	39.116	39.000
θ_F	deg	40.575	40.575	40.575
λ_I	deg	-5.327	-4.448	-3.325
λ_F	deg	-3.422	-3.422	-3.422
V_I	m/s	130	130	130
V_F	m/s	110	110	110
μ_I	deg	0	0	0
γ_I	deg	0	0	0
χ_I	deg	356	294	240
m_I	kg	65000	65000	65000

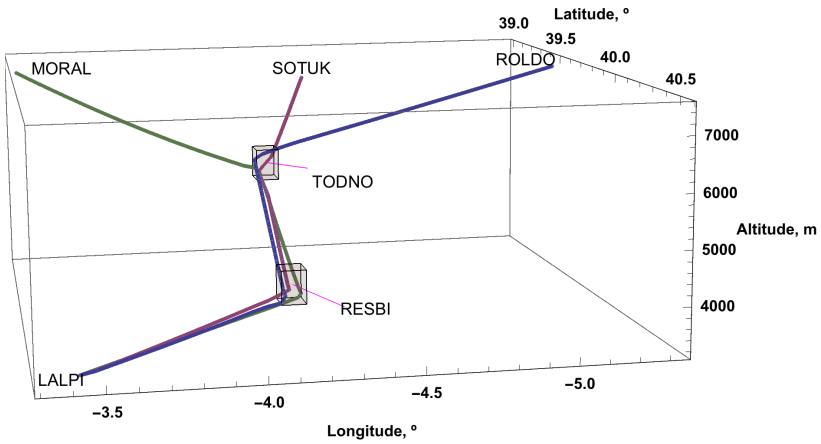

Figure 4.27: Experiment 3. Case study A. 3D view of the paths with waypoints constraints and without time-based separation constraints.

4.3.1 Case study A. Without time-based separation constraints

In a first instance, the problem has been formulated as an offline trajectory planning problem following Section 2.2, it has been solved following Section 2.3, and neither

time-based nor distance-based separation constraints have been included in the model. In Figure 4.2 the 3D view of the paths obtained in the solution are represented and in Figure 4.3 and Figure 4.4 the horizontal and vertical profiles, respectively, are shown for the three aircraft. The final mass for the three aircraft are depicted in Figure 4.5.

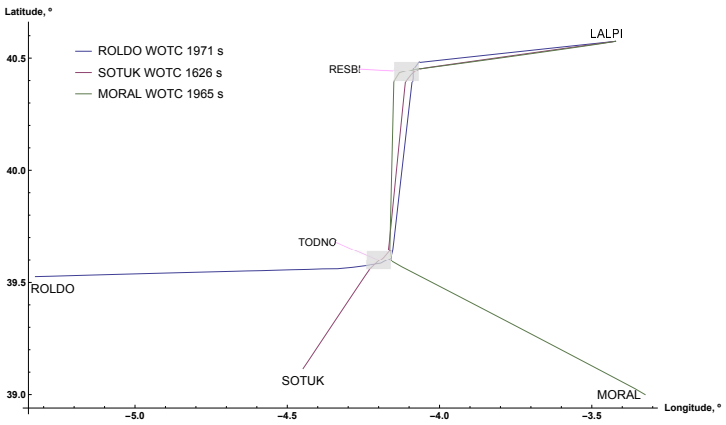

Figure 4.28: Experiment 3. Case study A. Horizontal profiles with waypoints constraints and without time-based separation constraints.

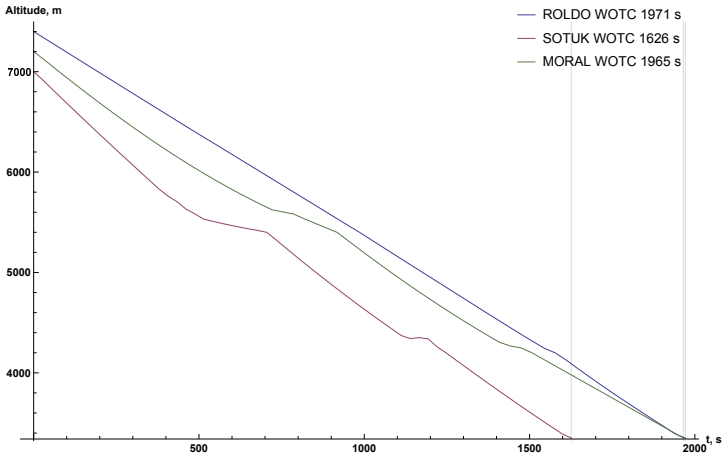

Figure 4.29: Experiment 3. Case study A. Vertical profiles with waypoints constraints and without time-based separation constraints.

The final time is 1971 s, 1626 s and 1965 s for Aircraft 1, Aircraft 2 and Aircraft 3, respectively, corresponding to 27-33 min of flight. In spite of the fact that the three aircraft have to pass through two waypoints, neither distance-based conflict nor time-based conflict arises during the flight except for the last part of the time discretization. In particular, Aircraft 1 and Aircraft 3 reach the `LALPI` waypoint with a time separation of 6 s only. This difference in time between both aircraft at `LALPI` waypoint is obviously below the required time separation of 200 s established above. Therefore, a new experiment has been conducted in order to fix the conflict observed in Case study A.

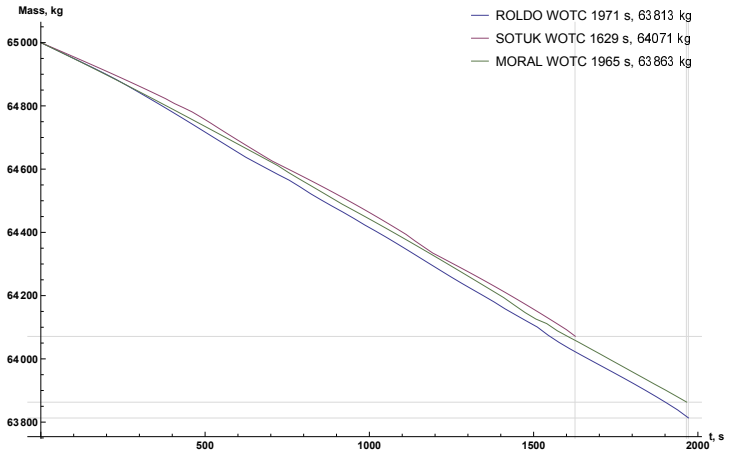

Figure 4.30: Experiment 3. Case study A. Mass consumption with waypoints constraints and without time-based separation constraints.

4.3.2 Case study B. With time-based separation constraints

In order to fix the conflict observed in the last part of the time discretization of Case study A, a second experiment has been conducted which, besides the formulation used to model Case study A with waypoint constraints, also includes time-based separation logical constraint of at least 200 s between aircraft as described in Section 3.2.1.

In Figure 4.31 the 3D view of the paths obtained in the solution are represented and in Figure 4.32 and Figure 4.33 the horizontal and vertical profiles, respectively, are shown for the three aircraft. The final mass for the three aircraft are depicted in Figure 4.34.

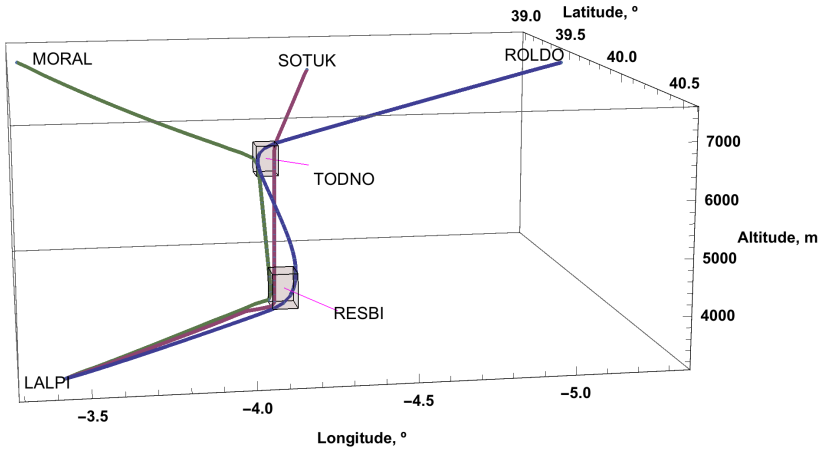

Figure 4.31: Experiment 3. Case study B. 3D view of the paths with waypoints and time-based separation constraints.

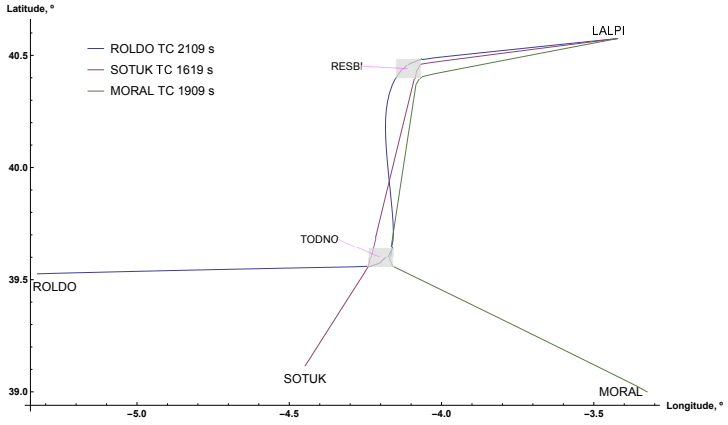

Figure 4.32: Experiment 3. Case study B. Horizontal profiles with waypoints and time-based separation constraints.

In this case, the final time is 2109 s, 1619 s and 1909 s for Aircraft 1, Aircraft 2 and Aircraft 3, respectively, corresponding to 27-35 min of flight. Now, the difference between the final time of Aircraft 1 and 3 is 200 s whereas the difference between the final time of Aircraft 3 and 2 is 290 s. Thus, these differences in time among the three aircraft at `LALPI` waypoint fulfil the required time separation established above.

4.3.3 Comparison and discussion on the results

In Figure 4.35 the 3D view of the paths obtained in the solution without time-based separation constraints are represented in thin lines whereas the 3D view of the

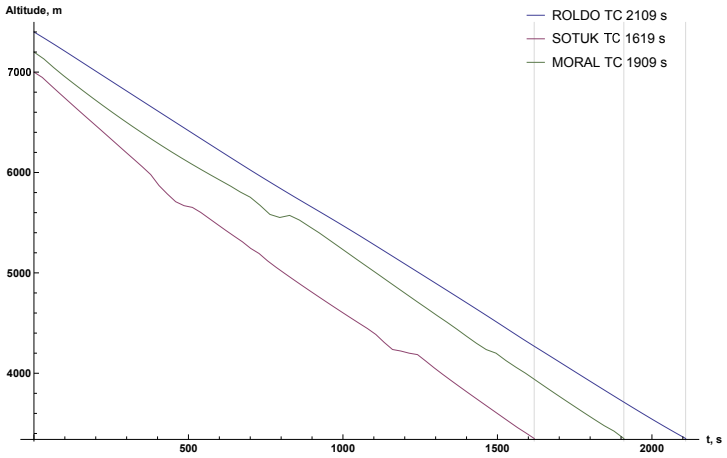

Figure 4.33: Experiment 3. Case study B. Vertical profiles with waypoints and time-based separation constraints.

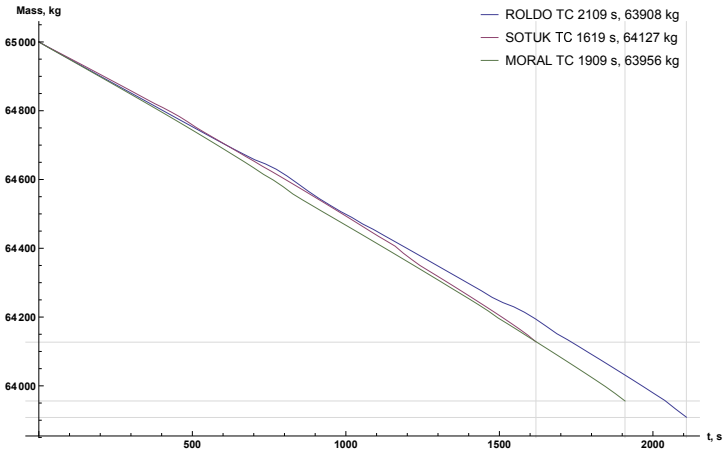

Figure 4.34: Experiment 3. Case study B. Mass consumption with waypoints and time-based separation constraints.

paths obtained in the solution with time-based separation constraints are represented in thick lines. In Figure 4.36 and Figure 4.37 the horizontal and vertical profiles, respectively, with time-based separation constraints are represented in solid lines whereas the horizontal and vertical profiles without time-based separation constraints are represented in dashed lines.

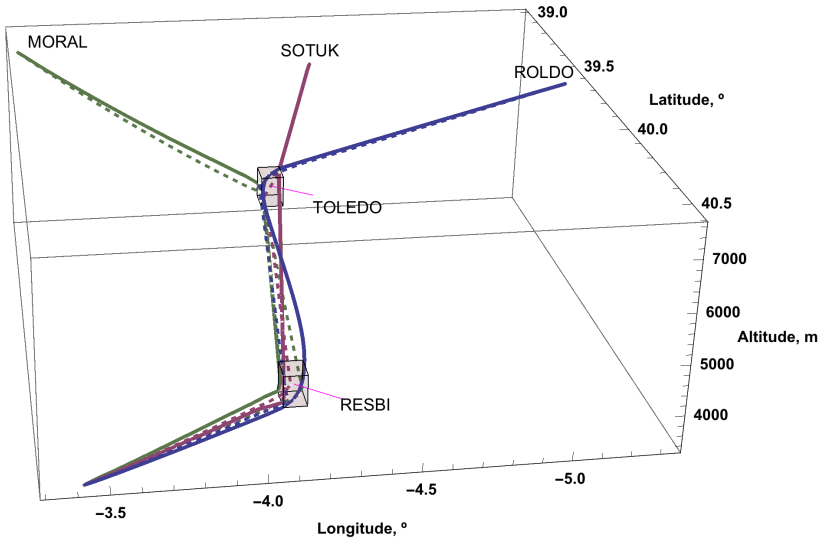

Figure 4.35: Experiment 3. Comparison. 3D view of the paths with (thick lines) and without (thin lines) time-based separation constraints.

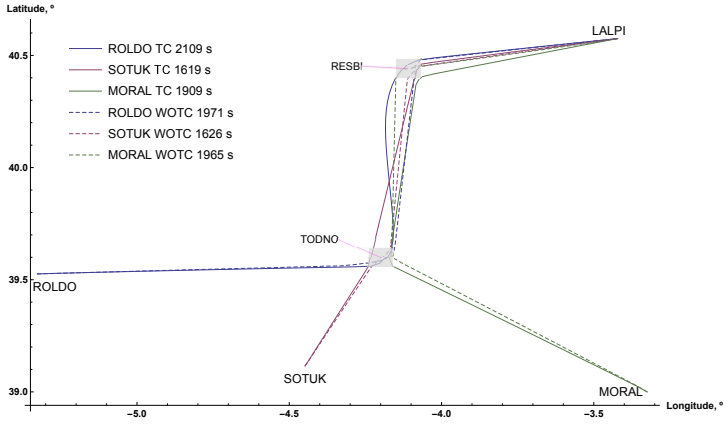

Figure 4.36: Experiment 3. Comparison. Horizontal profiles with (TC, solid lines) and without (WOTC, dashed lines) time-based separation constraints.

Note that in both cases the minimum-time STAR-based continuous descent path procedure is performed. However, due to the inclusion of the time-based separation constraints, there are changes in both the vertical and horizontal profiles for the three aircraft. In particular, changes in the horizontal profiles are especially significant. These differences also can be appreciated in the control variables profiles of the three aircraft.

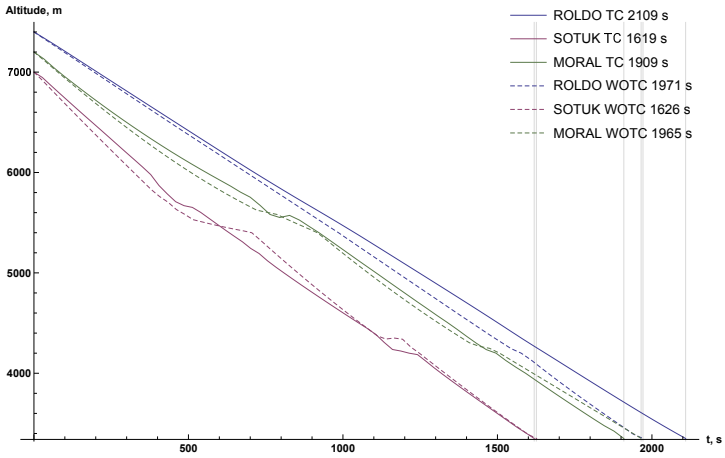

Figure 4.37: Experiment 3. Comparison. Vertical profiles with (TC, solid lines) and without (WOTC, dashed lines) time-based separation constraints.

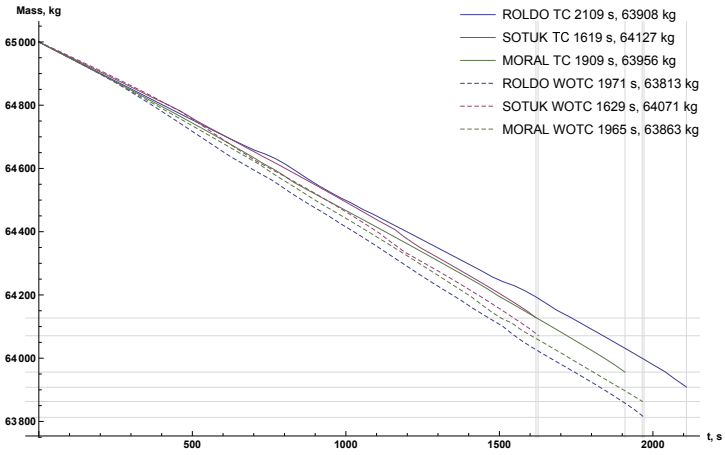

Figure 4.38: Experiment 3. Comparison. Mass consumption with (TC, solid lines) and without (WOTC, dashed lines) time-based separation constraints.

The final mass and time given by the solution with and without time-based separation constraints are reported for each aircraft in Table 4.7. The mass consumption is depicted in Figure 4.38, in which the solution with time-based separation constraints is represented in solid lines whereas the solution without time-based separation constraints is represented in dashed lines. It can be seen that introducing time-based separation constraints increases the mass consumption of the three aircraft. In all cases, this increment is lower than 100 kg.

Table 4.7: Results of Experiment 3

	# Aircraft	Final Time, s	Final mass, kg
Without logical constraints	1	1539	64023
	2	1419	64142
	3	1350	64151
With waypoint constraints	1	1971	63813
	2	1626	64071
	3	1965	63863
With waypoint and time constraints	1	2109	63908
	2	1619	64127
	3	1909	63956

Finally, notice that, unlike Experiment 1, Aircraft 2 and 3 in Case Study B do not maintain the minimum required time separation of 200 s. This is due to the fact that the performance index includes in this case, besides the minimization of the duration of the flights, the penalty term (3.24) associated to the waypoints constraints. Therefore, the saturation of the time-based constraints may not happen in this setting.

5

Multi-Aircraft Online Trajectory Planning

In this chapter, to show the effectiveness of the online trajectory planning methodology described in Section 2.4 and Section 3.2, the following two numerical experiments have been carried out:

- Experiment 4: minimum-time continuous descent of three aircraft along routes converging at the same waypoint with time-based separation constraint among them.
- Experiment 5: minimum-time STAR-based continuous descent of three aircraft along converging routes. This experiments implies sequencing the aircraft at a merging waypoint and passing through two other waypoints.

Experiments 4 and 5 are the online versions of the offline Experiments 1 and 3, respectively, described in Chapter 4. Thus, both numerical experiments involve the same Airbus A-320 BADA 3.14 aircraft models, in which the performance index is the sum of the duration of the flights of the three aircraft. Also, in both experiments, constraints derived from current flight regulation have been introduced. In the first one, time-base separation operational constraints have been imposed. The considered minimum time separation between aircraft has been 200 s. Again, this specific value has been chosen taking into account [46], which specifies that aircraft have to be separated by at least 3 NM or 3 min in the TMA. In the second experiment, constraints derived from a STAR procedure have been imposed, which imply passing through waypoints. However, unlike in Chapter 4, now a constant crosswind has been also considered along with a multi-cell storm in development whose cells grow and move in the same direction as the wind.

5.1 Experiment 4. Minimum-time continuous descent along converging routes

In this experiment, as in Experiment 1, a CDA under vectoring has been considered, that is, the lateral path followed by the aircraft has been assumed to be specified by the ATC. Again, the boundary conditions of the state variables have been selected from the chart of the Adolfo Suárez Madrid-Barajas (LEMD/MAD) TMA shown in Fig. 4.1. The initial positions of Aircraft 1, Aircraft 2, and Aircraft 3 have been assumed to be coincident with the ROLDO, SOTUK, and MORAL waypoints, respectively. Their common final position has been assumed to be the LALPI waypoint. It has been assumed that the three aircraft have been allowed by the ATC to go directly from their initial positions to the final waypoint.

Table 5.1: Boundary conditions for Experiment 4 and Experiment 5

Symbol	Unit	Aircraft 1	Aircraft 2	Aircraft 3
h_I	m	7400	7000	7200
h_F	m	3350	3350	3350
θ_I	deg	39.526	39.116	39.000
θ_F	deg	40.575	40.575	40.575
λ_I	deg	-5.327	-4.448	-3.325
λ_F	deg	-3.422	-3.422	-3.422
V_I	m/s	130	130	130
V_F	m/s	110	110	110
μ_I	deg	0	0	0
γ_I	deg	0	0	0
χ_I	deg	356	294	240
m_I	kg	65000	65000	65000

Table 5.2: Experiment 4: Boundary conditions for the cells of the storm

Symbol	Unit	Cell 1	Cell 2	Cell 3
h_I	m	5500	5500	5500
h_F	m	5500	5500	5500
θ_I	deg	39.7	39.7	40.0
θ_F	deg	39.7	39.7	40.0
λ_I	deg	-3.24	-3.9	-4.3
λ_F	deg	-3.53	-4.2	-4.63
V_S	m/s	18.5	18.5	18.5

5.1.1 Case study A. Without time-based separation constraints

In a first instance, the problem has been formulated and solved as an online trajectory planning problem following Section 2.4. However, neither time-based nor distance-based separation constraints have been included in the model.

A constant crosswind of 30 m/s westbound has been considered together with a multi-cell storm in development formed by three cells. Each cell has been modelled using a moving and growing ellipsoid as explained in Section 3.2.4. They are assumed to grow in dimension and move in the same direction as the wind but with a different speed of 18.5 m/s. In general, the cells growth could be described by increasing both the safety distances $d_{\lambda\theta_i}$ and d_{h_i} introduced in Section 3.2.4. In this experiment, only the $d_{\lambda\theta_i}$ distance has been increased from 7000 m to 10000 m. The experiment has been designed in such a way that there is a potential conflict among the cells of the storm and the aircraft. The initial mass of the three aircraft has been assumed equal to the maximum landing weight of the aircraft. The specific boundary conditions of the state variables are given in Table 5.1. and the boundary conditions of the cells of the storm are given in Table 5.2.

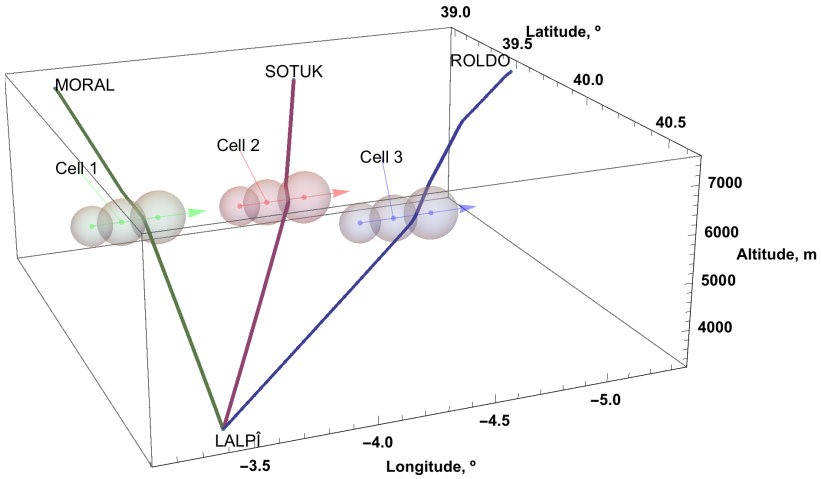

Figure 5.1: Experiment 4. Case study A. 3D view of the paths without time-based separation constraints.

In Figure 5.1 the 3D view of the paths obtained in the solution are represented and in Figure 5.2 and Figure 5.3 the horizontal and vertical profiles, respectively, are shown for the three aircraft. The final mass for the three aircraft are depicted in Figure 5.4.

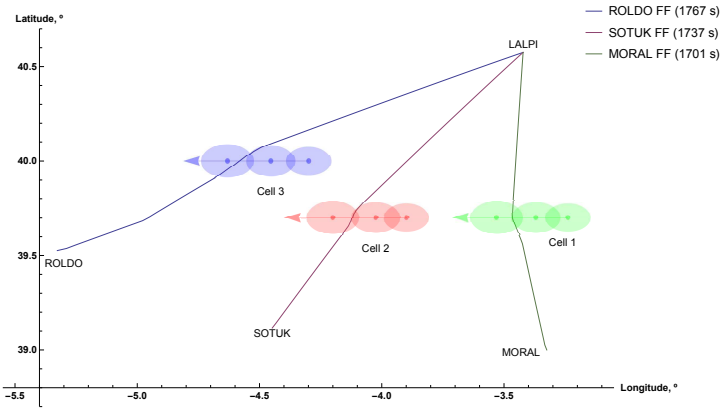

Figure 5.2: Experiment 4. Case study A. Horizontal profiles without time-based separation constraints.

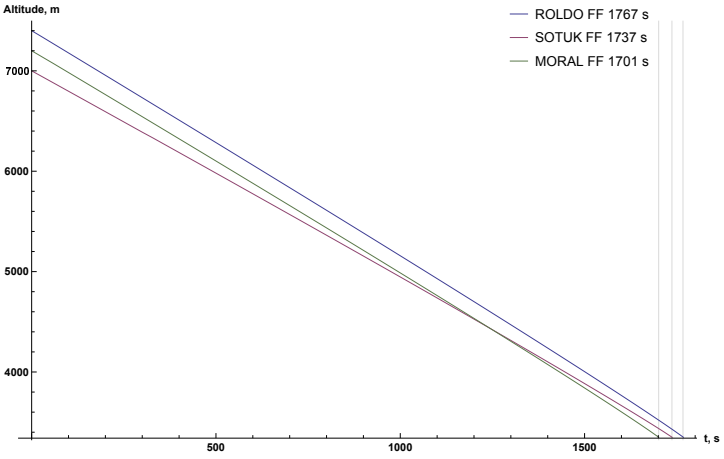

Figure 5.3: Experiment 4. Case study A. Vertical profiles without time-based separation constraints.

The final time is 1767 s, 1737 s and 1701 s for Aircraft 1, Aircraft 2 and Aircraft 3, respectively, corresponding to 28-30 min of flight. The difference between the final time of Aircraft 2 and 3 is 36 s, between Aircraft 1 and 2 is 30 s, and between Aircraft 1 and 3 is 66 s. As expected, these differences in time among the three aircraft at LALPI waypoint are below the required time separation of 200 s established above. Note that, as mentioned before, the chart in Figure 4.1 has been intentionally selected due to the high likelihood of potential conflicts that might arise among the involved aircraft. These potential conflicts are still present after the inclusion of the wind and the multi-cell storm in development in the model. Therefore, a new experiment has been conducted in order to fix the conflict observed in Case study A.

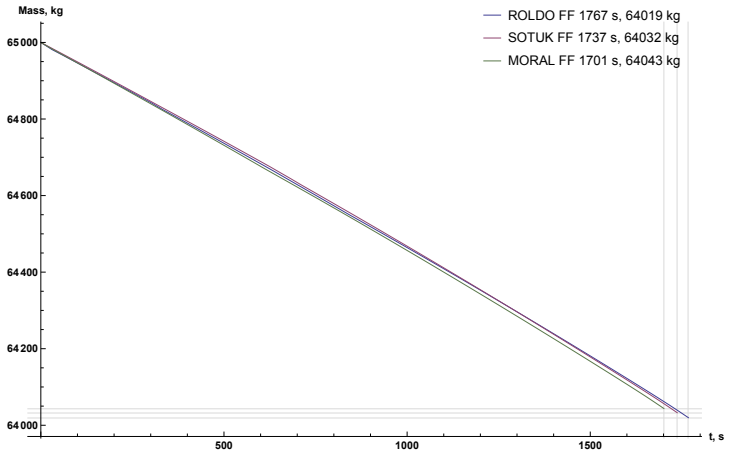

Figure 5.4: Experiment 4. Case study A. Mass consumption without time-based separation constraints.

5.1.2 Case study B. With time-based separation constraints

As mentioned above, a second experiment has been conducted which, besides the formulation used to model Case study A, includes time-based separation logical constraint of at least 200 s between aircraft at the `LALPI` waypoint as described in Section 3.2.1.

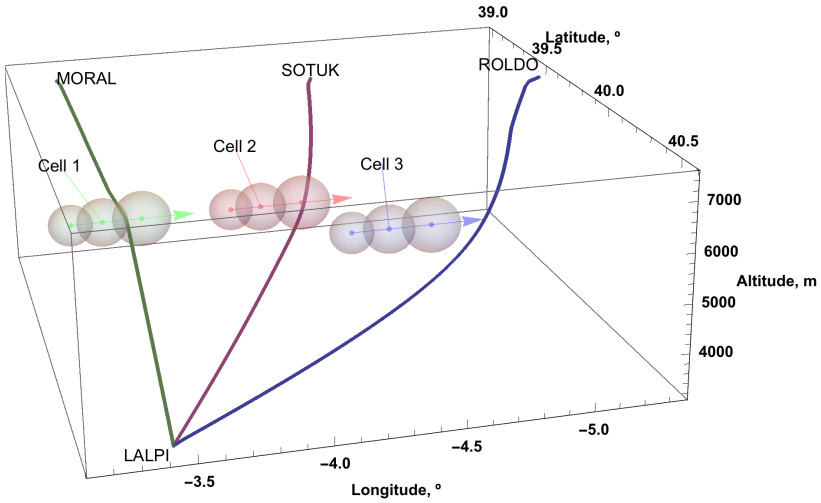

Figure 5.5: Experiment 4. Case study B. 3D view of the paths with time-based separation constraints.

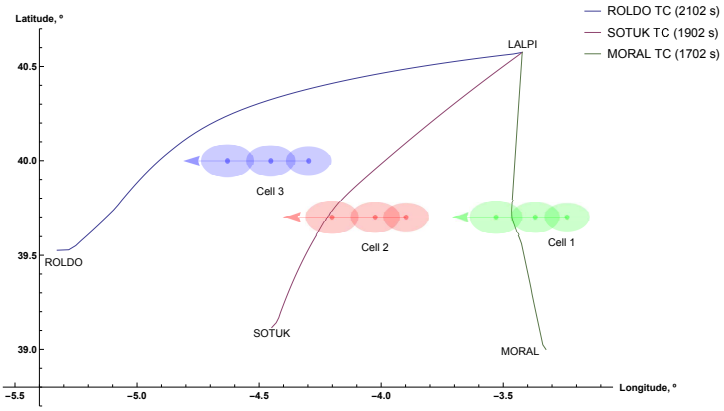

Figure 5.6: Experiment 4. Case study B. Horizontal profiles with time-based separation constraints.

In Figure 5.5 the 3D view of the paths obtained in the solution are represented and in Figure 5.6 and Figure 5.7 the horizontal and vertical profiles, respectively, are shown for the three aircraft. The final mass for the three aircraft are depicted in Figure 5.8.

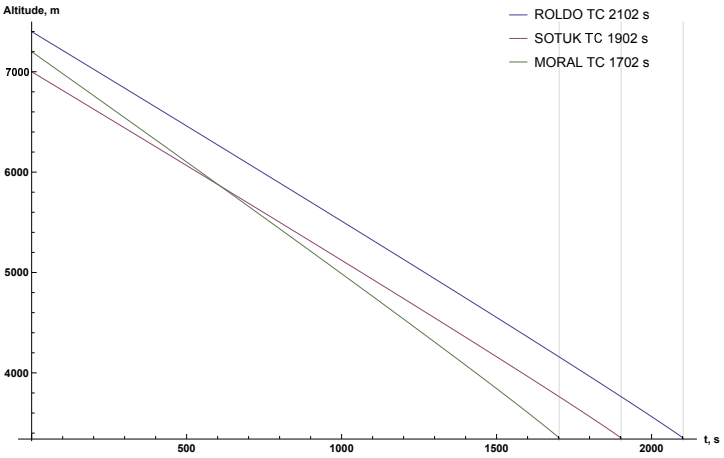

Figure 5.7: Experiment 4. Case study B. Vertical profiles with time-based separation constraints.

Now, the final time is 2102 s, 1902 s and 1702 s for Aircraft 1, Aircraft 2 and Aircraft 3, respectively, corresponding to 28-35 min of flight. The difference between the final time of aircraft is 200 s in all cases. Thus, as expected, these differences in time among the three aircraft at LALPI waypoint fulfil the required time separation established above.

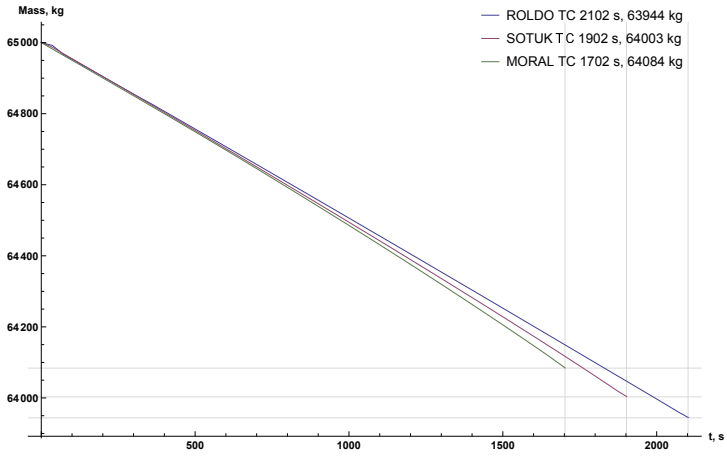

Figure 5.8: Experiment 4. Case study B. Mass consumption with time-based separation constraints.

5.1.3 Comparison and discussion on the results

In Figure 5.9 the 3D view of the paths obtained in the solution without time-based separation constraints are represented in thin lines whereas the 3D view of the paths obtained in the solution with time-based separation constraints are represented in thick lines. In Figure 5.10 and Figure 5.11 the horizontal and vertical profiles without time-based separation constraints are represented in dashed lines whereas the horizontal and vertical profiles with time-based separation constraints are represented in solid lines.

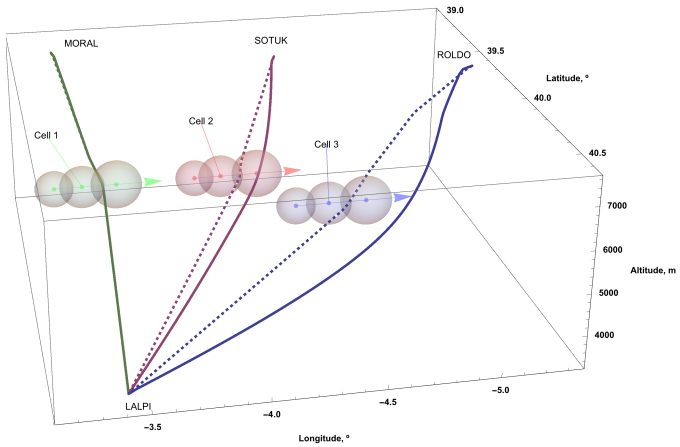

Figure 5.9: Experiment 4. Comparison. 3D view of the paths with (thick lines) and without (thin lines) time-based separation constraints.

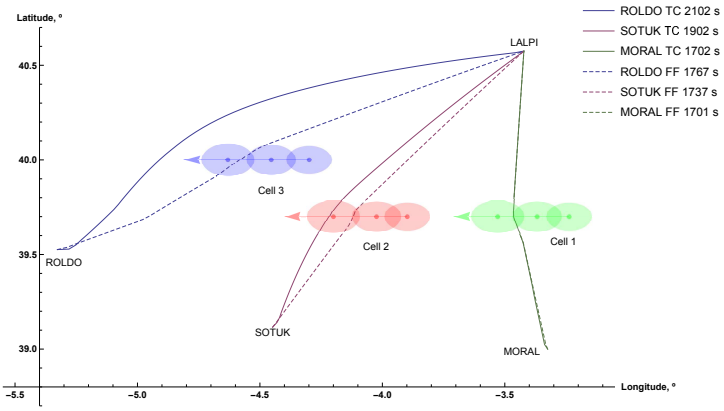

Figure 5.10: Experiment 4. Comparison. Horizontal profiles with (TC, solid lines) and without (FF, dashed lines) time-based separation constraints.

Note that whereas in Case Study A the three aircraft perform the minimum-time descent path by means of a CDA procedure at almost idle thrust, in Case Study B the horizontal and vertical profiles changed significantly for Aircraft 1 and Aircraft 2. These differences are obviously due to the inclusion of the time separation constraints which substantially modifies the control variables profiles of Aircraft 1 and Aircraft 2.

Table 5.3: Results of Experiment 4

	# Aircraft	Final Time, s	Final mass, kg
Without time constraint	Aircraft 1	1767	64019
	Aircraft 2	1737	64032
	Aircraft 3	1701	64043
With time constraint	Aircraft 1	2102	63944
	Aircraft 2	1902	64003
	Aircraft 3	1702	64084

The final mass and time given by the solution with and without time-based separation constraints are reported for each aircraft in Table 5.3. The mass consumption is represented in Figure 4.13, in which the solution without time-based separation constraints is represented in dashed lines whereas the solution with time-based separation constraints is represented in solid lines. It can be seen that introducing time separation constraints increases the mass consumption of Aircraft 1 and Aircraft 2 whereas that of Aircraft 3 decreases.

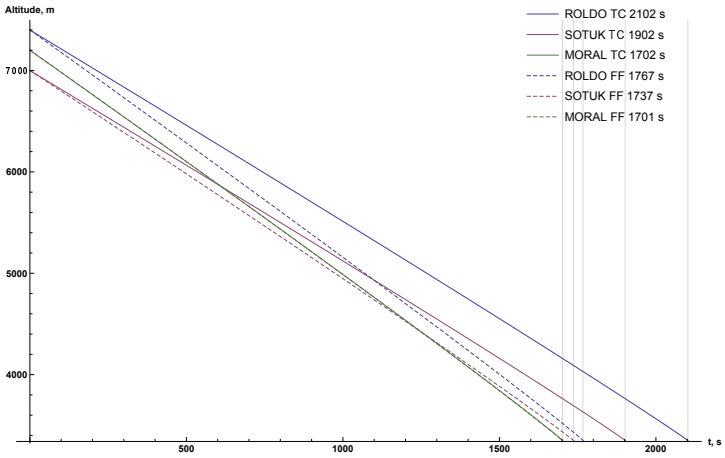

Figure 5.11: Experiment 4. Comparison. Vertical profiles with (TC, solid lines) and without (FF, dashed lines) time-based separation constraints.

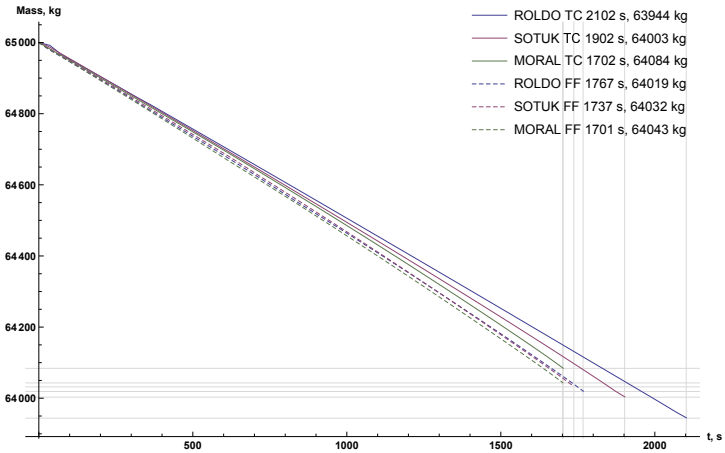

Figure 5.12: Experiment 4. Comparison. Mass consumption with (TC, solid lines) and without (FF, dashed lines) time-based separation constraints.

Finally, note that, since the objective functional to be minimized is the sum of the duration of the flights, time-based separation constraints are saturated in Case Study B and aircraft maintain mutually the minimum required time-based separation of 200 s. Moreover, it can be seen from Figure 5.9 and Figure 5.10 that in the experiment without time-based separation constraints the storm avoidance constraints are saturated by the three aircraft whereas in the experiment with time-based separation constraints they are not saturated by Aircraft 1 and Aircraft 2, due to the inclusion of the time-based separation constraints. The path of Aircraft 3 remains almost unchanged.

5.2 Experiment 5. Minimum-time STAR-based continuous descent along converging routes

In this experiment, as in Experiment 3, a STAR-based CDO has been considered, that is, the lateral path followed by the aircraft has been assumed to be specified in a navigation chart. In particular, the same boundary conditions of the state variables have been selected from the chart of the Adolfo Suárez Madrid-Barajas (LEMD/MAD) TMA shown in Figure 4.1. Again, the initial positions of Aircraft 1, Aircraft 2, and Aircraft 3 have been assumed to be coincident with the ROLDO, SOTUK and MORAL waypoints, respectively. In principle, the aircraft are constrained to pass through the TODNO and the RESBI waypoints and their common final position is assumed to be the LALPI waypoint. However, the presence of the multi-cell storm might lead to the negletion of this assumption as it will be explained later. Similarly to Experiment 3, for the setting of the cuboids centered at the given waypoints the modeling technique defined in (3.20) has been employed. In particular, the cuboid centered at the TODNO waypoint has been defined by the two corners $(39.560°, -4.24°, 5400\ \text{m})$ and $(39.640°, -4.160°, 6000\ \text{m})$, whereas the cuboid centered at the RESBI waypoint has been defined by the two corners $(40.400°, -4.150°, 4200\ \text{m})$ and $(40.480°, -4.070°, 4800\ \text{m})$. As in the previous experiments, the initial mass of the three aircraft has been assumed equal to the maximum landing weight of the aircraft. The specific boundary conditions of the state variables are the same as in Experiment 4 and are given in Table 5.1.

Table 5.4: Experiment 5: Boundary conditions for the cells of the storm

Symbol	Unit	Cell 1	Cell 2	Cell 3
h_I	m	5500	4500	5000
h_F	m	5500	4500	5000
θ_I	deg	39.6	40.44	40.0
θ_F	deg	39.6	40.44	40.0
λ_I	deg	-3.45	-3.95	-4.5
λ_F	deg	-3.78	-4.25	-4.8
V_S	m/s	18.5	18.5	18.5

As in Experiment 4, a constant crosswind of 30 m/s westbound has been considered together with a three-cell storm in development. These cells, which have been modelled as moving and growing ellipsoids, as explained in Section 3.2.4, are assumed to move in the same direction as the wind but with a different speed of 18.5 m/s. The specific boundary conditions of the cells of the storm are given in Table 5.4. The cells growth has been also modeled by increasing only the $d_{\lambda\theta_i}$ distance from 7000 m to 10000 m. Following the STAR procedure, in principle, the three aircraft are assumed to pass through both the TODNO and the RESBI waypoints. However, the experiment has been designed in such a way that one of the cells also passes through the RESBI waypoint

when the aircraft are approaching it, generating conflicts. To solve these conflicts, a decision making process has been included in the model, which attending to safety reasons, in case of spatio-temporal coincidence between a cell of the storm and a waypoint, establishes that avoiding the storm is preferable for the aircraft than crossing a waypoint. The effectiveness of this decision making process is guaranteed by the presence of the penalty term (3.24) for the waypoints constraints and the absence of the penalty term for the storm avoidance constraints. In the optimal solution, the former might not be fulfilled while the latter must be accomplished in any case.

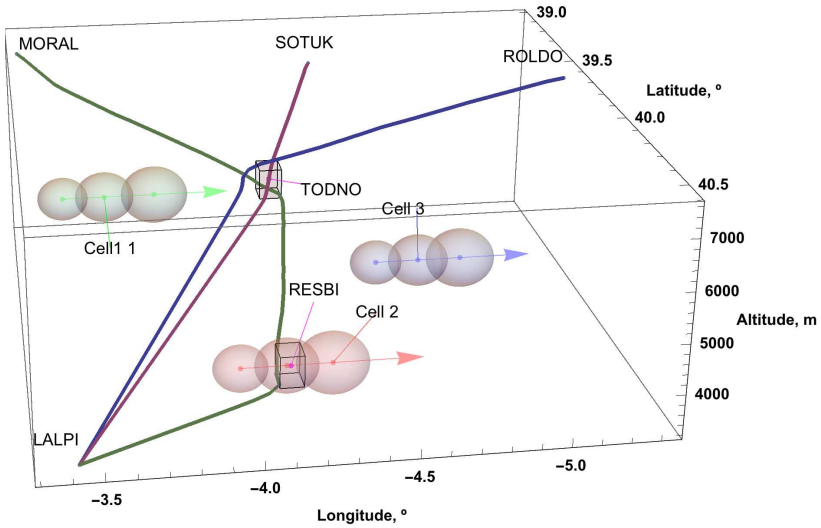

Figure 5.13: Experiment 5. Case study A. 3D view of the paths with storm and waypoints constraints.

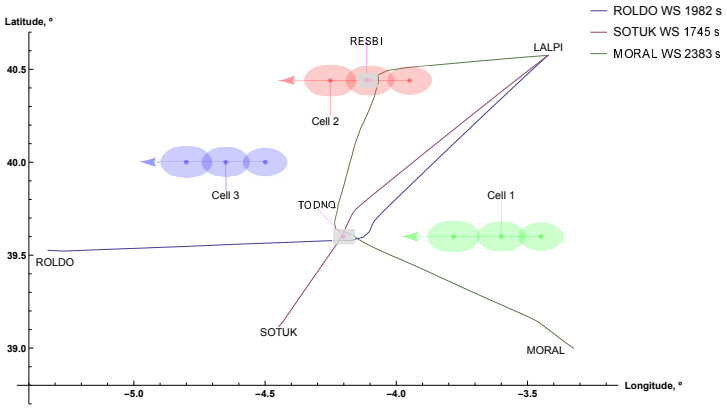

Figure 5.14: Experiment 5. Case study A. Horizontal profiles with storm and waypoints constraints.

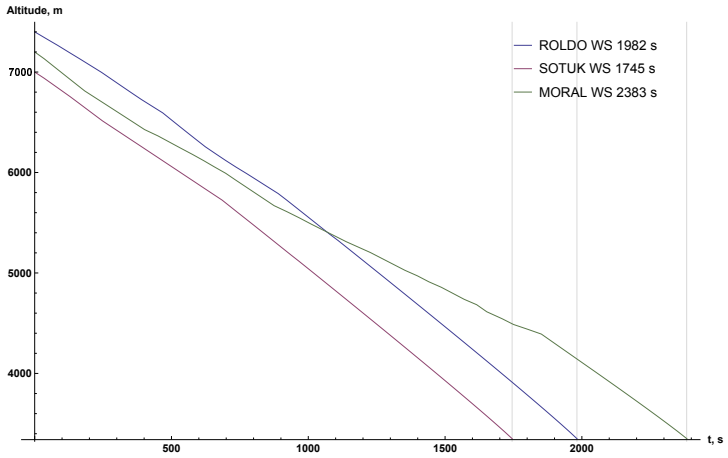

Figure 5.15: Experiment 5. Case study A. Vertical profiles with storm and waypoints constraints.

5.2.1 Case study A. With storm avoidance constraints

In a first instance, the problem has been formulated and solved as an online trajectory planning problem following Section 2.4 and neither time-based nor distance-based separation constraints have been included in the model. In Figure 5.13 the 3D view of the paths obtained in the solution are represented and in Figure 5.14 and Figure 5.15 the horizontal and vertical profiles, respectively, are shown for the three aircraft. The final mass for the three aircraft are depicted in Figure 5.16.

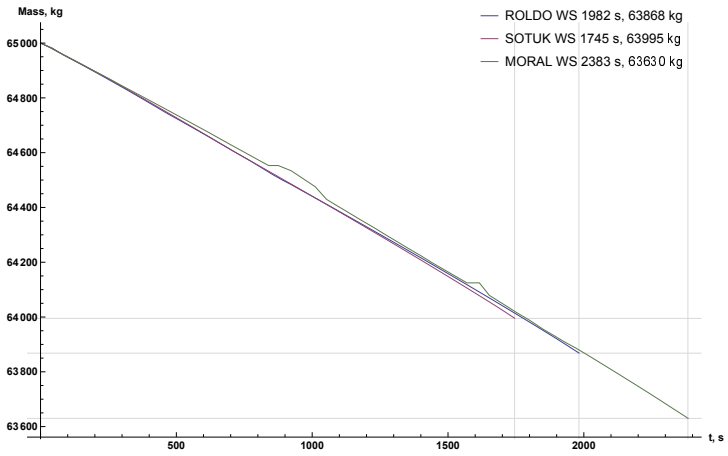

Figure 5.16: Experiment 5. Case study A. Mass consumption with storm and waypoints constraints.

The final time is 1942 s, 1742 s and 2287 s for Aircraft 1, Aircraft 2 and Aircraft 3, respectively, corresponding to 29–38 min of flight. In spite of the fact that the three aircraft have to pass through two waypoints, neither distance-based conflict nor time-based conflict arises during the whole flight. In particular, the difference between the final time of Aircraft 2 and 3 is 546 s, between Aircraft 1 and 2 is 201 s, and between Aircraft 1 and 3 is 345 s. All these differences in time among the three aircraft at the LALPI waypoint are above the required time-based separation of 200 s.

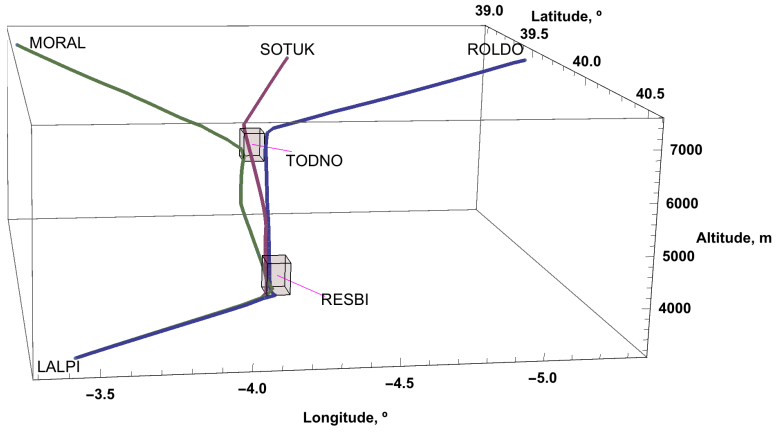

Figure 5.17: Experiment 5. Case study B. 3D view of the paths without storm constraints and with waypoints constraints.

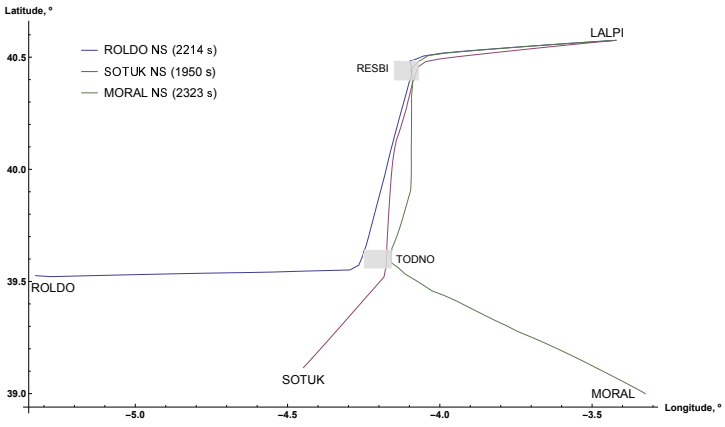

Figure 5.18: Experiment 5. Case study B. Horizontal profiles without storm constraints and with waypoints constraints.

5.2.2 Case study B. Without storm avoidance constraints

For the sake of comparison, the same experiment has been carried out following the same formulation used to model Case study A but without the storm avoidance constraints. In Figure 5.17 the 3D view of the paths obtained in the solution are represented and in figures Figure 5.18 and Figure 5.19 the horizontal and vertical profiles are shown for the three aircraft. The final mass for the three aircraft are depicted in Figure 5.20.

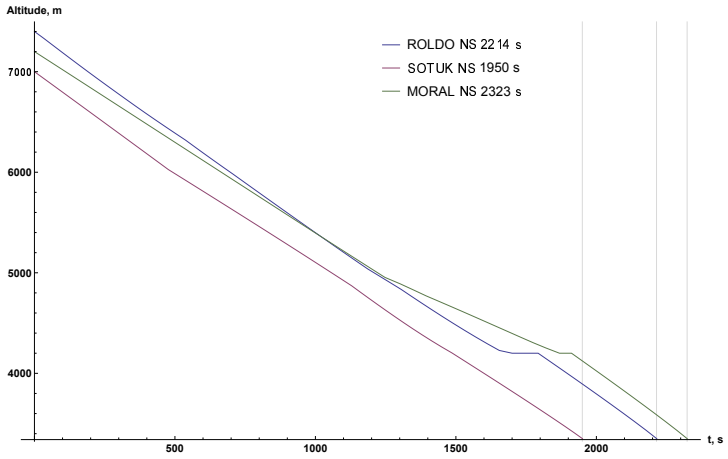

Figure 5.19: Experiment 5. Case study B. Vertical profiles without storm constraints and with waypoints constraints.

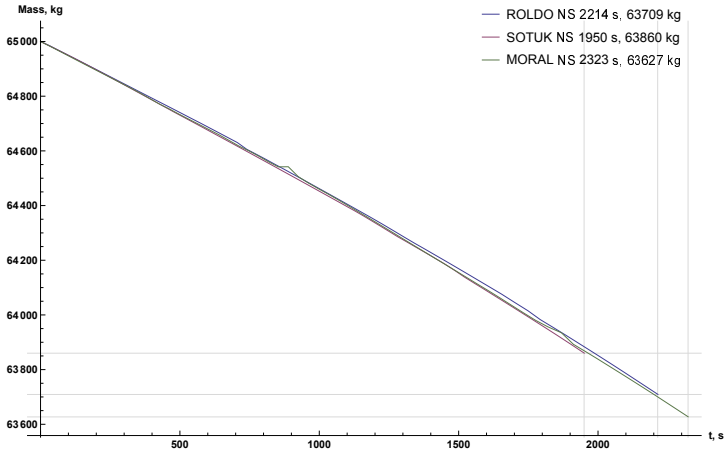

Figure 5.20: Experiment 5. Case study B. Mass consumption without storm constraints and with waypoints constraints.

Now, the final time is 2214 s, 1950 s and 2323 s for Aircraft 1, Aircraft 2 and Aircraft 3, respectively, corresponding to 32-39 min of flight. The difference between the final time of Aircraft 2 and 3 is 373 s, between Aircraft 1 and 2 is 264 s, and between Aircraft 1 and 3 is 109 s. Thus, the difference in time between Aircraft 1 and 3 at LALPI waypoint is below the required time separation of 200 s established above.

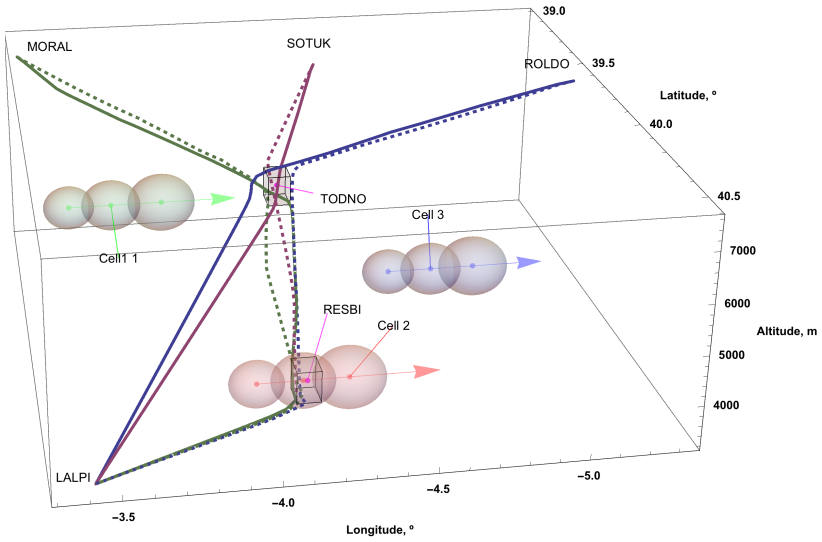

Figure 5.21: Experiment 5. 3D view of the paths with (thick lines) and without (thin lines) waypoints and time-based separation constraints.

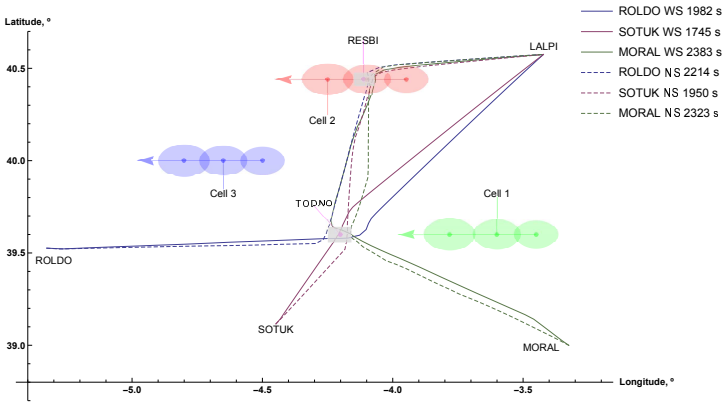

Figure 5.22: Experiment 5. Horizontal profiles with (WS, solid lines) and without (NS, dashed lines) storm avoidance constraints.

5.2.3 Comparison and discussion on the results

In Figure 5.21 the 3D view of the paths obtained in the solution with storm avoidance constraints are represented in thick lines whereas the 3D view of the paths obtained in the solution without storm avoidance constraints are represented in thin lines. In Figure 5.22 and Figure 5.23 the horizontal and vertical profiles with storm avoidance constraints are represented in solid lines whereas the horizontal and vertical profiles without storm avoidance constraints are represented in dashed lines. It can be seen that both the horizontal and the vertical profiles changed significantly.

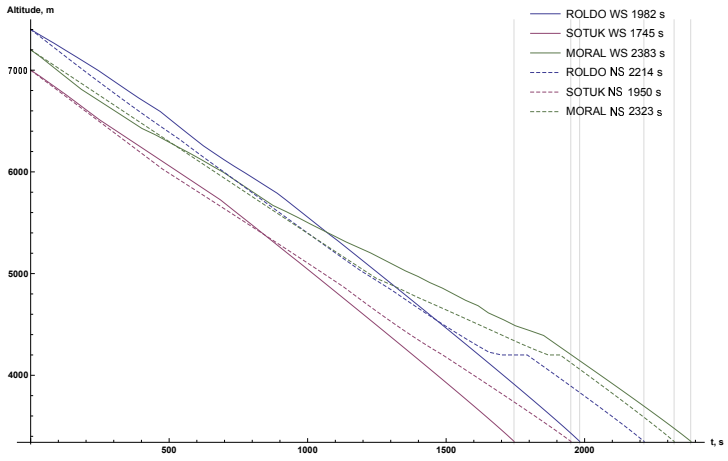

Figure 5.23: Experiment 5. Vertical profiles with (WS, solid lines) and without (NS, dashed lines) storm avoidance constraints.

In principle, the three aircraft are assumed to pass through both waypoints and, at the same time, avoid the storm. However, as it can be seen in 5.21, in Case Study A, only A aircraft 3 is able to avoid the storm and reach both waypoints `TODNO` and `RESBI`. The other two aircraft also avoid the storm but they are able only to reach the `TODNO` waypoint. This is due to the fact that the performance index includes in this case, besides the minimization of the duration of the flights, a penalty term associated to the waypoints constraints in such a way that, as explained above, the storm avoidance constraint is always preferable for safety reasons. On the other hand, in Case Study B, the three aircraft reach both waypoints since no storm is included in the model and thus, the penalty term associated to the waypoints constraints is enough to guarantee the fulfilment of the assumption.

Therefore, in Case Study B, the the minimum-time STAR-based continuous descent path procedure is performed by the three aircraft whereas this procedure is only performed by Aircraft 3 in Case Study A. Thus, due to the inclusion of the storm avoidance constraints, there are significant changes in both the vertical and horizontal profiles for the three aircraft. These differences also can be appreciated in the control variables profiles of the three aircraft.

Table 5.5: Results of Experiment 5

	# Aircraft	Final Time, s	Final mass, kg
Without storm avoidance constraints	Aircraft 1	2214	63709
	Aircraft 2	1950	63860
	Aircraft 3	2323	63627
With storm avoidance constraints	Aircraft 1	1982	63868
	Aircraft 2	1745	63995
	Aircraft 3	2383	63630

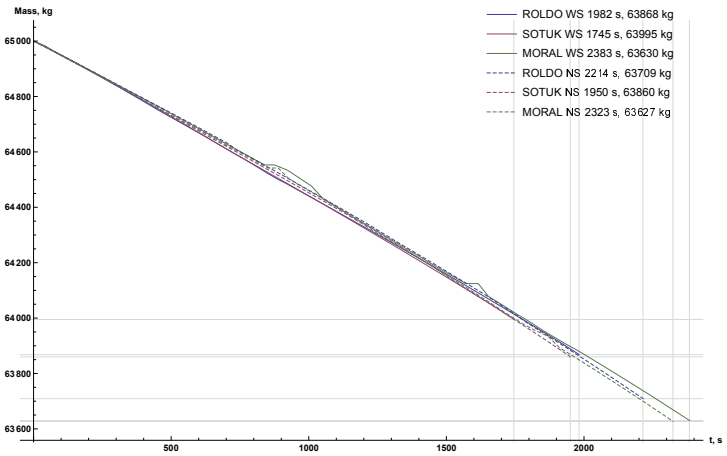

Figure 5.24: Experiment 5. Mass consumption with (WS, solid lines) and without (NS, dashed lines) storm avoidance constraints.

The final mass and time given by the solution with and without storm avoidance constraints are reported for each aircraft in Table 5.5. The mass consumption is depicted in Figure 5.24, in which the solution with storm avoidance constraints is represented in solid lines whereas the solution without storm avoidance constraints is represented in dashed lines. It can be seen that introducing the storm avoidance constraints decreases the mass consumption of the three aircraft.

Finally, notice that, unlike Experiment 1, aircraft 2 and 3 in Case Study B do not maintain the minimum required time separation of 200 s. This is due to the fact that the performance index includes in this case, besides the minimization of the duration of the flights, the penalty term (3.24) associated to the waypoints constraints. Therefore, the saturation of the time-based constraints may not happen in this setting.

5.3 Computational issues

In this section, the computational aspects of the proposed method for multi-aircraft optimal 4D online trajectory planning in the presence of a multi-cell storm in development will be discussed.

All the experiments presented in this dissertation have been carried out on an Intel Core i7 4 GHz CPU with 8 GB RAM. In both, Experiments 4 and 5, 60 iterations within the NMPC scheme are performed allowing up to 60 updates of the position and dimension of each cell of the multi-cell storm to be incorporated in the online trajectory planning problem.

Due to the NMPC scheme, where in the first iterations almost the complete trajectories are computed whereas in last iterations only the final trajectory segments are calculated, the observed computation times to solve the sequence of OLOCPs are not uniform over the iterations. For instance, the computation time observed in the first iteration of Experiment 5, the most demanding one from the computational point of view, has been 70.599 s, the computation time of the 30th iteration has been 19.38 s, and the computation time of the last iteration has been less than a second. The total computation time in Experiment 5 has been 1250.04 s, corresponding to approximately 20.8 min, while the total flight time has been 2287 s, corresponding to approximately 38 min. In Experiment 4 the computation time has been 283.552 s, corresponding to approximately 4.73 min, and the total flight time has been 1702 s, corresponding to approximately 28 min.

This confirms that the computational time of the proposed online trajectory planning paradigm is suitable for onboard implementation, since in both experiments the computation time is shorter than the flight time with the considered number of iterations in the NMPC scheme, which is much higher than the number of updates of the meteorological information available from current meteorological products.

This compatibility for online implementation allows the multi-aircraft optimal trajectory planning method presented in the manuscript to be integrated into an AMAN system like that proposed in [3], in which an architecture for future arrival management compatible with trajectory-based operations has been proposed. In [3], three technical challenges have been identified to support future AMAN: developing arrival scheduling algorithms, creating AMAN protocols and designing information flow models for air-ground, air-air, and ground-ground communications. It consists of three components called Route Analyzer (RA), Traffic Synthesizer (TS), and Dynamic Planner (DP).

The RA calculates aircraft trajectories from current positions to arrival airports following given flight plans and air traffic control interventions such as speed instructions and radar vectors. The TS calculates estimated time of arrival (ETA) at terminal airspace entry points. The DP generates an arrival schedule, which determines arrival sequences and scheduled times of arrival (STA) at terminal gates and runway thresholds using the ETA given by the TS. Input information, source and update timing of these components are specified. It can be seen that the method proposed in this paper combines the

functionalities of the RA and the DP components described in [3]. Moreover, input information, scheduling constraints and sequence constraints considered coincide in large extent.

6

Conclusions and Future Work

In this dissertation the in-flight 4D trajectory planning problem for multiple aircraft has been studied in converging and intersecting routes in presence of multi-cell storms in development along with time-based and distance-based separation between aircraft, obstacle avoidance and modelling passage through waypoints. The storm avoidance constraints have been enforced by approximating the cells of the storm as moving and growing ellipsoids, and the resulting problem has been solved by using nonlinear model predictive control based on hybrid optimal control with logical constraints in disjunctive form.

The logical constraints in disjunctive form have been transformed into inequality and equality constraints which involve only continuous auxiliary variables. In this way, the optimal control problem with logical constraints has been converted into a smooth optimal control problem, which has been solved very efficiently within a nonlinear model predictive control scheme for online trajectory planning.

Numerical experiments within the terminal manoeuvring area of the Adolfo Suárez Madrid-Barajas, which involve three aircraft and a three-cell storm in development, have been carried out to test the effectiveness of the proposed method, the most complex and computationally demanding of which is a minimum-time STAR-based continuous descent along converging routes. This experiment has been designed in such a way that a cell of the storm occupies a waypoint when the aircraft are approaching it. The contingency has been solved by a decision-making process included in the model to establish if the waypoint can be reached and the storm avoided or it is preferable for safety reasons to skip it. These numerical results show the effectiveness of the proposed technique, which is able to tackle all the aspects of the problem and optimally guide several aircraft in a STAR-based continuous descent along converging routes, separating and sequencing them while avoiding the cells of a storm in development.

Conclusions

According to the obtained results, three main conclusions can be drawned:

a) The hybrid optimal control approach is suitable for the definition of a framework to model efficient multiple-aircraft trajectories into a constrained-based in-flight trajectory planning paradigm.

b) The embedded optimal control approach allows to solve realistic flight plans for multiple aircraft by means of tackling logical constraints in disjunctive form, which gives the possibility to model both, meteorological and operational conditions, and decision-making processes.

c) The numerical techniques devised for both open-loop and closed-loop approaches are able to find solutions in time frames compatible not only with strategic and tactical planning but also with in-flight planning.

Overall, it can be concluded that the hybrid optimal control techniques proposed in this dissertation are able to define more efficient in-flight plans towards those operational concepts based on 4D business trajectories.

Open problems and future work

Several natural extensions of the study presented in this dissertation can be highlighted. First, more complex representations of the meteorological conditions could be considered to feed the multi-aircraft system. For instance, storms could be devised following curvilinear trajectories, changing velocity and with nonuniform size-changing. Moreover, data-driven approaches could be used to build both wind and storm models, and achieve more realistic and richer results. Second, a stochastic version of the embedded optimal control approach considered in this dissertation could be obtained by means of Monte Carlo or Polynomial Chaos techniques, which would improve the practical predictability of the aircraft trajectories. Finally, a computational improvement of the nonlinear model predictive control approach considered could be attained by means of a practical implementation based on a receding set of final positions of the aircraft instead of a single fixed final point position.

Bibliography

[1] A. Gardi, R. Sabatini, and S. Ramasamy, "Multi-objective optimisation of aircraft flight trajectories in the ATM and avionics context," *Progress in Aerospace Sciences*, vol. 83, pp. 1–36, 2016.

[2] International Civil Aviation Organization, "Continuous Descent Operations (CDO) Manual, Document 9931," tech. rep., ICAO, 2010.

[3] E. Itoh, M. Brown, A. Senoguchi, N. Wickramasinghe, and S. Fukushima, "Future arrival management collaborating with trajectory-based operations," in *Air Traffic Management and Systems II. Lecture Notes in Electrical Engineering, vol. 420* (Electronic Navigation Research Institute, ed.), pp. 137–156, Springer, 2017.

[4] "Nextgen: Concept of operations for the next generation air transport system." http://www.jpdo.gov/library/NextGen_v2.0.pdf., 2007.

[5] S. Consortium, "Air transport framework: the current situation, sesar definition phase milestone deliverable 1," tech. rep., SESAR Consortium, July 2006. http://www.eurocontrol.int/sesar/public [Retrieved 01/09/2009].

[6] S. Consortium, "The atm target concept, sesar definition phase milestone deliverable 3," tech. rep., SESAR Consortium, September 2007. http://www.eurocontrol.int/sesar/public [Retrieved 01/09/2009].

[7] S. Consortium, "The performance target, sesar definition phase milestone deliverable 2," tech. rep., SESAR Consortium, December 2006. http://www.eurocontrol.int/sesar/public [Retrieved 01/09/2009].

[8] M. Sauer, T. Hauf, and C. Forster, "Uncertainty analysis of thunderstorm nowcasts for utilization in aircraft routing," in *Proccedings of the 4th SESAR Innovation Days*, 2014.

[9] M. Matthews and R. DeLaura, "Evaluation of enroute convective weather avoidance models based on planned and observed flights," in *Proceedings of the 14th Conference on Aviation, Range, and Aerospace Meteorology*, 2010.

[10] K. Sheth, T. Amis, S. Gutierrez-Nolasco, B. Sridhar, and D. Mulfinger, "Development of a probabilistic convective weather forecast threshold parameter for flight-routing decisions," *Weather and Forecasting*, vol. 28, no. 5, pp. 1175–1187, 2013.

[11] V. Mouillet, "User Manual for the Base of Aircraft Data (BADA) Revision 3.14," tech. rep., EUROCONTROL Experimental Centre, Brétigny, France, 2017.

[12] L. Grüne and J. Pannek, *Nonlinear Model Predictive Control: Theory and Algorithms, Second Edition*. Springer-Verlag, London, 2017.

[13] S. C. Bengea and R. A. DeCarlo, "Optimal control of switching systems," *Automatica*, vol. 41, pp. 11–27, 2005.

[14] S. Wei, K. Uthaichana, M. Zefran, R. A. DeCarlo, and S. Bengea, "Applications of numerical optimal control to non-linear hybrid systems," *Nonlinear Analysis: Hybrid Systems*, vol. 1, no. 2, pp. 264–279, 2007.

[15] S. Wei, M. Zěfran, and R. A. DeCarlo, "Optimal control of robotic systems with logical constraints: Application to UAV path planning," in *Proceedings of the 2008 IEEE International Conference on Robotics and Automation*, (Pasadena, CA, USA), 2008.

[16] A. Andreeva-Mori, S. Suzuki, and E. Itoh, "Rule derivation for arrival aircraft sequencing," *Aerospace Science and Technology*, vol. 30, pp. 200–209, 2013.

[17] P. Bonami, A. Olivares, M. Soler, and E. Staffetti, "Multiphase mixed-integer optimal control approach to aircraft trajectory optimization," *Journal of Guidance, Control, and Dynamics*, vol. 36, no. 5, pp. 1267–1277, 2013.

[18] A. U. Raghunathan, V. Gopal, D. Subramanian, L. T. Biegler, and T. Samad, "Dynamic optimization strategies for three-dimensional conflict resolution of multiple aircraft," *Journal of Aircraft*, vol. 27, no. 4, pp. 586–594, 2004.

[19] K. Mohan, M. A. Patterson, and A. V. Rao, "Optimal trajectory and control generation for landing of multiple aircraft in the presence of obstacles," in *Proceedings of the AIAA Guidance, Navigation, and Control Conference*, (Minneapolis, MN, USA), 2012.

[20] S. G. Park and J.-P. Clarke, "Optimal control based vertical trajectory determination for continuous descent arrival procedures," *Journal of Aircraft*, vol. 52, no. 5, pp. 1469–1480, 2015.

[21] S. G. Park and J. P. Clarke, "Vertical trajectory optimization to minimize environmental impact in the presence of wind," *Journal of Aircraft*, vol. 53, no. 3, pp. 725–737, 2016.

[22] J. Pannequin, A. Bayen, I. Mitchell, H. Chung, and S. Sastry, "Multiple aircraft deconflicted path planning with weather avoidance constraints," in *Proceedings of the AIAA Guidance, Navigation and Control Conference and Exhibit*, (Hilton Head, SC, USA), 2007.

[23] M. Kamgarpour, V. Dadok, and C. Tomlin, "Trajectory generation for aircraft subject to dynamic weather uncertainty," in *Proceedings of the 49th IEEE Conference on Decision and Control*, (Atlanta, GA, USA), 2010.

[24] S. Summers, M. Kamgarpour, C. Tomlin, and J. Lygeros, "A stochastic reach-avoid problem with random obstacles," in *Proceedings of the 14th ACM International Conference on Hybrid Systems: Computation and Control*, (Chicago, IL, USA), 2011.

[25] M. Sauer, M. Steiner, R. D. Sharman, J. O. Pinto, and T. Hauf, "Flight execution and route adaptation considering multiple weather hazard," in *Proccedings of the WMO Aeronautical Meteorology Scientific Conference*, 2017.

[26] D. Hentzen, M. Kamgarpour, M. Soler, and D. González-Arribas, "On maximizing safety in stochastic aircraft trajectory planning with uncertain thunderstorm development," *Aerospace Science and Technology*, vol. 79, pp. 543–553, 2018.

[27] B. Zhang, L. Tang, and M. Roemer, "Probabilistic planning and risk evaluation based on ensemble weather forecasting," *IEEE Transactions on Automation Science and Engineering*, vol. 15, no. 2, pp. 556–566, 2018.

[28] E. Sontag, *Mathematical Control Theory, 2nd edn*, vol. 6 of *Texts in Applied Mathematics*. Springer, New York, 1998.

[29] J. Richalet, A. Rault, J. Testud, and J. Papon, "Model predictive heuristic control: Applications to industrial processes," *Automatica*, vol. 14, pp. 413–428, 1978.

[30] C. Cutler and B. Ramaker, "Dynamic matrix control: a computer control algorithm," in *Proceedings of the Joint Automatic Control Conference*, pp. 13–15, 1980.

[31] C. García, D. Prett, and M. Morari, "Model predictive control: Theory and practice: a survey," *Automatica*, vol. 25, no. 3, pp. 335–348, 1989.

[32] R. Bitmead, M. Gevers, and V. Wertz, *Adaptive Optimal Control. The Thinking Man's GPC*. International Series in Systems and Control Engineering, Prentice Hall, New York, 1990.

[33] S. Keerthi and E. Gilbert, "Optimal infinite-horizon feedback laws for a general class of constrained discrete-time systems: stability and moving-horizon approximations," *J. Optim. Theory Appl.*, vol. 57, no. 2, pp. 265–293, 1988.

[34] C. Chen and L. Shaw, "On receding horizon feedback control," *Automatica*, vol. 18, no. 3, pp. 349–352, 1982.

[35] D. Mayne and H. Michalska, "Receding horizon control of nonlinear systems," *IEEE Trans. Automat. Control*, vol. 35, no. 7, pp. 814–824, 1990.

[36] C. R. Hargraves and S. W. Pairs, "Direct trajectory optimization using nonlinear programming and collocation," *Journal of Guidance, Control, and Dynamics*, vol. 10, no. 4, pp. 338–342, 1987.

[37] O. von Stryk and R. Bulirsch, "Direct and indirect methods for trajectory optimization," *Annals of Operations Research*, vol. 37, no. 1, pp. 357–373, 1992.

[38] A. L. Herman and B. A. Conway, "Direct optimization using collocation based on high-order gauss-lobatto quadrature rules," *Journal of Guidance, Control, and Dynamics*, vol. 19, no. 3, pp. 592–599, 1996.

[39] D. Xiu, *Numerical Methods for Stochastic Computations: A Spectral Method Approach*. Princeton University Press, 2010.

[40] A. Herman, *Improved Collocation Methods with Application to Direct Trajectory Optimization*. PhD thesis, University of Illinois at Urbana-Champaign, Urbana, Illinois, USA, 1995.

[41] U. Eren, A. Prach, B. B. Koçer, S. V. Raković, E. Kayacan, and B. AçÄśkmeşe, "Model predictive control in aerospace systems: Current state and opportunities," *Journal of Guidance, Control, and Dynamics*, vol. 40, no. 7, pp. 1541–1566, 2017.

[42] A. Wachter and L. Biegler, "On the implementation of an interior-point filter line-search algorithm for large-scale nonlinear programming," *Mathematical Programming*, vol. 106, no. 1, pp. 25–57, 2006.

[43] T. M. Cavalier, P. M. Pardalos, and A. L. Soyster, "Modeling and integer programming techniques applied to propositional calculus," *Computers and Operations Research*, vol. 17, no. 6, pp. 561–570, 1990.

[44] S. Hao, S. Cheng, and Y. Zhang, "A multi-aircraft conflict detection and resolution method for 4-dimensional trajectory-based operation," *Chinese Journal of Aeronautics*, vol. 31, no. 7, pp. 1579–1593, 2018.

[45] S. Wei, K. Uthaichana, M. Zefran, and R. A. DeCarlo, "Hybrid model predictive control for the stabilization of wheeled mobile robots subject to wheel slippage," *IEEE Transactions on Control Systems Technology*, vol. 21, pp. 2181–2193, 2013.

[46] I. C. A. Organization, "Procedures for air navigation services: Air traffic management," Tech. Rep. 4444, ICAO, 2016.